Nonlinear optics of normal-mode-coupling semiconductor microcavities

G. Khitrova and H. M. Gibbs

Optical Sciences Center, University of Arizona, Tucson, Arizona 85721

F. Jahnke, M. Kira, and S. W. Koch

Department of Physics and Material Sciences Center, Philipps-University Marburg, Renthof 5, 35032 Marburg, Germany

The authors review the nonlinear optical properties of semiconductor quantum wells that are grown inside high-Q Bragg-mirror microcavities. Light-matter coupling in this system is particularly pronounced, leading in the linear regime to a polaritonic mixing of the excitonic quantum well resonance and the single longitudinal cavity mode. The resulting normal-mode splitting of the optical resonance is observed in reflection, transmission, and luminescence experiments. In the nonlinear regime the strong light-matter coupling influences the excitation-dependent bleaching of the normal-mode resonances for nonresonant excitation, leads to transient saturation and normal-mode oscillations for resonant pulsed excitation and is responsible for the density-dependent signatures in the luminescence characteristics. These and many more experimental observations are summarized and explained in this review using a microscopic theory for the Coulomb interacting electron-hole system in the quantum well that is nonperturbatively coupled to the cavity light field.
[S0034-6861(99)01005-3]

CONTENTS

I. INTRODUCTION

A. What questions does this field address?

What happens when a quantum well is grown in the center of a semiconductor microcavity? If the quantum well exhibits a pronounced exciton resonance and if the widths of the degenerate exciton and empty-cavity lines are both small enough, one sees two transmission peaks and two reflection dips (Weisbuch *et al.*, 1992). This result of light-matter interaction is called here excitonic normal-mode coupling (NMC). It is often related to vacuum-field Rabi splitting of atoms or to a polariton describing light-propagation in a dielectric medium.

The study of vacuum-field Rabi splitting has been an exciting subfield of atomic physics for 15 years. After a decade of gradual improvements, Rabi splitting was seen with a single atom (Thompson *et al.*, 1992; Haroche, 1992). This led recently to the first clear demonstration of the discrete nature of the coherent exchange of energy between the atom and the quantized electromagnetic field (Brune *et al.*, 1996). For such a truly quantum system the optical properties are changed by the addition of a single photon or single atom, which is often referred to as the quantum statistical limit.

In the opposite limit of many atoms the system behaves semiclassically, i.e., the light-matter interaction can be described equally well on the basis of a classical field. For atoms in a cavity one finds a sinusoidal cycling of energy between the atom and the cavity field. What complicates the comparison between the single-atom and the many-atom systems is the fact that both systems show the same response to a weak probe field (Carmichael *et al.*, 1994). These insights lead to a number of stimulating new questions: Is putting a single quantum well in a semiconductor microcavity equivalent to putting a single atom into one of the atomic cavities? Can present-day semiconductor microcavities provide tiny, monolithic, ''permanent'' quantum gates exhibiting the quantum entanglements needed for quantum computing? To find out, one must answer the question: how many photons does it take to see detectable changes in the properties of a current normal-mode-coupling microcavity? In other words, one must perform and analyze nonlinear optical experiments, the primary focus of this review.

To understand the nonlinear response, one must first understand the linear response. How does one design an NMC microcavity? Could the measured linear optical response be useful in this design? Are there any curious effects arising from the capability to grow a quantum well where one wants in the microcavity spacer, i.e., in a field antinode, or node, or anywhere in between? This static spatial arrangement is a clear advantage of quantum wells relative to atoms.

Then, to return to the nonlinear response, what happens to the reflectivity, transmission, absorption, and photoluminescence of an NMC microcavity as the number of excitations in the system is increased? Does the NMC splitting change with the first excitation? Could the measured nonlinear response of the bare quantum well be useful in understanding the nonlinear response of the composite system? How does one go about computing the nonlinear optical properties, for example, when the excitations occur at a constant rate by carrier injection or by optical pumping above the band gap? What about the case of resonant excitation with a short pulse with a broad spectrum overlapping both NMC peaks? Can one excite the microcavity in a way that causes the energy to go back and forth between the excitons in the quantum well and the photons bouncing between the mirrors? If so, what determines the rate of oscillation? What happens for resonant narrow band excitation into one peak and probing the other? Can one achieve coherent control of a probe by coherent deexcitation?

Another interesting topic is the propagation of light through an NMC microcavity. The interaction of the light field with a single resonance of an infinite medium leads to a new quasiparticle, the polariton (Hopfield, 1958). Using the appropriate boundary conditions, one can similarly introduce a cavity polariton (Andreani *et al.*, 1994). Does the curvature of the dispersion curve of such a cavity polariton correspond to the effective mass of this quasi-particle? Since the mass of this exciton-photon ''molecule'' is much smaller than that of an exciton, does a cavity polariton have a much larger de Broglie wavelength? Does that mean it is much easier to achieve Bose condensation of cavity polaritons than of excitons? Could such a condensation result in coherent light emission at lower thresholds than ordinary semiconductor lasers or vertical-cavity surface-emitting lasers (VCSEL's)? Is it possible that in one of these tiny semiconductor microcavities one could observe both the long sought for Bose condensation in a semiconductor and an atom laser? How does the photoluminescence for off-resonant cw excitation depend upon excitation density? Can it be described by electrons and holes having Fermi-Dirac distributions trying to emit from within a two-peaked microcavity? Must one quantize the electromagnetic field in order to compute it?

Yet another topic involves deviations from perfect systems in real devices. Does a larger de Broglie wavelength result in better averaging over structural disorder such as interface fluctuations, interface diffusion, alloy fluctuations, etc.?

Normal-mode coupling is also related to device questions. What distinguishes a microcavity that exhibits normal-mode coupling from a VCSEL? Can one utilize the phenomenon of normal-mode coupling to produce more efficient light-emitting diodes or lower-threshold coherent light emitters? Does normal-mode coupling occur only at low temperatures?

B. Historical perspective

The optical properties of semiconductors and semiconductor structures have been the subject of intense experimental and theoretical investigation during recent decades. Consequently, many of the basic physical properties are understood very well and even used in commercial devices such as semiconductor lasers. To some degree it is the huge success of these devices as well as the desire for faster operational speeds and higher levels of on- and off-chip integration that drives the development of smaller and smaller semiconductor structures.

A recent example in this context is the novel VCSEL structure in which thin layers of semiconductor material inside high-finesse microcavities function as very efficient miniature laser systems (Soda *et al.*, 1979; Passner *et al.*, 1980; Iga *et al.*, 1988; Jewell *et al.*, 1988; Gourley *et al.*, 1989; Jewell *et al.*, 1991; Koch *et al.*, 1995). Interestingly enough, basically the same structures show very interesting light-matter coupling effects even under low excitation conditions, where the excitonic resonances dominate the optical semiconductor properties.

The detailed analysis of strong light-matter coupling and its manifestation in the linear and nonlinear optical properties of semiconductor quantum-well structures inside high-finesse microcavities is the main theme of this review article. A schematic picture of a microcavity system is shown in Fig. 1. Of particular interest is the so-called nonperturbative regime in which the coupling between the material response and photons in the

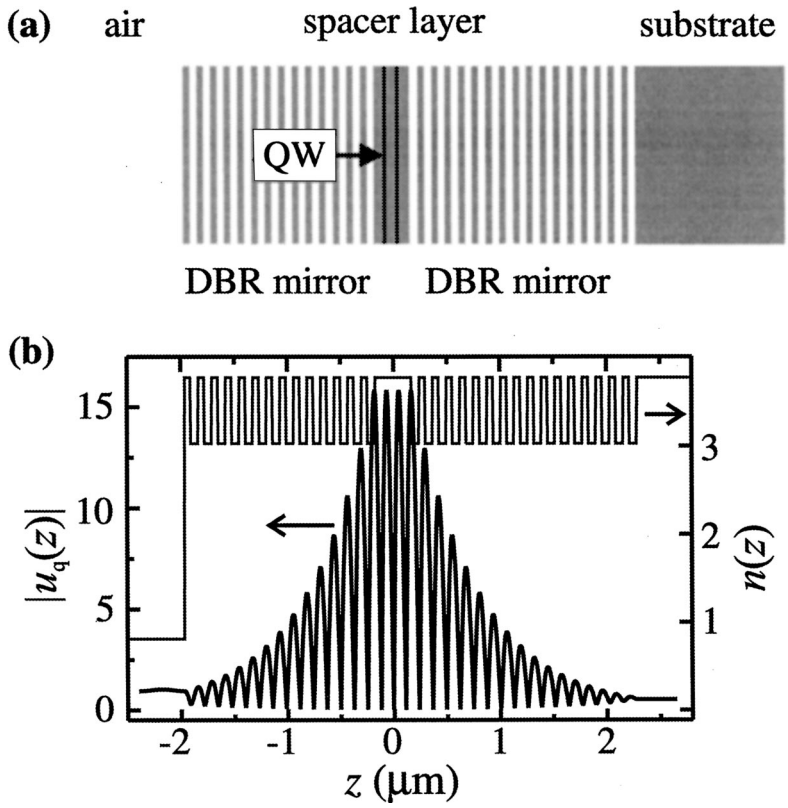

FIG. 1. Schematic of a planar microcavity consisting of two distributed Bragg reflectors (DBR), spacer layers, and a quantum well in the cavity-field antinode.

semiconductor microcavity exceeds the decay rates of both. The resulting normal-mode coupling of exciton and cavity mode was first observed by Weisbuch *et al.*, 1992; see also Burstein and Weisbuch, 1995; Weisbuch *et al.*, 1995; Rarity and Weisbuch, 1996.

For atomic systems it has been known for many years that the spontaneous emission lifetime and angular distribution are not determined by the atom alone but can be altered appreciably by the environment around the atom (Purcell, 1946; Drexhage, 1974; Haroche, 1984, 1992; Meystre, 1992; Berman, 1994; Goldstein and Meystre, 1995). Modifications of the radiation rates and patterns of semiconductor media in the spacer of a semiconductor microcavity have been studied in the perturbative or weak-coupling regime of irreversible emission.[1]

The current studies of normal-mode coupling in semiconductor systems benefit from the gradual improvement of semiconductor Fabry-Pérot interferometers used in the research on optical bistability, nonlinear etalons, and—more recently—VCSEL's. In the 1980s nonlinear Fabry-Pérot etalons were studied extensively as potential optical switches, logic gates, and optically bistable memory devices (Miller *et al.*, 1981; Abraham and Smith, 1982; Gibbs, 1985; Mandel *et al.*, 1987; Warren *et al.*, 1987) based on large band-edge nonlinearities discovered in the late 1970s (Shah *et al.*, 1977; Gibbs *et al.*, 1979; Klingshirn and Haug, 1980; Miller *et al.*, 1981; Chemla *et al.*, 1984; Klingshirn, 1995). One began to understand the physics behind these nonlinearities in the 1980s,[2] but the more sophisticated experimental techniques available today still show that many aspects of such systems need to be analyzed in further detail (Chemla, 1999).

Many of the early experimental studies in quantum well structures were done in samples having linewidths of several meV. The nonlinearities in such inhomogeneously broadened systems were based on the bleaching and/or shift of an exciton or band edge, resulting in a change in transmission and/or shift of the single peak of the cavity. In the late 1980s great progress was made both in the growth of high-finesse monolithic semiconductor microcavities that spawned VCSEL's and in narrower-linewidth quantum wells (Weisbuch and Vinter, 1991; Weisbuch, 1994a, 1994b). At low temperatures a modern-day quantum well sample can have a narrow linewidth of less than one meV. This results in very pronounced index changes in the vicinity of the exciton resonance so that the Fabry-Pérot resonance condition, requiring an integral number of wavelengths

[1]Papers include those of (Yokoyama *et al.*, 1990; Yamamoto, Machida, and Björk, 1991; Nishioka *et al.*, 1993; Yamamoto *et al.*, 1993; Burstein and Weisbuch, 1995; Tanaka *et al.*, 1995; Yamanishi, 1995).

[2]See, for example, Haug and Schmitt-Rink, 1984; Bányai and Koch, 1986; Schmitt-Rink and Chemla, 1986; Lee *et al.*, 1986; Koch, Peyghambarian, and Gibbs, 1988; Zimmermann, 1988; Schäfer, 1988; Koch, Peyghambarian, and Lindberg, 1988; Schmitt-Rink *et al.*, 1989; Haug and Koch, 1994.

between the two mirrors, can be satisfied at three different frequencies. In the NMC case, the high absorption at line center destroys the transmission at the central-frequency Fabry-Pérot solution. That leaves the two sideband solutions giving the characteristic NMC two-peaked transmission spectrum first observed by Weisbuch *et al.* (1992; Weisbuch and Rarity, 1996).

Generalizing the well known concept of exciton polaritons in bulk semiconductors (Hopfield, 1958; Hopfield and Thomas, 1965; Agranovich and Dubovskii, 1966), the linear exciton-photon coupling in microcavities was discussed by Weisbuch *et al.* (1992) and Houdré, Weisbuch, *et al.* (1994) in terms of cavity polaritons. Andreani (1995a) gives an excellent review of excitons, polaritons, and radiative lifetimes in bulk and low-dimensional semiconductor structures. Andreani *et al.* (1994), Andreani and Panzarini (1995), and Savona *et al.* (1995) extend the theory to cavity polaritons.

II. OSCILLATOR MODEL OF NORMAL-MODE COUPLING

In this section the basic ideas of semiconductor NMC are introduced for the example of an ensemble of oscillators in a planar Fabry-Pérot interferometer with metal mirrors (Zhu *et al.*, 1990; Ell *et al.*, 1999). We use this simple system to discuss the concepts and to provide the background for the results presented in the following sections. The equations for the simple oscillator model are evaluated for conditions and parameter values that are typical for a number of recent experiments in semiconductors.

Even though for many configurations the oscillator model would allow us to obtain the linear optical properties in a simple way, this is often not the case for experiments on semiconductors, where sample characteristics and the unavailability of perfect structures can make it necessary to use indirect methods of experimental observation, which are therefore also discussed for the model system. In the simple analysis presented in this section we characterize light-matter interaction via absorption and refractive index. This general concept will have to be modified later when we deal with a set of quantum wells in a microcavity. For such a spatially inhomogeneous situation we need an explicit solution of Maxwell's equations (see Sec. III). Nevertheless, many aspects of microcavity physics can be understood on the basis of the simple oscillator model discussed here.

The linear susceptibility of a system of Lorentz oscillators can be found by solving the optical Bloch equations in steady state [see, for example, Haug and Koch (1994); Loudon (1973)]. The result can be written as

$$\chi_{res}=\frac{G}{(\hbar\omega-\hbar\omega_A)+i\gamma}, \tag{1}$$

where ω and ω_A are the radial frequencies of electromagnetic field and the oscillator resonance, G is proportional to the oscillator strength depending on the transition dipole moment and the density of oscillators, and γ is the homogeneous oscillator HWHM linewidth.

For wave propagation in a spatially homogeneous medium, Maxwell's equations reduce to the traveling-wave equation

$$\Delta\mathbf{E}(\mathbf{r},\omega)+\frac{\omega^2}{c_0^2}\varepsilon(\omega)\mathbf{E}(\mathbf{r},\omega)=0, \tag{2}$$

where c_0 is the vacuum speed of light. The dielectric function

$$\varepsilon(\omega)=\varepsilon_B+\frac{\chi_{res}(\omega)}{\varepsilon_0} \tag{3}$$

contains a nonresonant background contribution ε_B in addition to the resonant contribution of the dipole oscillators. For plane-wave solutions of Eq. (2),

$$\mathbf{E}(\mathbf{r},\omega)=\mathbf{E}_0(\omega)e^{i\mathcal{K}(\omega)z}, \tag{4}$$

one can introduce a complex wave number $\mathcal{K}(\omega)$, which can be traced back to the dielectric function ε or a complex refractive index $\tilde{n}$ according to

$$\mathcal{K}^2(\omega)=\frac{\omega^2}{c_0^2}\varepsilon(\omega)=\frac{\omega^2}{c_0^2}\tilde{n}^2(\omega). \tag{5}$$

The wave number $\mathrm{Re}\,\mathcal{K}(\omega)$ and the decay constant $\mathrm{Im}\,\mathcal{K}(\omega)$ of the wave propagating in the medium are then $n(\omega)q(\omega)$ and $\kappa(\omega)$, where

$$n(\omega)=\mathrm{Re}\,\tilde{n}(\omega),$$

$$\kappa(\omega)=\frac{\omega}{c_0}\mathrm{Im}\,\tilde{n}(\omega), \tag{6}$$

and $q(\omega)=\omega/c_0=2\pi/\lambda_0$. Hence linear wave propagation in a homogeneous three-dimensional medium can be described in terms of the renormalized refractive index $n(\omega)$ and the intensity absorption coefficient $\alpha(\omega)=2\kappa(\omega)$.

If one considers a situation in which the medium fills the space between two ideal metal mirrors having intensity reflectivity R_M, transmission T_M, and no losses ($R_M+T_M=1$), the boundary conditions for the right and left traveling waves at the two mirrors result in the Fabry-Pérot formula for transmission and reflection (Born and Wolf, 1980):

$$T(\omega)=\frac{T_M^2e^{-\alpha(\omega)L}}{|1-R_Me^{i\phi(\omega,L)-\alpha(\omega)L}|^2},$$

$$R(\omega)=R_M\frac{|1-e^{i\phi(\omega,L)}|^2}{|1-R_Me^{i\phi(\omega,L)-\alpha(\omega)L}|^2}, \tag{7}$$

where $\alpha(\omega)L$ describes light absorption and $\phi(\omega,L)=2n(\omega)q(\omega)L$ is the phase shift caused by one optical round trip of the light between mirrors separated by a distance L. For an empty cavity, the reflection becomes zero and transmission unity (resonance) when the phase shift is an integral multiple of 2π.

To determine the basic properties of the Fabry-Pérot mirrors, we first consider the empty-cavity case. Then $n(\omega)$ and $\alpha(\omega)$ are described by the constant background index of refraction n_B and absorption α_B, respectively. For a small deviation from the cavity reso-

nance, $q=m_R\pi/(n_BL)+\Delta q$ with $m_R=1,2,\ldots,$ the transmission can be expressed using the expansion $e^{i\phi(\omega,L)}=1+i2n_BL\Delta q$,

$$T(\omega)=\frac{T_M^2e^{-\alpha_BL}}{|(1-R')-i2n_BLR'\Delta q|^2}, \tag{8}$$

with the notation $R'=R_Me^{-\alpha_BL}$. Then the Fabry-Pérot transmission has a Lorentzian form, $T\propto|\Delta E-i\delta_c|^{-2}$ with the energetic HWHM

$$\delta_c=\frac{\hbar c_0}{2n_BL}\frac{1-R'}{\sqrt{R'}}. \tag{9}$$

This result illustrates that both transmission through the mirrors and background absorption are loss mechanisms for the light, resulting in a decay rate proportional to $T_M+\alpha_BL$ when both are small.

For later reference we define linear dispersion theory as the computation of a structure's transmission, reflection, and absorption using Maxwell's equation with the input of the actual linear susceptibility of the detailed structure (Andreani, 1995a, Andreani *et al.*, 1994). For the case of a microcavity with Bragg mirrors, Maxwell's wave equation can be solved conveniently using transfer-matrix techniques, with the medium susceptibility of each layer as an input (Yariv and Yeh, 1983; MacLeod, 1986; Andreani, 1994; Coldren and Corzine, 1995; Pau, Björk, Jacobson, Cao, and Yamamoto, 1995a). Linear dispersion theory can be based on a theoretical nonlocal susceptibility (Andreani and Bassani, 1990; Andreani, 1994; Andreani, 1995a) that emerges from the microscopic physics; see Sec. III. This approach is referred to as "nonlocal semiclassical theory" by Andreani (1995a; see also Andreani *et al.*, 1994; Savona *et al.*, 1995). Or it can be based on an experimentally measured (or from measurements reconstructed) linear susceptibility averaged over a quantum well. This corresponds to the semiclassical "local linear dispersion model" in the nomenclature of Savona *et al.* (1995).

The correct susceptibility is essential to an understanding of the NMC system response. Consequently much theoretical effort is focused on the microscopic origin of the susceptibility, and experimental attempts to fit the NMC spectra involve careful reconstructions of the susceptibility from measurements of the optical spectra. In this section the spacer between the cavity mirrors is assumed to be filled with Lorentz oscillators described by the model susceptibility of Eq. (1); and for planar metal mirrors the transfer-matrix approach reduces to the Fabry-Pérot formula (Zhu *et al.*, 1990). This is called the semiclassical "atomic model" by Savona *et al.* (1995); it was first applied to semiconductor normal-mode coupling by Weisbuch *et al.* (1992); see also Ell *et al.* (1999).

The empty-cavity Fabry-Pérot formula for the representative values $R_M=0.9989$, $\alpha_B=1.5\times10^{-6}\,\mathrm{nm}^{-1}$, $n_B=3.616$, $L=230$ nm, and $\alpha_BL=0.000\,35$ gives a single transmission peak with HWHM linewidth of 0.175 meV $=0.097$ nm, typical of semiconductor microcavities. These values are used in all Fabry-Pérot figures in Sec. II. The Lorentzian oscillator model absorption has an energy HWHM linewidth of $\gamma=0.25$ meV and a peak absorption coefficient $\alpha_0=0.75\,\mu\mathrm{m}^{-1}$. When the Lorentzian susceptibility is used in Eq. (7), Fig. 2 results, showing two peaks in transmission, two dips in reflection, and two peaks in absorption $A=1-R-T$. These two peaks and two dips are the signatures of normal-mode coupling. The two peaks are approximately Lorentzian in shape and occur at the frequencies $\Delta\equiv\hbar(\omega-\omega_A)=\pm\Omega_0/2$ (Agarwal, 1984; Haroche, 1984; Zhu *et al.*, 1990; Kimble, 1994), where

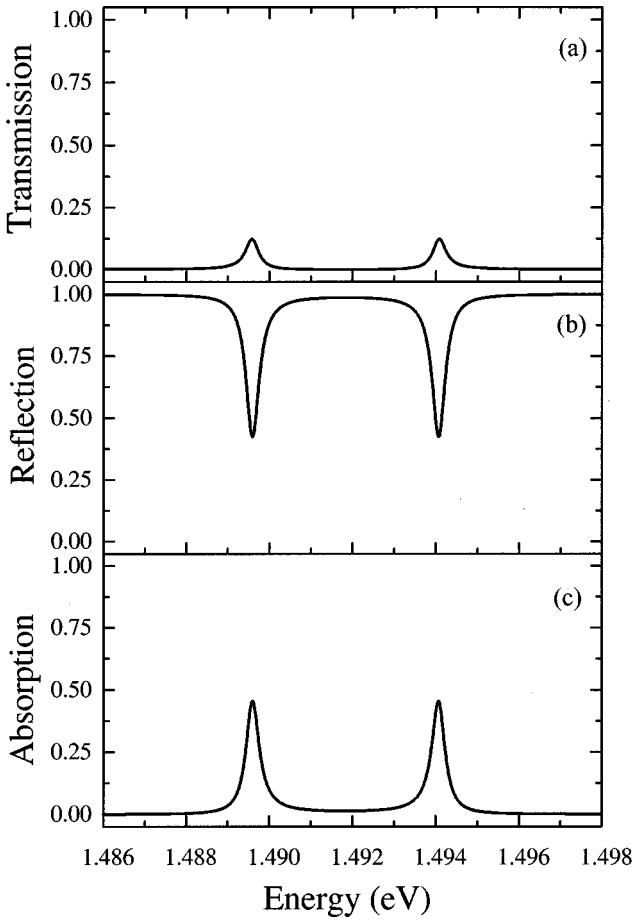

FIG. 2. Spectra of a Fabry-Pérot cavity containing Lorentz oscillators: (a) transmission; (b) reflection; (c) absorption.

$$\Omega_0=\sqrt{2\varepsilon_0\hbar\omega_AG/n_B^2-(\gamma-\delta_c)^2}. \tag{10}$$

Here $G=(n_Bc_0\alpha_0\gamma)/(\varepsilon_0\omega_A)$ relates G to the peak absorption coefficient α_0. Since the oscillator strength is proportional to the density of the oscillators, the NMC splitting depends on the square root of the number of oscillators and inversely on the square root of the cavity length. The HWHM width of each of the two peaks is $(\gamma+\delta_c)/2$, so that normal-mode coupling is observed only if the splitting exceeds each of the linewidths. When $\Omega_0\gg\gamma,\delta_c$, the splittings seen in R, T, and A are almost the same. But it is possible to choose other parameters for which they differ greatly; for $R_M=0.90$,

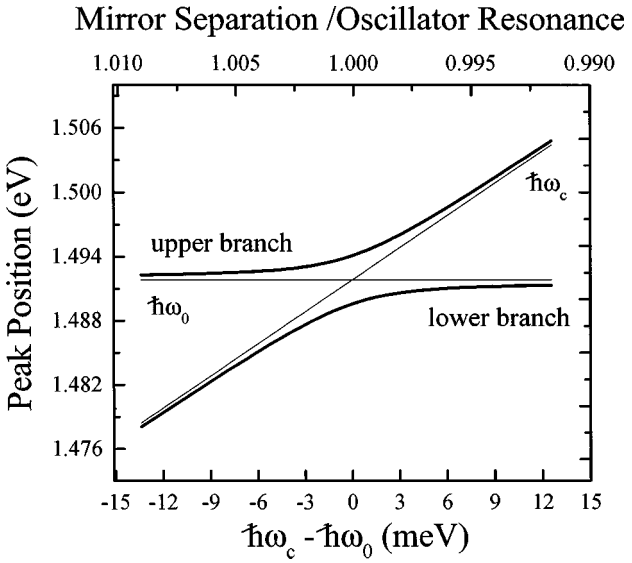

FIG. 3. NMC anticrossing curve vs oscillator-cavity detuning: heavy solid lines, transmission peak positions; thin solid lines, uncoupled oscillator and cavity positions.

there is a splitting in R and T, but not in A (Houdré *et al.*, 1993; Savona *et al.*, 1995).

In Fig. 3 the energies of the peaks in T are plotted as a function of detuning between oscillator and cavity resonance. The result is the characteristic anticrossing curve typical of any two coupled oscillators: $\Omega=(\Omega_0^2+\Delta^2)^{1/2}$. This anticrossing is consistent with the fact that in the weak excitation limit the coupled Maxwell-Bloch equations reduce to the equations for two coupled oscillators.

Further insight into normal-mode coupling can be gained from a graphical solution to the refractive index that influences the Fabry-Pérot resonance condition $\phi(L)=2n(\omega)qL=2\pi m_R$ $(m_R=1,2,\ldots)$ obtained when the cavity resonance was determined in Eq. (8). Using $q=2\pi/\lambda_0$ we get

$$n(\lambda_0)+n_B=\frac{n_B\lambda_0}{\lambda_R}, \tag{11}$$

where λ_R is the value of λ_0 at the cavity peak. For an empty cavity, the left side of Eq. (11) is just a constant n_B and the right side is a straight line, as shown in Fig. 4(a); the single intersection gives the wavelength of the single longitudinal mode of the cavity. Note that since the right-hand side of Eq. (11) is linear in λ_0 (and not strictly so versus ω), the x axis is the wavelength for this one figure. For a many-oscillator cavity the left-hand side of Eq. (11) varies rapidly in the vicinity of the resonance; if the transition is sufficiently narrow and strong, three intersections result, as depicted in Fig. 4(b). The very high absorption at the central solution results in very low transmission there; the other two solutions give the wavelengths of the two NMC peaks. This is analogous to the Casperson (1978) single-mode instability, where two side modes build up when the lasing mode burns a narrow hole in an inhomogeneously broadened gain spectrum. For arbitrary absorption lineshapes, one

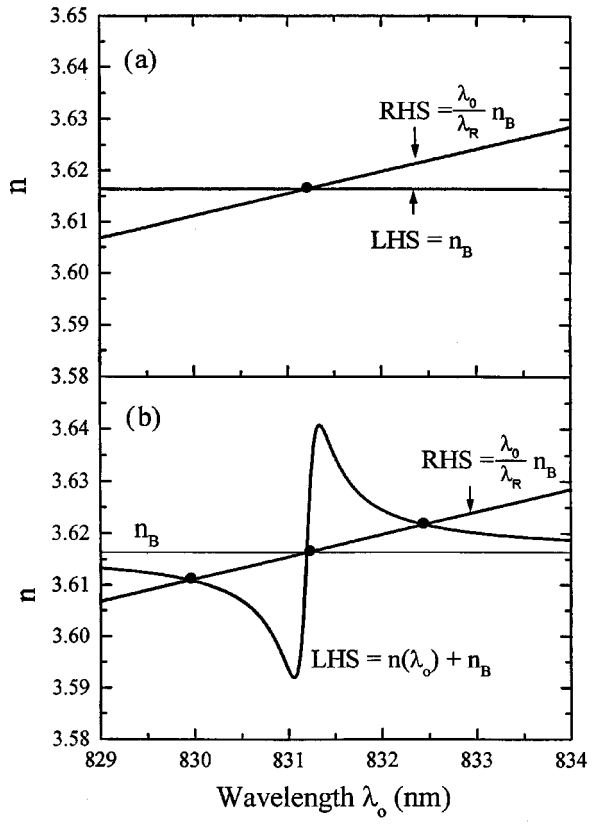

FIG. 4. Graphic solution for the peak positions of a Fabry-Pérot resonator for (a) a constant refractive index n_B and (b) a Lorentz oscillator index $n(\lambda)$.

can use Kramers-Kronig relations to obtain $n(\lambda_0)$ and use this graphical method to find the NMC peak positions as a function of detuning determined by L.

In Fig. 3 we have plotted the anticrossing curve for normal incidence as was done by Weisbuch *et al.* (1992) in the first observation of normal-mode coupling. The Fabry-Pérot analysis can be extended to light propagation at angle θ with respect to the normal of the mirrors by replacing L by $L/\cos\theta$ in $T(\omega)$, $R(\omega)$, and R' and by $L\cos\theta$ in $\phi(\omega,L)$. The dashed curve in Fig. 5(a) shows an empty-cavity dispersion curve, i.e., $\hbar\omega_P(\theta)$ from the Fabry-Pérot formula. The uncoupled oscillator resonance is also shown as the dotted straight line independent of θ. When the cavity-oscillator interaction is turned on by placing the oscillators inside the cavity, the NMC splitting at each θ can now be computed from the Fabry-Pérot formula to obtain the cavity polariton dispersion curve; see solid curves in Fig. 5(a). If the cavity peak at $\theta=0$ is at slightly lower energy than the oscillator resonance, then the minimum splitting occurs for finite θ, as illustrated in Fig. 5(b). Since the Fabry-Pérot dispersion is well known, one can deduce the cavity polariton dispersion curve from the $\theta=0$ anticrossing curve. However, for NMC splittings approaching the linewidths, Fabry-Pérot plots of R, T, and A extrema can differ appreciably (Savona *et al.*, 1995).

The upper (u) and lower (l) NMC peaks have a width (HWHM) of

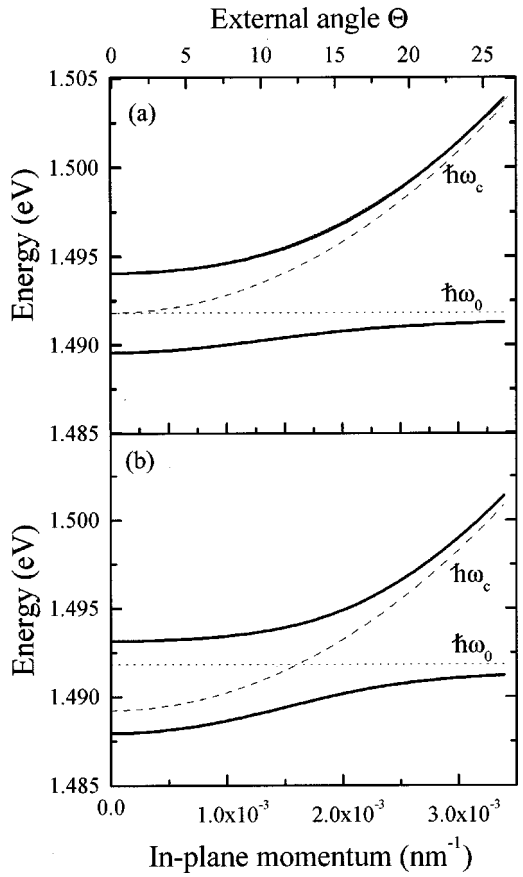

FIG. 5. Cavity-polariton dispersion curve (heavy solid lines) and oscillator and cavity dispersions for zero detuning, i.e., (a) $\hbar\omega_o=\hbar\omega_c(\Theta=0)$ and (b) $\hbar\omega_o>\hbar\omega_c(\Theta=0)$; dotted line, oscillator dispersion; dashed lines, cavity dispersions.

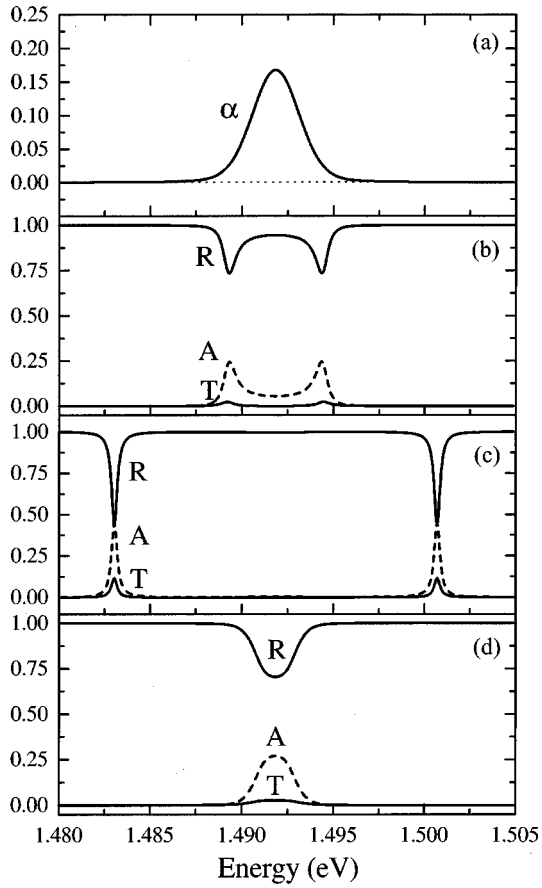

FIG. 6. Symmetrically inhomogeneously broadened oscillator: (a) absorption coefficient; (b)–(d) Corresponding $\Theta=0$ NMC transmission (T, solid lines), reflection (R, solid lines), and absorption (A, dashed lines) spectra for (b) splittings of 5 meV; (c) splittings of 17.6 meV; (d) splittings of 2 meV.

$$\delta_u=\delta_l=(\gamma+\delta_c)/2 \tag{12}$$

for zero detuning. Thus the two linewidths are equal to the average of the uncoupled oscillator and cavity widths. However, this is not a general result, since it depends upon the particular line shapes of the susceptibility and cavity. Note that linear dispersion theory using a measured absorption profile does not require an understanding of the nature of the broadening giving rise to the measured line shape. However, if the total linewidth γ_{ex} is much broader than the homogeneous linewidth γ, then the on-resonance NMC linewidth can be much less than $(\delta_c+\gamma_{ex})/2$ (Houdré *et al.*, 1996); in fact, for $\Omega_0\gg\gamma_{ex}$, it approaches $(\delta_c+\gamma)/2$. This is illustrated in Fig. 6, in which a total HWHM linewidth of $\gamma_{ex}=1.51$ meV is obtained by a Gaussian distribution of energies for oscillators having a homogeneous linewidth of $\gamma=0.25$ meV. For $\Omega_0=5$ meV, $\delta_u=\delta_l=0.46$ meV is clearly less than $(\delta_c+\gamma_{ex})/2=0.82$ meV. For $\Omega_0=17.6$ meV, $\delta_u=\delta_l$ approaches $(\delta_c+\gamma)/2$. The NMC peaks are so far removed from the absorption peak that the index in the vicinity of each peak, which determines the linewidths, is almost the same as if the line were not inhomogeneously broadened. For $\Omega_0=2$ meV, Fig. 6(d), the increased ratio of inhomogeneous broadening to normal-mode coupling prevents the appearance of two clear peaks as shown by Pau, Björk, Jacobson, Cao, and Yamamoto (1995a; see also Pau, Björk, Cao, Hanamura, and Yamamoto, 1995).

For real quantum well systems the line shapes of the excitonic resonances at very low densities are still being investigated extensively. Generally the $1s$ exciton line shape is asymmetric, falling off faster on the low-energy side. As a result, equalizing the transmission peaks requires a positive detuning, such that $\alpha(\omega_u)=\alpha(\omega_l)$. The transmission peaks and reflection dips depend upon the local absorptions at the two peaks, which may not be related by a simple formula to the peak absorption and linewidth as they are for a Lorentzian line shape. This can be illustrated using two inhomogeneously broadened oscillator resonances as shown in Fig. 7. This case is close to that discussed at the beginning of Sec. V.C, where it is also mentioned that δ_l can be much less than $(\delta_c+\gamma_{ex})/2$. Note that part of the reason why δ_l is less than δ_u is that at energies above ω_l, α increases very rapidly, sending T to zero and resulting in a very asymmetric T around ω_l with narrower δ_l. This illustrates that δ_u and δ_l not only are influenced by R' (if R_M and α change slowly around ω_u and ω_l) but can be changed drastically by rapid changes in α and/or n in the vicinity of ω_u and ω_l.

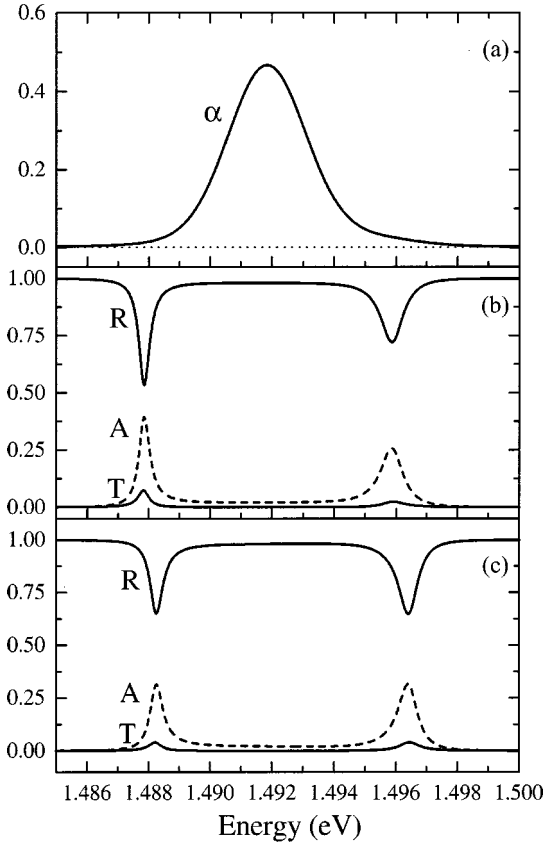

FIG. 7. Asymmetrically, inhomogeneously broadened oscillator system: (a) Absorption coefficient: (b) and (c) Corresponding $\Theta=0$ NMC transmission (T, solid lines), reflection (R, solid lines), and absorption (A, dashed lines) spectra at a detuning of (b) 0 and (c) 1.02 meV.

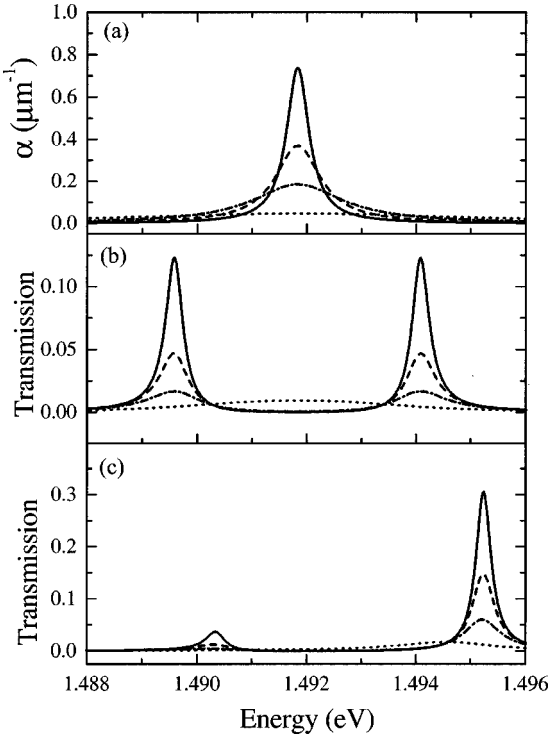

FIG. 8. Effect of homogeneous broadening on NMC transmission for large splitting-to-linewidth ratio: (a) Oscillator absorption coefficient for various HWHM homogeneous broadenings: solid lines, $\gamma=0.25$ meV; dashed lines, 0.5 meV, dashed-dotted lines, 1.0 meV, and dotted lines, 4.0 meV. Corresponding $\Theta=0$ NMC transmission spectra for the case $\Omega \gg \gamma_{ex}, \delta_c$: (b) zero detuning and (c) $\hbar\omega_c > \hbar\omega_o$.

It will be shown in Sec. III.B that, as an increasing incoherent equilibrium carrier density is generated in the quantum wells, the exciton saturation leads to broadened absorption with negligible change in oscillator strength. This behavior can be mimicked by our oscillator susceptibility, assuming broadening of the form $\gamma=\gamma_0+\gamma_P C_{ex}$ where C_{ex} is the external control parameter (carrier density in the exciton system). Figure 8 illustrates linear dispersion theory (Fabry-Pérot formula with broadened γ in α and n) for the case of line broadening with no change in oscillator strength. Note that the NMC transmission goes to zero with little change in splitting. The line broadening increases the absorption at the energies of the two NMC peaks, thereby causing the transmissions to decrease. But since the oscillator strength is constant, there is little change in the NMC splitting. As we shall see later, this behavior illustrates very well the carrier density dependence of normal-mode coupling for a microcavity with a large splitting-to-linewidth ratio. The behavior is quite different when Ω is not much larger than $2\gamma_0$, as shown in Fig. 9. Then the difference term in Eq. (10) for Ω becomes large, causing the NMC splitting to decrease.

If the system inside the NMC microcavity has considerable inhomogeneous broadening, the effects of density-dependent broadening may be masked. At sufficiently high carrier density the oscillator strength will decrease. This is mimicked here by plotting in Fig. 10 the NMC transmission as a function of α_0 for fixed γ. As expected, the splitting Ω_0 decreases proportional to $\sqrt{\alpha_0}$.

Inside a Fabry-Pérot cavity the forward and backward traveling waves interfere to produce a standing wave whose amplitude is $\mathcal{E}$, and spatial distribution can be described by a field mode function $E(z)$. Then αL and nL in the Fabry-Pérot formulae must be replaced by $\int_0^L \alpha(z)E(z,\omega)dz$ and $\int_0^L n(z)E(z,\omega)dz$. In a semiconductor system one typically uses thin quantum well layers as a medium whose thickness is typically 5–20 nm, i.e., much thinner than the distance $\lambda_0/2n \approx 116$ nm between field antinodes, as shown in Fig. 1. This ability to position quantum wells enhances interference effects (radiative coupling), leading to enhanced (superradiant) or suppressed (subradiant) emission.

To conclude this section, we should point out that what we have presented so far is an attempt to separate cavity physics from the behavior of the medium. In the linear regime this separation is usually well justified. However, in the general nonlinear situation one needs not only a consistent theory for interacting electron-hole pairs but also a self-consistent treatment of the properties of the medium and the light. Such a theory will be outlined in the remainder of this paper.

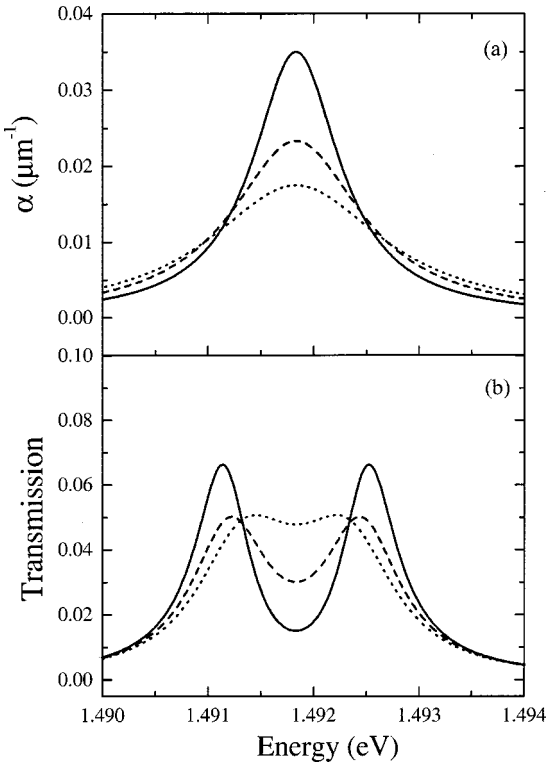

FIG. 9. Effect of homogeneous broadening on transmission for barely resolved normal-mode coupling: (a) Oscillator absorption coefficient for a constant oscillator strength and HWHM homogeneous broadenings: solid lines, $\gamma=0.5$ meV; dashed lines, 0.75 meV; dotted lines, 1.0 meV. (b) Corresponding $\Theta=0$ NMC transmission spectra at zero detuning for $\Omega\approx\gamma_{ex}$.

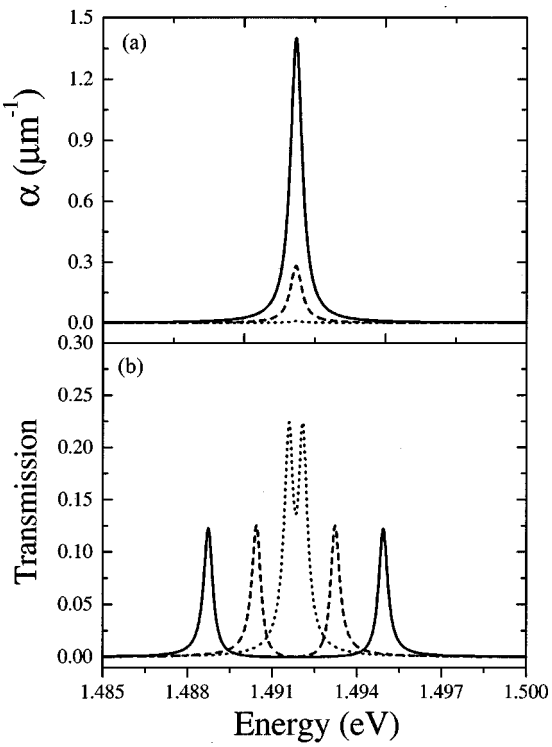

FIG. 10. Dependence of NMC transmission on oscillator strength: (a) Oscillator absorption coefficient for a constant HWHM broadening of $\gamma=0.25$ meV and various oscillator strengths: solid lines, $\alpha_0=1.40\,\mu\text{m}^{-1}$; dashed lines, $0.28\,\mu\text{m}^{-1}$; dotted lines, $0.0084\,\mu\text{m}^{-1}$. (b) Corresponding $\Theta=0$ NMC transmission spectra.

III. LINEAR AND NONLINEAR LIGHT PROPAGATION IN QUANTUM WELLS AND MICROCAVITIES

A. Light propagation in layered microstructures

The semiclassical description of light propagation in quantum wells is an interesting topic on its own. Quantum well polaritons and radiatively coupled multiple quantum wells have been intensively studied recently. After the prediction of radiative broadening in semiconductor nanostructures without translational symmetry (Agranovich and Dubovskii, 1966; Orrit *et al.*, 1982; Hanamura, 1988; Andreani *et al.*, 1991; Citrin, 1993) and the experimental observation of radiative broadening (Devaud *et al.*, 1991), radiatively coupled quantum wells were theoretically studied.[3] Few attempts were made to investigate the nonlinear propagation of ultrashort, intense pulses in quantum wells (Manzke and Henneberger, 1988; Kim *et al.*, 1993) or to study the influence of light propagation or radiative coupling effects on four-wave mixing and pump-probe signals (Rappen *et al.*, 1993; Hübner *et al.*, 1996; Weber *et al.*, 1996; Haas *et al.*, 1997).

Propagation effects in quantum wells are part of coherent microcavity physics in a nonperturbative regime. In several recent publications (Citrin, 1994b; Jorda, 1994; Savona *et al.*, 1995) the theoretical description of quantum well polaritons in semiconductor microcavities has been based on a linear dispersion theory of an exciton Hamiltonian. These approaches have been successfully applied for a linear treatment of the light-matter interaction, i.e., to the regime of weak-light-field reflection, transmission, and absorption experiments. However, the extension of these approaches to the nonlinear regime is not straightforward. The linear dispersion theory is naturally based on optical susceptibilities that are independent of the exciting field(s). On the other hand, a first-principles quantum-mechanical treatment of the semiconductor leads to a Hamiltonian for electrons and holes interacting via a Coulomb interaction. To simplify the description of bound states in the system, one can introduce exciton operators. Using these operators, it is possible to construct a so-called exciton Hamiltonian which describes the linear optical properties correctly (Haug and Schmitt-Rink, 1984); for a review see Haug and Koch (1994). However, the excitation of free carriers, which often cannot be avoided, e.g., in short-pulse experiments, and the resulting influence of free-carrier screening and scattering can not be included since such a Hamiltonian contains only electron-hole pair processes. Even if one considers only exciton-

[3]See, for example, Ivchenko, 1991; Andreani, 1994; Citrin, 1994a; Ivchenko *et al.*, 1994a, 1994b; Andreani, 1995a, 1995b; Andreani and Panzarini, 1995; Stroucken *et al.*, 1996.

exciton interactions, different expansions are used in the low-density and high-density regimes, with no solution in between (Steyn-Ross and Gardiner, 1983).

The aim of our review is to discuss nonlinear effects in semiconductor microcavities that exhibit normal-mode coupling. In Sec. III.A, we focus on effects that can be described on the level of a semiclassical light-matter interaction. We start with a general treatment of the light propagation that is valid under linear as well as nonlinear excitation conditions. Using macroscopic Maxwell's equations, we derive in Sec. III.A.1 a wave equation for the light field that contains the full space-time dynamics of the optical field to describe optical coupling between quantum wells, the interplay of the quantum well emission with cavity mirrors, and the reflected and transmitted field components of the entire system.

The weak-field regime is defined through a linear dependence of the induced quantum well polarization on the light field. The theoretical treatment of this case is reviewed in Sec. III.A.2. The quantum well polarization can be determined from a field-independent optical susceptibility and the field at the quantum well's position. Hence we can describe the coupled light-matter system with two independent parts. Calculation of the quantum well's susceptibility involves only the electronic properties, including the Coulomb interaction and quantum confinement. The light propagation problem can be solved in terms of a given quantum well susceptibility and confinement wave functions. For multilayer systems like quantum wells or microcavities, the linear solution of the light propagation problem can be readily formulated using the transfer-matrix technique. The result unifies earlier approaches (Andreani, 1994; Ivchenko *et al.*, 1996) in which the treatment is restricted, for example, to $1s$ excitons; it also allows a direct extension to plasma nonlinearities, discussed below. At the end of Sec. III.A.2 we study linear reflection, transmission, and absorption spectra of quantum wells and the physics of radiative exciton broadening and radiative coupling between quantum wells.

In Sec. II, a simple picture of normal-mode coupling for Lorentz oscillators in a Fabry-Pérot interferometer was developed. Using the results of Sec. III.A, we can generalize this approach to quantum-confined excitons in semiconductor microcavities. Theoretical results for excitonic normal-mode coupling and the corresponding experimental results are reviewed in Sec. III.A.3. Through a comparison of theoretical and experimental results the influences of radiative coupling, broadening, and disorder effects are discussed.

1. Wave equation

Our starting point is Maxwell's equations averaged over macroscopic regions that are large compared to the atomic scale of the semiconductor crystal but small compared to the light wavelength. We consider only intrinsic (undoped) semiconductors without external charges or currents. Then the divergence of $\mathbf{D}=\varepsilon_0\mathbf{E}+\mathbf{P}$ vanishes where ε_0 is the vacuum permeability (using *SI* units) and $\mathbf{P}$ is the induced macroscopic polarization of the semiconductor. Using $\varepsilon_0 \operatorname{div}\mathbf{E}=-\operatorname{div}\mathbf{P}$, we obtain from these macroscopic Maxwell's equations the inhomogeneous wave equation

$$\left[\Delta-\frac{1}{c_0^2}\frac{\partial^2}{\partial t^2}\right]\mathbf{E}(\mathbf{r},t)=\mu_0\frac{\partial^2}{\partial t^2}\mathbf{P}(\mathbf{r},t)-\frac{1}{\varepsilon_0}\operatorname{grad}\operatorname{div}\mathbf{P}(\mathbf{r},t). \tag{13}$$

In the following we consider standard (type-*I*) quantum wells in which a thin layer of lower band gap material is epitaxially grown between larger layers of bandgap buffer material to ensure efficient carrier confinement. In a semiconductor microcavity, quantum wells are placed between Bragg mirrors which consist of quarter-wavelength dielectric layers. Quantum well buffer layers and mirror layers are usually nonabsorbing and optically inactive for frequencies close to the quantum well band edge. Then the light field interacts nonreasonantly with the buffer layers and the mirror layers and resonantly with the quantum wells. The nonresonant polarization can be calculated from a background susceptibility using $\mathbf{P}_B(\mathbf{r},t)=\chi_B(\mathbf{r})\mathbf{E}(\mathbf{r},t)$ where the background susceptibility can be traced back to an excitation-independent refractive index $n_B^2(\mathbf{r})=1+\chi_B(\mathbf{r})/\varepsilon_0$. In the simplest approximation, this refractive index is real and frequency independent. For quantum wells the resonant interaction of the states close to the band edge is described by the polarization $\mathbf{P}_{QW}$. Using $\mathbf{P}=\mathbf{P}_{QW}+\mathbf{P}_B$ we obtain from Eq. (13)

$$\left[\Delta-\frac{n_B^2(\mathbf{r})}{c_0^2}\frac{\partial^2}{\partial t^2}\right]\mathbf{E}(\mathbf{r},t)=\mu_0\frac{\partial^2}{\partial t^2}\mathbf{P}_{QW}(\mathbf{r},t)-\frac{1}{\varepsilon_0}\operatorname{grad}\operatorname{div}\mathbf{P}(\mathbf{r},t). \tag{14}$$

The second term on the right side of Eq. (14) describes contributions to the longitudinal part of the field. The remaining wave equation for the transverse optical field can be further simplified for light propagation orthogonal to the layers of quantum wells and Bragg mirrors,

$$\left[\frac{\partial^2}{\partial z^2}-\frac{n_B^2(z)}{c_0^2}\frac{\partial^2}{\partial t^2}\right]\mathbf{E}(z,t)=\mu_0\frac{\partial^2}{\partial t^2}\mathbf{P}_{QW}(z,t), \tag{15}$$

where the right side contains only the transverse part of the polarization. For a heavy-hole exciton of the lowest quantum well subband, the polarization itself is transversal and can be directly used in Eq. (15).

In the remainder of this section we describe linear light propagation in quantum wells and quantum well microcavities. The extension to the nonlinear regime will be given in Secs. III.B and III.C.

2. Linear theory for quantum wells: Radiative broadening and radiative coupling

The quantum well polarization $\mathbf{P}_{QW}(z,t)$, which enters Eq. (15), can be calculated from a microscopic semiconductor theory. Referring the reader to Appendix A

for a general derivation, we summarize here only the ingredients for a linear description of the medium. In the linear regime, it is convenient to introduce a Fourier-transformed polarization,

$$\mathbf{P}_{QW}(z,t)=\int \frac{d\omega}{2\pi}\, e^{-i\omega t}\mathbf{P}_{QW}(z,\omega), \tag{16}$$

and similarly a Fourier-transformed optical field $\mathbf{E}(z,\omega)$. The spatial extension of the polarization $\mathbf{P}_{QW}(z,\omega)$ is restricted to the quantum well layers; the z dependence of $\mathbf{P}_{QW}(z,\omega)$ is determined by the carrier confinement wave functions. Taking for simplicity the same confinement wave functions $\xi(z)$ for electrons and holes of the lowest quantum well subband, we obtain the corresponding polarization,

$$\mathbf{P}_{QW}(z,\omega)=\mathbf{P}_{QW}(\omega)|\xi(z)|^2. \tag{17}$$

The matrix element $\mathbf{P}_{QW}(\omega)$ contains the sum over all possible dipole transitions. In a quantum well Bloch basis with the in-plane carrier momentum $\mathbf{k}$, we use

$$\mathbf{P}_{QW}(\omega)=\frac{1}{S}\sum_{\mathbf{k}} \mathbf{d}_{cv}^{*}P_{\mathbf{k}}(\omega)+\text{c.c.} \tag{18}$$

with the dipole matrix element $\mathbf{d}_{cv}$ and quantum well area S. If the polarization depends only linearly on the light field, the carrier-momentum-dependent transition probability $P_{\mathbf{k}}(\omega)$ obeys the Wannier equation,

$$(\epsilon_{\mathbf{k}}^{eh}-\hbar\omega-i\gamma)P_{\mathbf{k}}(\omega)=\mathbf{d}_{cv}\mathbf{E}_{QW}(\omega)+\frac{1}{S}\sum_{\mathbf{k}'} V_{\mathbf{k}-\mathbf{k}'}P_{\mathbf{k}'}(\omega), \tag{19}$$

which is an inhomogeneous version of the two-particle Schrödinger equation for an exciton's relative motion; for a review see Haug and Koch (1994). The Wannier equation contains the free-carrier energies $\epsilon_{\mathbf{k}}^{eh}$, the polarization dephasing γ, and the quantum well matrix elements of the bare Coulomb potential $V_{\mathbf{k}-\mathbf{k}'}$ (discussed in Appendix A). Entering into the driving term of the Wannier equation is the effective field component which interacts with the quantum well subband,

$$\mathbf{E}_{QW}(\omega)=\int dz\, \mathbf{E}(z,\omega)|\xi(z)|^2. \tag{20}$$

For typical quantum wells, the optical field is practically constant over the extension and $\mathbf{E}_{QW}(\omega)$ is simply the optical field at the quantum well position. The linear polarization resonantly excited by the field $\mathbf{E}(z,\omega)$ follows from Eqs. (17)–(20). The solution of Eqs. (18) and (19) can be expressed through a linear susceptibility $\chi(\omega)$, with

$$\mathbf{P}_{QW}(\omega)=\chi(\omega)\mathbf{E}_{QW}(\omega). \tag{21}$$

In the case of ideal two-dimensional carrier confinement, the analytical result for $\chi(\omega)$ can be given by an Elliot formula which contains a sum over all excitonic bound and continuum states. Optical susceptibilities of such a system of finite-width quantum wells can be calculated numerically using a matrix inversion approach. Both analytical and numerical methods are discussed by Haug and Koch (1994).

With Eqs. (17), (20), and (21) a closed integral equation for the optical field can be obtained from the wave equation (15) in which the properties of the semiconductor quantum wells enter only through the independently calculated susceptibility $\chi(\omega)$ and the confinement wave function $\xi(z)$,

$$\left[\frac{\partial^2}{\partial z^2}+\frac{\omega^2}{c_0^2}\,n_B^2(z)\right]\mathbf{E}(z,\omega) =-\mu_0\omega^2\chi(\omega)|\xi(z)|^2\int dz'\,\mathbf{E}(z')|\xi(z')|^2. \tag{22}$$

The main advantage of this equation is that it can be solved analytically for a single quantum well. Such an approach, introducing the nonlocal integral of the field, has frequently been used to describe multiple quantum wells alone and in a microcavity by formulating the solution of Eq. (22) in terms of a transfer matrix (Andreani, 1994; Savona *et al.*, 1995; Ivchenko *et al.*, 1996; Jahnke, Kira, and Koch, 1997). In this approach the nonlocal linear quantum well response, radiative broadening, and coupling effects are fully included.

For a single quantum well, the wave equation (22) describes the propagation of light through forward- and backward-propagating waves in the buffer and quantum well material at normal incidence. Exact analytical solutions for quantum wells of arbitrary thickness have been discussed in detail by Jahnke, Kira, and Koch (1997). However, for increasing thickness, additional subbands have to be included, where for every subband transition a separate Eq. (19) has to be solved. In the following we consider the typical case of a narrow quantum well in which the well width is small compared to the wavelength of light. Then on the right side of Eq. (22) one can use $|\xi(z)|^2=\delta(z-z_0)$, where z_0 is the quantum well's position. The solution of the resulting wave equation,

$$\left[\frac{\partial^2}{\partial z^2}+\frac{\omega^2}{c_0^2}\,n_B^2(z)\right]\mathbf{E}(z,\omega) =-\mu_0\omega^2\chi(\omega)\mathbf{E}(z_0,\omega)\,\delta(z-z_0), \tag{23}$$

is even simpler. The homogeneous solutions in the buffer layers,

$$\mathbf{E}_L(z,\omega)=L_+e^{iqnz}+L_-e^{-iqnz}, \tag{24}$$

$$\mathbf{E}_R(z,\omega)=R_+e^{iqnz}+R_-e^{-iqnz}, \tag{25}$$

for $z<z_0$ and $z>z_0$, respectively, describe forward- and backward-traveling waves with $q=\omega/c_0$ and the buffer refractive index n. From Eq. (23) we can also deduce boundary conditions at the quantum well position,

$$\mathbf{E}_L(z_0,\omega)=\mathbf{E}_R(z_0,\omega), \tag{26}$$

$$\mathbf{E}_L'(z_0,\omega)+\mathbf{I}=\mathbf{E}_R'(z_0,\omega), \tag{27}$$

where Eq. (26) describes the continuity of the field and Eq. (27) leads to a step in the first derivative of $\mathbf{E}(z,\omega)$

at $z=z_0$ with $\mathbf{I}=-\mu_0\omega^2\chi(\omega)\mathbf{E}(z_0,\omega)$ so that the second derivative contains a δ function. With Eqs. (26) and (27) two of the four coefficients in Eqs. (24) and (25) can be determined. The connection between the coefficients can be formulated as a transfer matrix $\hat{M}_{QW}$,

$$\begin{pmatrix} R_+ \\ R_- \end{pmatrix} = \hat{M}_{QW} \begin{pmatrix} L_+ \\ L_- \end{pmatrix}, \tag{28}$$

which yields the field in the right buffer layer in terms of the field in the left buffer layer. For $\hat{M}_{QW}$ one readily obtains

$$\hat{M}_{QW} = \begin{pmatrix} 1+Y & Ye^{-2iqnz_0} \\ -Ye^{2iqnz_0} & 1-Y \end{pmatrix} \tag{29}$$

with $Y=i(q/2\varepsilon_0 n)\chi(\omega)$. From a given transfer matrix $\hat{M}_{QW}$ the transmission $t=R_+/L_+$ and the reflection $r=L_-/L_+$ for an incident wave from the left side can be directly determined. Solving

$$\begin{pmatrix} t \\ 0 \end{pmatrix} = \hat{M}_{QW} \begin{pmatrix} 1 \\ r \end{pmatrix} \tag{30}$$

for r and t leads to

$$r(\omega) = -\frac{M_{21}}{M_{22}} = \frac{i(q/2\varepsilon_0 n)\chi(\omega)}{1-i(q/2\varepsilon_0 n)\chi(\omega)}\, e^{2iqnz_0}, \tag{31}$$

$$t(\omega) = \frac{M_{11}M_{22}-M_{12}M_{21}}{M_{22}} = \frac{1}{1-i(q/2\varepsilon_0 n)\chi(\omega)}, \tag{32}$$

where M_{ij} are the matrix elements of $\hat{M}_{QW}$. The advantage of the transfer-matrix formulation is that it can be easily extended to multiple quantum wells at arbitrary positions. Since the transfer matrix determines the field coefficients on one side of the quantum well in terms of coefficients on the other side, a transfer matrix for the combined system of several quantum wells follows from successively multiplying the transfer matrices of the individual quantum wells,

$$\hat{M}_{MQW} = \hat{M}^N_{QW} \cdot \hat{M}^{N-1}_{QW} \cdot \cdots \cdot \hat{M}^2_{QW} \cdot \hat{M}^1_{QW}, \tag{33}$$

where $\hat{M}^1_{QW}$ ($\hat{M}^N_{QW}$) is the transfer matrix of the outermost left (right) quantum well. Then from Eq. (30) reflection and transmission spectra of the combined system can be directly determined.

For completeness we should like to note that the solution for quantum wells of thickness L, Eq. (69) in Jahnke, Kira, and Koch (1997), reduces to Eq. (29) in the limit $L\to 0$.

3. Analytical solutions for 1*s* excitons

Restricting the analysis to $1s$ excitons for this subsection only, we obtain from the two-dimensional Elliot formula,

$$\chi_{1s} = -g\frac{|d_{cv}|^2}{\hbar\omega - E_{1s} + i\gamma} = -\frac{2\varepsilon_0 n\Gamma/q}{\hbar\omega - E_{1s} + i\gamma}, \tag{34}$$

where E_{1s} is the $1s$-exciton energy, γ is the nonradiative homogeneous exciton broadening, and a radiative broadening,

$$\Gamma = \frac{q}{2\varepsilon_0 n} g|d_{cv}|^2, \tag{35}$$

has been introduced. The oscillator strength is determined by the dipole coupling matrix element d_{cv} and the $1s$ wave function entering $g=|\phi^{2D}_{1s}(r=0)|^2$. Using χ_{1s}, we can evaluate the transfer matrix for a single quantum well,

$$\hat{M}_{QW} = \frac{1}{\hbar\omega - E_{1s} + i\gamma} \times \begin{pmatrix} [\hbar\omega - E_{1s} + i(\gamma-\Gamma)] & -i\Gamma e^{-2iqnz_0} \\ i\Gamma e^{2iqnz_0} & [\hbar\omega - E_{1s} + i(\gamma+\Gamma)] \end{pmatrix}. \tag{36}$$

With Eqs. (36) we can determine the $1s$-exciton reflection, transmission, and absorption spectra of a single quantum well,

$$R(\omega) = |r(\omega)|^2 = \frac{\Gamma^2}{(\hbar\omega - E_{1s})^2 + (\gamma+\Gamma)^2}, \tag{37}$$

$$T(\omega) = |t(\omega)|^2 = \frac{(\hbar\omega - E_{1s})^2 + \gamma^2}{(\hbar\omega - E_{1s})^2 + (\gamma+\Gamma)^2}, \tag{38}$$

$$A(\omega) = 1 - R(\omega) - T(\omega) = \frac{2\gamma\Gamma}{(\hbar\omega - E_{1s})^2 + (\gamma+\Gamma)^2}. \tag{39}$$

The appearance of the additional radiative broadening Γ in the denominator is a consequence of spatial boundary conditions that have to be satisfied by the solutions of the interacting light-exciton system. Even though in this section the response of semiconductor quantum wells is described with a linear susceptibility, the polarization that follows from Eqs. (17), (20), and (21) fulfills the self-consistency requirement if calculated together with the wave equation (15).

Radiative broadening and its explicit form have been studied by Tassone *et al.* (1992); Andreani (1994); Savona *et al.* (1995); Stroucken *et al.* (1996); and Jahnke, Kira, and Koch (1997). Its physical origin stems from the lack of momentum conservation in the quantum well growth direction. A light field that is resonant with the exciton can propagate in a three-dimensional semiconductor as a polariton mode. The propagation is limited only by intrinsic semiconductor dephasing as well as material imperfections and the boundary of the crystal where polaritons decay into light. For light propagating through a quantum well, only the in-plane momentum has to be conserved. Hence the excited quantum well polarization can decay due to radiation emitted in the forward and backward directions, as pointed out by Agranovich and Dubovskii (1966). This leads to an additional decay channel, which in good samples is the dominant one. For GaAs parameters, we obtain from Eq. (35) a radiative lifetime $T_{rad}=\hbar/\Gamma\approx 13$ ps.

Using the analytical results for quantum well spectra, Eqs. (37)–(39), we can discuss two limiting cases. For small radiative coupling, $\Gamma \ll \gamma$, the quantum well transmission approaches unity while reflection and absorption vanish. On the other hand, for vanishing dephasing γ, only the absorption vanishes. However, if there is inhomogeneous broadening, the true absorption A is nonzero even if $\gamma=0$ (Ivchenko *et al.*, 1994a); this is because the emission of the oscillators distributed over frequency are no longer suppressed via destructive interference at finite detunings.

Multiple quantum wells exhibit interesting optical coupling effects. For two quantum wells analytical results can be obtained by multiplying two transfer matrices [Eq. (36)]. Assuming a distance $\lambda/2$ between the quantum wells (the Bragg condition), we find the reflectivity

$$R_{\lambda/2}=\frac{4\Gamma^2}{(\hbar\omega-E_{1s})^2+(\gamma+2\Gamma)^2}. \tag{40}$$

In comparison to the single quantum well, the radiative broadening is enhanced by a factor of 2 and the reflectivity at the $1s$-exciton resonance is increased by a factor $4[(\gamma+\Gamma)^2/(\gamma+2\Gamma)^2]$ due to in-phase coupling of the quantum well fields. For N quantum wells, 2Γ is replaced by $N\Gamma$ in Eq. (40). For a $\lambda/4$ distance between the quantum wells (anti-Bragg condition), destructive interference reduces the reflectivity. The reflectivity spectrum,

$$R_{\lambda/4}=\frac{2\Gamma^2}{(\hbar\omega-E_{1s}-\Gamma)^2+(\gamma+\Gamma)^2}\times\frac{2\Gamma^2}{(\hbar\omega-E_{1s}+\Gamma)^2+(\gamma+\Gamma)^2}, \tag{41}$$

contains a product of two Lorentzians, each of which is shifted by radiative broadening Γ. Correspondingly, in the limit, $\gamma<\Gamma$, a double-peak structure can be obtained (Stroucken *et al.*, 1996). Signatures of these coupling effects have been observed in four-wave mixing experiments (Hübner *et al.*, 1996).

4. Linear regime normal-mode coupling

a. Linear regime computations

The linear treatment of light propagation in quantum wells and multiple quantum wells can be readily extended to quantum wells in a semiconductor microcavity. The distributed Bragg mirrors consist of quarter-wavelength layers with alternating refractive index. In the ideal case of nonabsorbing mirror layers, we can assume free light propagation within the layers. For adjacent layers, the field is described by forward and backward traveling field components similar to those in Eqs. (24) and (25). The boundary conditions for the optical field require the continuity of $\mathbf{E}(z,\omega)$ and $\partial\mathbf{E}(z,\omega)/\partial z$. As discussed above, for every surface between two mirror layers, the resulting constraint for the coefficients can be cast in the form of a transfer matrix,

$$\hat{M}=\frac{1}{2}\begin{pmatrix}\left(1+\frac{q_0}{q_1}\right)e^{i(q_0-q_1)a} & \left(1-\frac{q_0}{q_1}\right)e^{-i(q_0+q_1)a}\\ \left(1-\frac{q_0}{q_1}\right)e^{i(q_0+q_1)a} & \left(1+\frac{q_0}{q_1}\right)e^{-i(q_0-q_1)a}\end{pmatrix}, \tag{42}$$

where $q_i=(\omega/c_0)n_i$ and n_0 (n_1) is the refractive index of the left (right) layer with a surface at $z=a$. By multiplying the matrices of the dielectric layers, one can obtain a transfer matrix for both mirrors of a microcavity. The successive multiplication of the transfer matrices for the first mirror, the quantum wells, and the second mirror leads to a transfer matrix for the microcavity (Yariv and Yeh, 1983; MacLeod, 1986; Andreani, 1994; Coldren and Corzine, 1995; Pau, Björk, Jacobson, Cao, and Yamamoto, 1995a).

The resulting semiclassical treatment of the light propagation, which incorporates a linear quantum well susceptibility, describes normal-mode coupling in linear reflection, transmission, and absorption spectra (Andreani *et al.*, 1994, 1998; Andreani and Panzarini, 1995; Kavokin and Kaliteevski, 1995; Panzarini and Andreani, 1995b; Lindmark *et al.*, 1996; Tredicucci *et al.*, 1996). This approach has been compared with a quantum theory of the light field together with a description of quantum well excitons with a Bose Hamiltonian (Citrin, 1994b; Jorda, 1994; Savona *et al.*, 1995). In analogy to the semiclassical and quantum theory of polaritons, the results are equivalent. However, such theories are restricted to the weak-field regime, since excitons lose their Bosonic nature for nonlinear excitation. This and the microcavity photoluminescence are further addressed in Sec. IV.

An alternative method for the description of light propagation in semiconductor microcavities is the recursive Green's-function technique. The method is not restricted to layers with constant refractive index and can also treat three-dimensional light propagation in waveguide geometries (Kahen, 1992, 1993). Jahnke and Koch (1995) did a full quantum theory for lasing in VCSEL structures using a nonequilibrium Green's-function approach. Even though it is possible in principle to extend this approach into the excitonic regime, it is technically easier to use equations of motion for the individual photon and system operators. This way one directly obtains the fully quantum-mechanical version of the semiconductor Bloch equations.

In Fig. 11 we show linear normal-mode spectra that are calculated numerically from the susceptibility of 8-nm quantum wells and a microcavity transfer matrix that follows from Eqs. (29), (33), and (42). The exciton binding energy in the quantum well is about $2.4E_B$, where E_B is the three-dimensional binding energy. We consider a cavity with two Bragg mirrors of 99.6% reflectivity. The left mirror (exposed to air) and right mirror (on a GaAs substrate) contain 14 and 16.5 quarter-wave pairs of GaAs $(n=3.61)$ and AlAs $(n=2.95)$, respectively. A $\frac{3}{2}\lambda$ GaAs spacer between the mirrors leads to two central antinodes of the static cavity field. For the solid line in Fig. 11(a), in each of the cavity

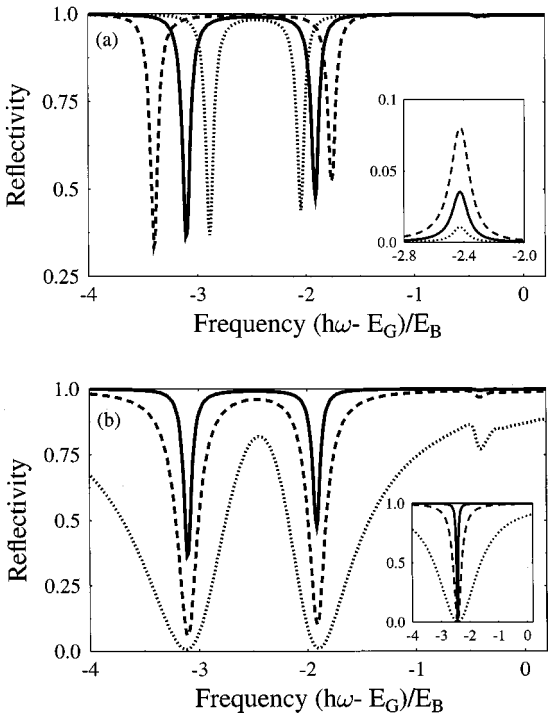

FIG. 11. Computed dependence of NMC reflectivity upon number of quantum wells and mirror pairs: (a) Linear reflectivity spectra for an NMC microcavity with 8-nm quantum wells: dashed line, four quantum wells: solid line, two quantum wells; dotted line, one quantum well. The inset shows the reflectivity spectrum for four quantum wells: dashed line, two pairs at $\lambda/2$ distance; solid line, two wells at $\lambda/2$; dotted line, a single quantum well. (b) Reflectivity spectrum for a microcavity with two quantum wells and 14/16.6 (solid line), 10/12.5 (dashed line), and 6/8.5 (dotted line) quarter-wave pair mirror layers. The inset draws the corresponding reflectivity spectrum of the microcavity without quantum wells.

antinodes a single 8-nm $In_{0.04}Ga_{0.96}As$ quantum well is located. For two quantum wells in every field antinode (dashed line), the larger oscillator strength of the system leads to an increase in normal-mode splitting by a factor $\sqrt{2}$. If only a single quantum well is placed in one of the two cavity antinodes (dotted line), the normal-mode splitting is reduced by a factor $1/\sqrt{2}$. The corresponding reflectivity of the quantum well(s) without microcavity is shown in the inset. In Fig. 11(b) we compare cavities with two quantum wells (one in each of the two cavity antinodes) and a reduced number of mirror layers. For 6 and 8.5 quarter-wave pair layers and a reflectivity of 88.3% and 86.0%, respectively, normal-mode coupling is still possible (dotted line). However, due to broadening of the cavity resonance (shown in the inset) the normal-mode peaks are strongly washed out.

b. Linear regime steady-state experiments

In their seminal paper reporting normal-mode coupling in a semiconductor microcavity, Weisbuch, Nishioka, Ishikawa, and Arakawa (1992) made a remarkable number of contributions: first observation of normal-mode coupling in a semiconductor microcavity (Fig. 12),

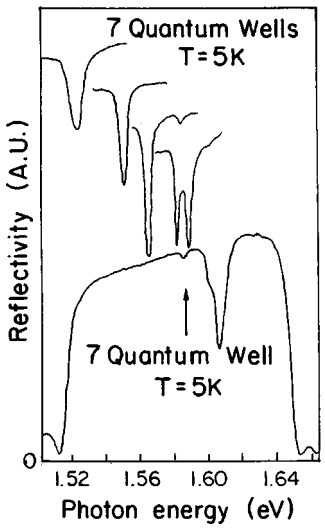

FIG. 12. 5-K reflectivity curves on a seven-quantum well microcavity structure. Various detuning conditions between cavity and quantum well exciton frequencies are obtained by choosing various points on the wafer, typically 0.5 mm apart. Note the line narrowing approaching and at resonance, the resonance mode splitting, and the indication of a light-hole exciton mode splitting around 1.605 eV for the lowest trace. From Weisbuch *et al.*, 1992.

anticrossing curve of dip positions (Fig. 13), narrowing of the cavitylike dip close to resonance, good agreement with Fabry-Pérot formula linear dispersion theory, and detection of normal-mode coupling up to 77 K with the prediction that it should be observable even at room temperature. Their structures had $R=98\%$ left (12 periods) and right (16.5 periods) $GaAs/Al_{0.4}Ga_{0.6}As$ distributed Bragg reflector mirrors with a λ $Al_{0.2}Ga_{0.8}As$ spacer and one or several 7.6-nm GaAs quantum wells grown in the center by metal organic chemical vapor deposi-

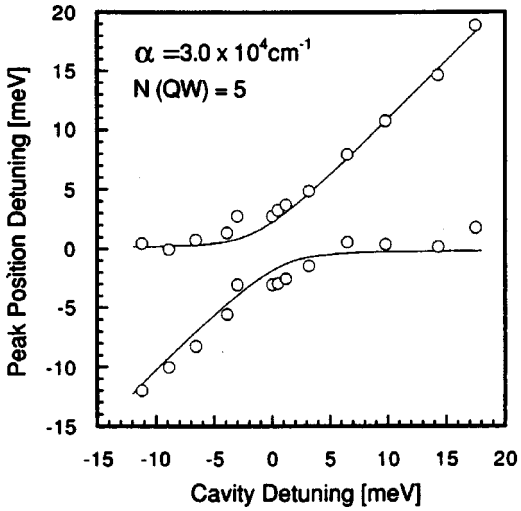

FIG. 13. Reflectivity peak positions as a function of cavity tuning for a five quantum well sample at $T=5$ K. The theoretical fit is obtained through a standard multiple-interfere analysis of the distributed-Bragg-reflector-Fabry-Pérot-quantum well structure. From Weisbuch *et al.*, 1992.

tion. With a single quantum well, normal-mode coupling was not seen. However, with seven quantum wells, two well-resolved reflectivity dips were seen on resonance; see Fig. 12 and compare with Fig. 11. The anticrossing curve, Fig. 13, was mapped out by scanning across the sample.

Note that the cavity peak scans much more rapidly with a percentage change in length than the exciton peak. For the cavity peak, given by $2L=m\lambda$, one finds $d\lambda/\lambda=dL/L$, whereas for the exciton confinement energy, which is proportional to the inverse square of the quantum well thickness w, we obtain $d\lambda/\lambda=2dw/w$, which scans twice as fast. However the exciton peak is determined by the sum of the exciton confinement energy, typically several meV, and the well band-gap energy (about 1.52 eV for GaAs at 4 K), so the exciton peak hardly changes as the cavity peak is tuned through it.

Using the linear dispersion theory approach of Sec. II and modeling the exciton resonance by a two-level dielectric function with Lorentzian HWHM linewidth $\gamma=1$ meV and peak absorption $\alpha_0=3\times10^4$ cm^{-1}, Weisbuch *et al.* (1992) fitted the anticrossing data of Fig. 13. They also observed that the linewidth of the cavitylike dip narrowed as the cavity resonance was tuned toward the exciton resonance. They point out that in atomic physics experiments usually the cavity finesse is very high, so it is the atomlike resonance that narrows. Whichever peak is broader becomes narrower at resonance. Note that already in this first observation, the higher-energy linewidth is broader than the lower-energy; detailed studies show that this is generally the case.

Is there something special about the sample used to see normal-mode coupling, relative to earlier samples used for optical bistability and VCSEL's? Since the observed on-resonance splitting was about $\Omega_0=4$ meV, it is clear that the NMC condition $\Omega_0>\delta_c+\gamma$ does not impose very stringent requirements on either the cavity or the exciton linewidth at low temperatures. In fact, the 98% reflectivity is higher than the 90% often used for bistability and low compared with the >99.9% used for VCSEL's. More than likely normal-mode coupling could have been seen several years sooner if the high-reflectivity Bragg mirrors developed for VCSEL's had been grown with intermediate reflectivity and with reasonably narrow-linewidth exciton absorption. That is, if one had been smart enough to look for it. Of course, the design and growth would have had to be optimized for low temperature, whereas bistability and VCSEL samples were usually designed for 300 K. The very high finesse achieved by Stanley, Houdré, Oesterle, Gailhanou, and Ilegems (1994) is not necessary for seeing normal-mode coupling. The relative ease with which it can now be achieved is illustrated by the rapidity with which the first work was extended. Since the NMC splitting Ω_0 is proportional to the product of the dipole moment times the cavity field at the quantum well position, below we divide the experiments into those that change the dipole moment, those that change the cavity mode functions and their overlap with the excitonic polarization, and those that change the exciton-cavity detuning.

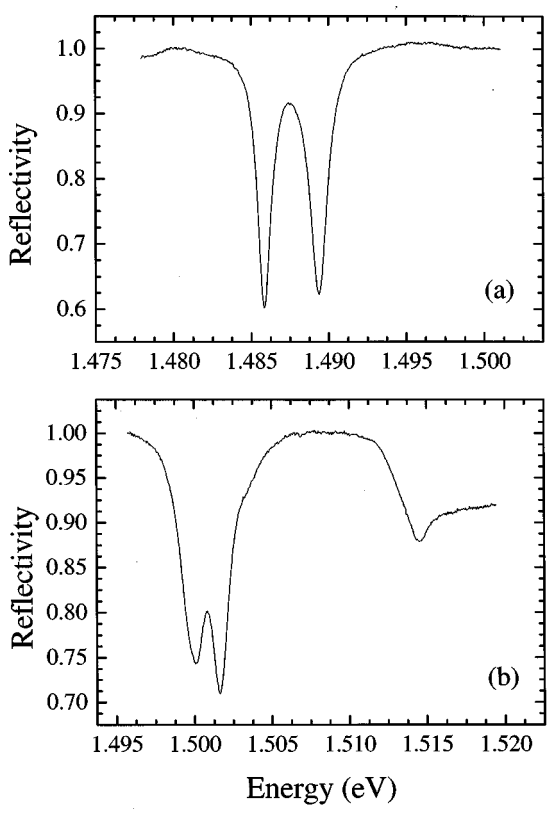

FIG. 14. Normal-mode coupling with a single quantum well in a 1λ cavity (sample NMC28) with 5/12.5 quarter-wave pair mirror layers (97.7%): (a) zero detuning from the heavy-hole transition and (b) close to the light-hole transition. From Nelson, Lindmark, *et al.*, 1996.

(1) Changing the exciton dipole moment. Soon normal-mode coupling was observed using a single 20-nm GaAs quantum well embedded in a λ microcavity [Yamamoto *et al.*, 1993; see Figs. 14(a) and 11(a)] and using two quantum wells in a λ/2 AlAs spacer whose low index prevented guided modes (Abram *et al.*, 1994). Normal-mode coupling of the light hole (Fisher *et al.*, 1995) has also been reported with a single quantum well (Goobar *et al.*, 1996; Lindmark *et al.*, 1996; Nelson, Lindmark, *et al.*, 1996); see Fig. 14(b). Normal-mode coupling with a very high splitting-to-linewidth ratio has been achieved; see Fig. 15. The large oscillator strength of ZnCdSe quantum wells has yielded a very large value, $\Omega_0=17.5$ meV, for normal-mode coupling in II-VI semiconductor microcavities (Kelkar *et al.*, 1995).

For a spacer filled with bulk GaAs, normal-mode coupling was obtained with $\Omega_0=3$ meV, which is almost as large as that for a single well because the greater thickness compensates for the smaller oscillator strength of the three-dimensional exciton (Chen *et al.*, 1993, 1995; Tredicucci, Chen, Pellegrini, and Deparis, 1995; Nelson, Lindmark, *et al.*, 1996). A λ/2 spacer is sufficiently short that the quantization of the center-of-mass motion of the exciton results in levels separated by more than 0.5 meV, which have been resolved in the NMC reflectivity;

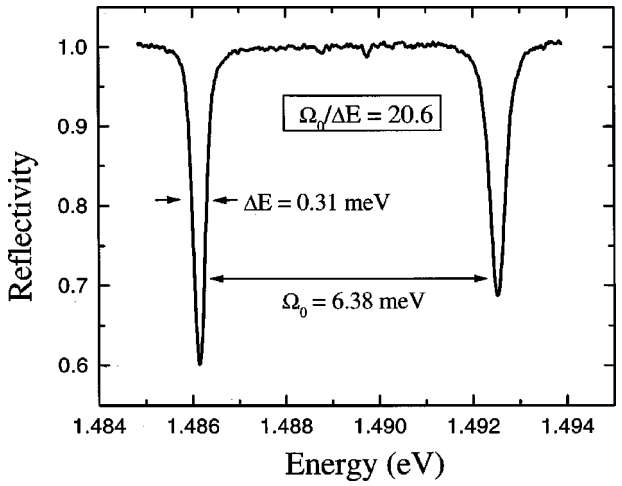

FIG. 15. Normal-mode coupling at zero detuning with ten quantum wells in a $11\lambda/2$ microcavity (sample NMC66) with mirrors designed for 99.94%.

see Fig. 16 (Tredicucci, Chen, Pellegrini, Börger, *et al.*, 1995).

An electric field, through the quantum confined Stark effect, reduces the overlap of the first electron and first heavy-hole states; this reduces d_{cv} and hence Ω_0 by 20% at 38 kV/cm (Fisher *et al.*, 1995; Whittaker *et al.*, 1995). A magnetic field increases the electron-hole overlap thereby increasing the NMC splitting by 40% in 14 T (Tignon *et al.*, 1995; Whittaker *et al.*, 1995; Berger *et al.*, 1996; Fisher *et al.*, 1996; Tanaka *et al.*, 1996). A magnetic field can even break up a continuum into discrete Landau levels, causing a transition from weak to nonperturbative coupling (Tignon *et al.*, 1995).

Systems resembling three coupled oscillators have been studied. For two cavities and one quantum well, the coupling between cavities is controlled by the transmission of their common mirror (Stanley, Houdré, Oesterle, Ilegems, and Weisbuch, 1994). Panzarini and Andreani (1995a, 1995b) predicted three reflectivity dips for a single cavity containing two nonidentical quantum wells with exciton energies close enough to simultaneously couple to the single-cavity mode; this was seen by Lindmark *et al.* (1996). Armitage *et al.* (1998) investigated four coupled oscillators consisting of one quantum well in each of two coupled cavities.

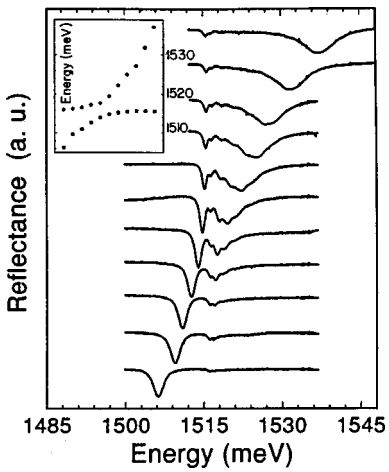

FIG. 16. Reflectance spectra of the $\lambda/2$ cavity; each curve refers to a different cavity thickness, with increasing thickness from top to bottom. The resonance condition ($\lambda_{exc}/2 \approx L_{cav}$) is at about the seventh curve from the top. The inset shows the energy position of the two main peaks for the various cavity thicknesses. From Tredicucci, Chen, Pellegrini, Börger, Sorba, Beltram, and Bassani, 1995.

(2) Changing the overlap of the exciton polarization and cavity mode function. Zhang *et al.* (1994) grew four 6.2-nm quantum wells in the center of a λ spacer (optical-field antinode position) plus two 9.0-nm quantum wells in each of the optical-field node positions. Normal-mode coupling occurred with the cavity tuned to the quantum wells in the antinode but not to those in the node, showing that the exciton-light coupling depends upon the position of the quantum well in the optical standing wave as expressed by Eqs. (22) and (23). However, calculations by Kira, Jahnke, and Koch (1997) show that quantum wells in cavity-node positions can be excited with ultrafast laser pulses propagating through the mirror layers.

Normal-mode coupling at 300 K was barely resolved using conventional DBR's (Houdré *et al.*, 1993; Houdré, Stanley, Oesterle, Ilegems, and Weisbuch, 1994). Slightly better resolution was achieved utilizing native-oxide AlAs/GaAs mirrors to improve the cavity field confinement and shorten the effective length of the cavity (Nelson, Khitrova, *et al.*, 1996; Graham *et al.*, 1997); see Fig. 17.

(3) Changing the exciton-cavity detuning. Often the cavity mode is scanned through the exciton energy by moving the probe spot across the sample as was done in the first experiment by Weisbuch *et al.* (1992). This works well if the sample quality is quite uniform. However, the scan is not linear, making it nontrivial to convert the scan to detuning in absolute energies. Abram *et al.* (1994) and Long *et al.* (1995) recorded photoluminescence using this technique to scan more than 30 meV away from the minimum splitting in both directions, enabling them to map out a beautiful anticrossing curve with very straight excitonlike and photonlike lines far from resonance. Stanley *et al.* (1996) mapped out the anticrossing curve in both photoluminescence and true absorption A; in addition, they showed that photoluminescence out the side is single-peaked when it is double-peaked out the front.

Fisher *et al.* (1995) and Goobar *et al.* (1996) employed temperature tuning, taking advantage of the strong temperature dependence of the exciton energy and weak temperature dependence of the cavity mode. Houdré *et al.* (1993), Fisher *et al.* (1995), and Kelkar *et al.* (1995) showed reduced splitting when the broadening with increased temperature causes γ to approach Ω_0. Such broadening-reduced splitting has been modeled, for example, by Jahnke, Ruopp, Kira, and Koch (1997).

The energy of the cavity mode can also be tuned by changing the angle of incidence of the light. Both Houdré, Weisbuch, Stanley, Oesterle, Pellandini, and Il-

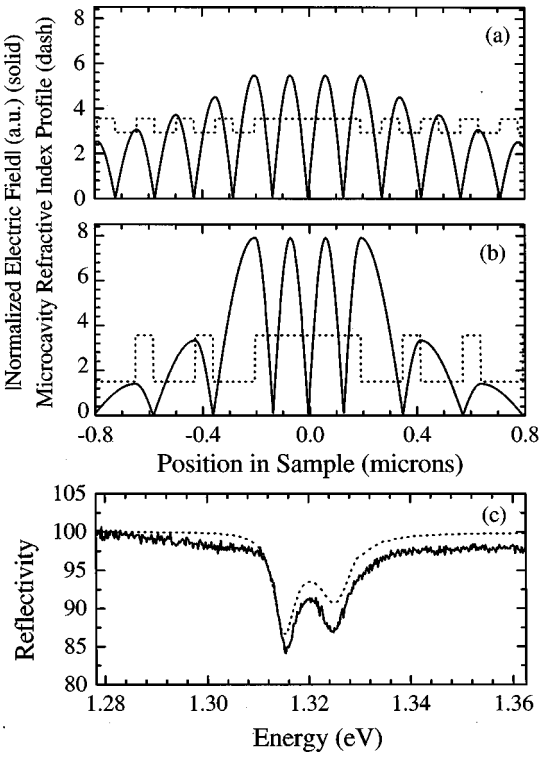

FIG. 17. The absolute value of the intracavity field amplitude and microcavity refractive index profile vs position in the cavity for (a) a $3\lambda/2$ GaAs spacer etalon with 28 left and 33 right mirror layers of GaAs/AlAs (99.5%); (b) a $3\lambda/2$ GaAs spacer etalon utilizing 6 left and 7 right native-oxide AlAs/GaAs mirror layers (99.4%). The origin of the horizontal axis is taken as the cavity center. (c) Measured (solid) and calculated (dashed) NMC reflectivity near zero detuning. From Nelson, Khitrova, *et al.*, 1996.

egems (1994), and Kelkar *et al.* (1995) used angle tuning to map out the cavity polariton in-plane dispersion curves, i.e., the energies of the two coupled modes as a function of $\mathbf{q}_\parallel$, which is the in-plane momentum for light propagating in the $\mathbf{q}=(\mathbf{q}_\parallel, q_z)$ direction; see Fig. 18 and compare with Fig. 5 of Sec. II and Savona *et al.* (1996). Since the values of $|\mathbf{q}_\parallel|$ are very small compared with those needed to see curvature in the quantum well in-plane dispersion curve, the cavity polariton dispersion is dominated by the photon dispersion, which appears curved when only the $|\mathbf{q}_\parallel|$ component is taken. The internal angle ϕ_i is related to the external angle of observation ϕ_e by $n \sin\phi_i = \sin\phi_e$ and $|\mathbf{q}|\sin\phi_i = |\mathbf{q}_\parallel|$. For large splitting-to-linewidth ratio, the in-plane dispersion curves are the positions of the two transmission peaks as a function of the tilt angle given by the Fabry-Pérot formula.

Combining tilting with an electric field, Kadoya *et al.* (1996) achieved the minimum splitting at different oscillator strengths.

B. Steady-state incoherent saturation of quantum well excitons and excitonic normal-mode coupling

Nonlinear exciton saturation is an intricate process that has been intensively studied in the past. The presence of unbound carriers, e.g., generated through an additional optical pulse resonant with the interband continuum, can efficiently bleach the exciton resonances. Phase-space filling and screening cause a reduction in the exciton oscillator strength and binding energy and lead to band-gap renormalization (Haug and Schmitt-Rink, 1984; Bányai and Koch, 1986; Schmitt-Rink *et al.*,

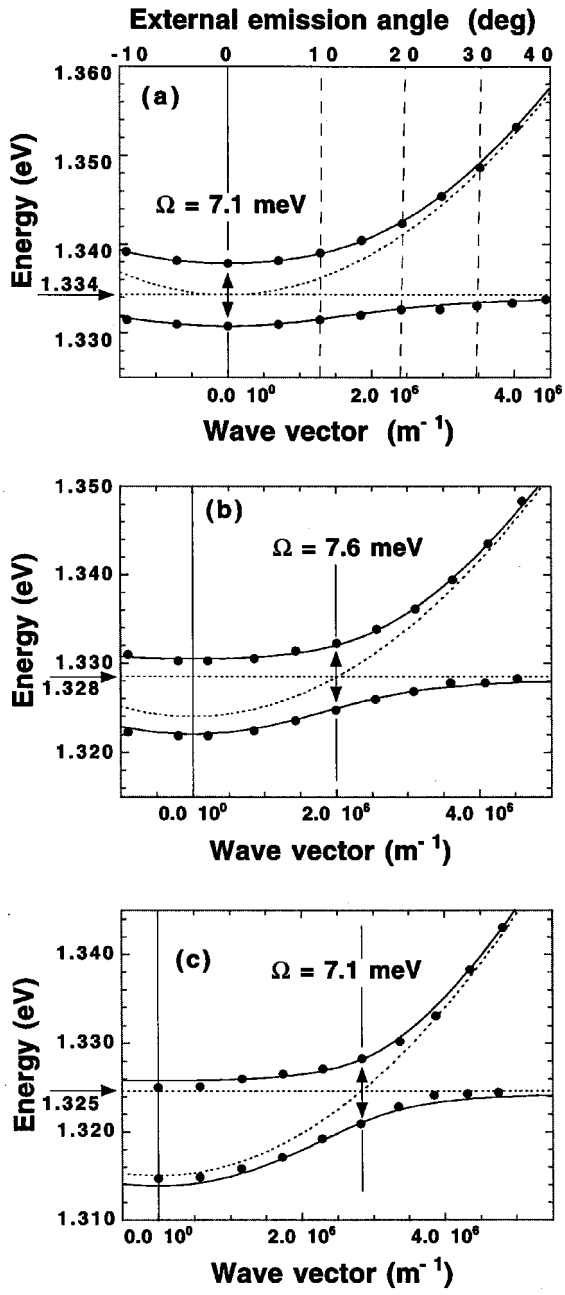

FIG. 18. Cavity-polariton dispersion curves, deduced from angle-resolved photoluminescence measurements, for different resonance conditions. Resonance at (a) $\theta=0°$, (b) $\theta=17°$, and (c) $\theta=24°$. The continuous lines are computed and the dashed lines are the uncoupled exciton and cavity dispersion curves. The interaction energy Ω and exact resonance position are determined from the minimum splitting between both photoluminescence lines. An external emission angle grid is drawn on (a). From Houdré, Weisbuch, *et al.*, 1994.

1989). Free carriers can scatter among each other and with the excitonic polarization. The corresponding dephasing leads to broadening of the excitonic resonances. Excitonic bound states in the presence of an electron-hole plasma have been treated in the past using a Bethe-Salpeter equation (Haug and Tran Thoai, 1978; Zimmermann *et al.*, 1978; Haug and Schmitt-Rink, 1985; Schäfer *et al.*, 1986), whereas the coherent exciton dynamics is described by semiconductor Bloch equations. Only recently a microscopic analysis of excitonic broadening due to carrier-carrier interaction has been presented (Wang *et al.*, 1993; Hu *et al.*, 1994; Rappen *et al.*, 1994; Schäfer *et al.*, 1994).

To reveal the physical nature of exciton saturation, one has to distinguish between a reduction in the exciton oscillator strength and resonance broadening, both of which reduce the peak absorption coefficient. The transmission and reflection of microcavities in the nonperturbative regime can help distinguish between these effects. The magnitude of the NMC splitting depends only on the oscillator strength in the limit of large NMC splitting-to-linewidth ratio. However, the transmission percentages and widths are sensitive to absorption in the vicinity of the peaks, so they are influenced by excitonic broadening.

In this section, we consider a weak external field that probes excitonic properties in the presence of unbound electrons and holes. For an interacting electron-hole plasma, it is well known that phase-space filling, screening, and dephasing due to carrier Coulomb interaction lead to nonlinear saturation with increased excitation density. At the same time, the wave equation for the light field interacting with the many-body system can be solved in linear approximation as long as the applied optical field is sufficiently weak. This is only possible when the optical field does not introduce optical nonlinearities into the system (through changes of the carrier occupation probability and nonlinear changes of the quantum well polarization).

The excitation of the system can be described in a Bloch basis with the momentum-dependent carrier occupation probabilities $f_{\mathbf{k}}^{e,h}$, defined in Eq. (A9). For a sufficiently long time delay between the electron-hole-pair generation and the weak optical probe pulse, carrier-carrier and carrier-phonon scattering leads to a quasiequilibration of the carriers within their bands, so that $f_{\mathbf{k}}^{e,h}$ can be taken as Fermi-Dirac distributions.

Next we have to extend the Wannier equation (19), which is the general basis for the calculation of a linear optical susceptibility, to include quasiequilibrium plasma nonlinearities. For this purpose we use the dynamic polarization equation (A33),

$$\left[i\hbar\frac{\partial}{\partial t}-\varepsilon_{\mathbf{k}}^{e}(t)-\varepsilon_{\mathbf{k}}^{h}(t)\right]P_{\mathbf{k}}(t)+[1-f_{\mathbf{k}}^{e}-f_{\mathbf{k}}^{h}]\Omega_{\mathbf{k}}(t)$$
$$=-i\tilde{\Gamma}_{\mathbf{k}}P_{\mathbf{k}}(t)+i\sum_{\mathbf{k}'}\tilde{\Gamma}_{\mathbf{k},\mathbf{k}'}P_{\mathbf{k}+\mathbf{k}'}(t), \tag{43}$$

whose derivation is outlined in Appendix A, together with the generalized optical Rabi energy,

$$\Omega_{\mathbf{k}}(t)=\mathbf{d}_{cv}\mathbf{E}_{QW}(t)+\frac{1}{S}\sum_{\mathbf{k}'}V_{\mathbf{k}-\mathbf{k}'}P_{\mathbf{k}'}(t). \tag{44}$$

Inserting Eq. (44) and setting $f_{\mathbf{k}}^{e,h}=0$, the left side of Eq. (43) reduces to a real-time version of the Wannier equation. Hence, for the unexcited system, we recover the linear susceptibility describing excitonic bound and continuum states. On the other hand, the left side of Eq. (43) is similar to the optical Bloch equation of atomic systems for the off-diagonal density-matrix elements. Pairs of electron-hole Bloch states with carrier momentum $\mathbf{k}$ correspond to various two-level systems, and the macroscopic polarization,

$$\mathbf{P}_{QW}(t)=\frac{1}{S}\sum_{\mathbf{k}}\mathbf{d}_{vc}P_{\mathbf{k}}(t)+\text{c.c.}, \tag{45}$$

is the dipole density of the ensemble. Already at the mean-field or Hartree-Fock level, the Coulomb interaction leads to a coupling of various $\mathbf{k}$ states. Correspondingly, $\Omega_{\mathbf{k}}(t)$ can be viewed as a renormalized Rabi energy and

$$\varepsilon_{\mathbf{k}}^{a}(t)=\epsilon_{\mathbf{k}}^{a}-\frac{1}{S}\sum_{\mathbf{k}'}V_{\mathbf{k}-\mathbf{k}'}f_{\mathbf{k}'}^{a}(t) \tag{46}$$

is the renormalized interband transition energy of the system. In terms of plasma density nonlinearities, the left side of Eq. (43), i.e., the semiconductor density-matrix equation in Hartree-Fock approximation, includes phase-space filling via the $1-f_{\mathbf{k}}^{e}-f_{\mathbf{k}}^{h}$ term and energy renormalization via Eq. (46). However, to consider screening of the Coulomb interaction and resonance broadening due to interaction-induced dephasing, one has to go beyond the Hartree-Fock level. Using quantum-statistical methods (e.g., nonequilibrium Green's functions) one can classify correlation contributions with respect to powers of the screened Coulomb interaction, as discussed in detail in Appendix A. The resulting terms on the right side of Eq. (43) describe excitation-induced resonance broadening and higher-order renormalizations of the transition energies (including band-gap shrinkage).

From a numerical solution of Eqs. (43)–(46), together with a calculation of $\tilde{\Gamma}_{\mathbf{k}}$ and $\tilde{\Gamma}_{\mathbf{k},\mathbf{k}'}$, we can directly obtain the optical susceptibility of the system, which is linear in terms of a weak probe field but nonlinear in terms of the plasma carrier density. Reflection, transmission, and absorption spectra can be calculated from the Fourier-transformed optical susceptibility with the transfer-matrix technique, as discussed in Sec. III.A.

1. Quantum wells

As a first step, we study the saturation of the excitonic susceptibility in the presence of a free-carrier plasma. Figure 19(a) shows the computed exciton spectrum for a given carrier density and temperature. The solid line is obtained if all correlation terms in Eqs. (A34) and (A35) are considered. For comparison, the dashed line shows the result if exchange contributions $\propto W_{\mathbf{k}'}W_{\mathbf{k}-\mathbf{k}''}$ are neglected in Eqs. (A34) and (A35). Then the broadening

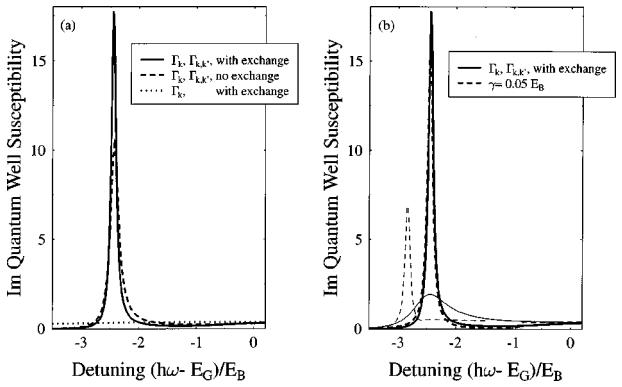

FIG. 19. Dependence of theoretical susceptibility upon exchange interaction and scattering: (a) Imaginary part of the optical susceptibility for an 8-nm quantum well and plasma excitation with $10^{10}\,\mathrm{cm}^{-2}$ at 77 K: solid line, with full dephasing; dashed line, without exchange interaction; dotted line, without off-diagonal scattering $\tilde{\Gamma}_{\mathbf{k},\mathbf{k}'}$. (b) Comparison of full dephasing (solid lines) and constant damping (dashed lines). The carrier densities are 10^{10} cm^{-2} (thick lines) and 10^{11} cm^{-2} (thin lines). From Jahnke *et al.*, 1996.

increases by almost a factor of 2. In the frequently used pure dephasing limit, where only diagonal contributions due to carrier-carrier scattering according to Eq. (A34) are considered and off-diagonal contributions from Eq. (A35) are neglected, the broadening is strongly overestimated (dotted line). Off-diagonal dephasing compensates for diagonal dephasing to a large extent. Somewhat similar behavior has been found for resonant interband excitation, where the generation process of free carriers is accurately described only if diagonal and off-diagonal dephasing contributions are considered (Rossi *et al.*, 1994). Furthermore, it has been shown that the lineshape problem of semiconductor gain spectra is solved by including off-diagonal dephasing (Chow *et al.*, 1997; Girndt *et al.*, 1997).

Surprisingly, already at the relatively low carrier-plasma density of $10^{10}\,\mathrm{cm}^{-2}$ the diagonal dephasing corresponds to a T_2 time faster than 100 fs. These values are usually expected only for high carrier densities, where sufficiently many scattering partners are available. However, at high carrier densities the Coulomb potential is strongly screened, whereas at the low carrier density used in Fig. 19(a) only weak Coulomb screening is present, so that the large scattering cross section compensates for the lower carrier density. Only at even smaller carrier densities does the carrier-carrier scattering efficiency decrease significantly.

In Fig. 19(b), the full calculation is compared with the common approximation in which correlation contributions are neglected, dephasing is described with a constant damping rate γ, and the bare Coulomb potential in the Hartree-Fock terms, Eqs. (44) and (46), is replaced by a screened potential. Then the so-called Coulomb-hole contribution has to be added to Eq. (46); compare Haug and Koch (1994). For a small carrier density ($10^{10}\,\mathrm{cm}^{-2}$) the full calculation (thick solid line) can be

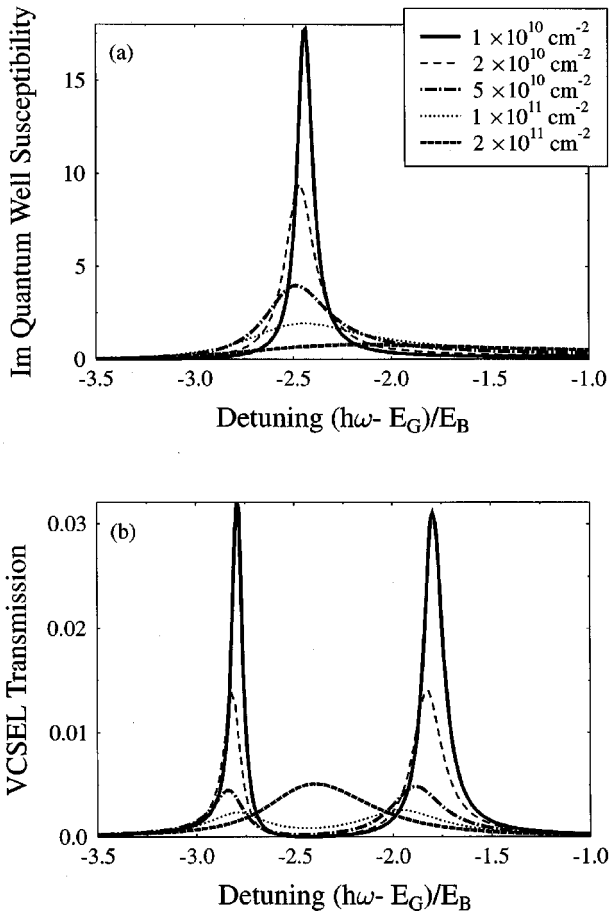

FIG. 20. Computed quantum-well susceptibility and corresponding NMC transmission as a function of carrier density: (a) Imaginary part of the optical susceptibility for an 8-nm quantum well and plasma excitation with various densities at carrier temperature 77 K. (b) Calculated transmission of the quantum well microcavity for increasing plasma density and bleaching of the exciton according to Fig. 20(a). The cavity resonance has been tuned from $-2.05E_B$ (full line) to $-2.14E_B$ (short dashed line) to compensate for the small numerical exciton shift. From Jahnke *et al.*, 1996.

fitted by a constant dephasing rate $\gamma=0.05E_B$ (thick dashed line). Increasing the carrier density to $10^{11}\,\mathrm{cm}^{-2}$, we obtain with constant damping and static screening the well-known artificial shift of the $1s$ exciton, whereas the full dephasing calculation does not exhibit this shift. For a higher carrier density and the same constant damping, the height of the $1s$-exciton peak is only reduced by a factor of about 2.5 due to phase-space filling and screening. If the increased broadening is also taken into account within the full calculation, the height of the $1s$-exciton peak is reduced almost by an order of magnitude.

Figure 20(a) shows the saturation of the $1s$ exciton for increasing plasma density, computed within the full dephasing model. Good agreement is obtained with Fig. 21(a), showing the measured absorption of a 20 quantum well sample.

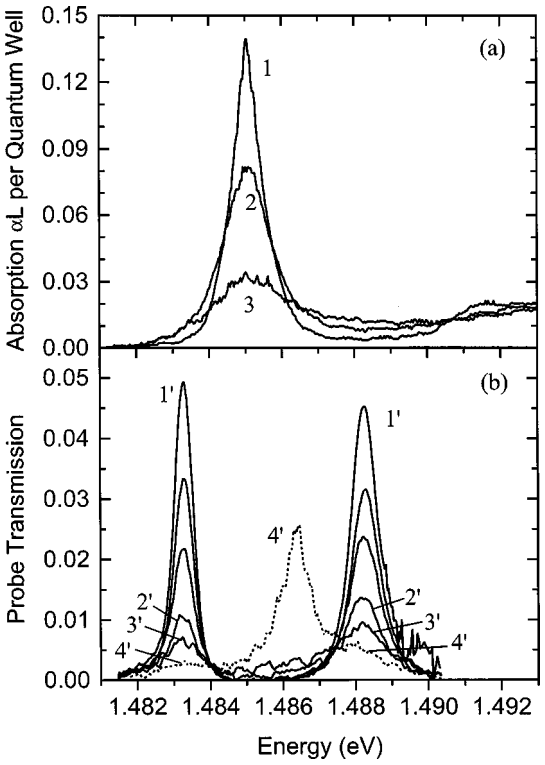

FIG. 21. Experimental probe transmission spectra with increasing pumping at 787 nm for (a) exciton absorption of 20 quantum wells like the two in the microcavity and (b) microcavity normal-mode coupling. Since absolute densities were not measured, curves in (a) and (b) cannot be compared directly; however, Kramers-Kronig transfer-matrix microcavity calculations using the nonlinear data in (a) show that $2'$ corresponds closely to 2 and $3'$ to 3. Noise from photoluminescence prevented determining the probe transmission when the exciton is completely saturated ($4'$). Stronger pumping in (b) results in lasing at a wavelength close to the $4'$ peak. From Jahnke *et al.*, 1996.

2. Normal-mode coupling

To determine the normal-mode coupling spectrum for a microcavity containing quantum wells, we use the quantum well susceptibility within a transfer-matrix calculation for the microcavity design. We consider a cavity with a $\frac{3}{2}\lambda$ GaAs spacer between GaAs/AlAs mirrors. For the left mirror (exposed to air) and right mirror (on a substrate) a reflectivity of 99.6% is obtained with 14 and 16.5 quarter-wave pairs. A single 8-nm $In_{0.04}Ga_{0.96}As$ quantum well is placed in each of the two cavity antinodes. The cavity wavelength is chosen to coincide with the $1s$-exciton resonance of the quantum wells. The calculated microcavity transmission is shown in Fig. 20(b). For increasing broadening of the $1s$-exciton resonance with increasing carrier density, we find a strong reduction of the NMC peak height with only a small reduction in NMC splitting. The reduced transmission and the increased widths of the individual NMC peaks indicate strong broadening of the exciton resonance, whereas the small reduction of the splitting clearly reveals the minor reduction of the exciton oscillator strength within a large plasma density range. With increasing plasma density the renormalized band edge approaches the energetically stable $1s$-exciton resonance. The rather abrupt replacement of the NMC doublet by a single transmission peak occurs when the cavity resonance becomes degenerate with the band edge. This corresponds to a transition from the nonperturbative regime to the perturbative regime due to strong dephasing of interband states.

The dramatic effect of excitonic broadening on normal-mode coupling has been seen in measurements with 8-nm $In_{0.04}Ga_{0.96}As$ quantum wells within the above-discussed cavity design (Khitrova *et al.*, 1996; Jahnke *et al.*, 1996; Gibbs *et al.*, 1997). The In concentration is sufficiently large for the heavy-hole exciton peak to be around 834 nm at 4 K, so that the GaAs substrate does not have to be removed for transmission studies. Nonetheless the strain shifts the light-hole exciton peak to 826 nm, 13 meV above the heavy-hole exciton, so that it does not interfere with NMC studies with the heavy-hole exciton. The results for three samples having small exciton HWHM linewidths ($\gamma_{ex} \approx 0.5\,\text{meV} = 0.3\,\text{nm}$ at 4 K) are as follows. The ratio of splitting to linewidth was found to be 41(13.6; 4.6) for Bragg mirrors consisting of 19/21.5(14/16.5; 5/12.5) periods for the left and right mirrors, respectively. The calculated reflectivities of the cavities were 99.94% (99.6%; 97.7%); see Figs. 15 (21; 14). The second sample will also be used to illustrate time-resolved normal-mode oscillations (Fig. 25 in Sec. III.C.1), nonlinear pulse propagation (Fig. 28) in Sec. III.C.2), and nonlinear and time-dependent photoluminescence (Figs. 34–39 in Sec. IV).

Experimental results for cw pump-probe excitation of quantum wells and the corresponding exciton saturation are shown in Fig. 21(a), in agreement with Fig. 20(a). With increased excitation, there is little change in oscillator strength (integrated absorption) but considerable broadening (Fehrenbach *et al.*, 1982; Wang *et al.*, 1993). This broadening increases the absorption at the energies of the two peaks, thereby decreasing their transmission as shown in Fig. 21(b), in agreement with Fig. 20(b). This curious behavior was illustrated in Fig. 8 in Sec. II. When the exciton is completely saturated, the transmission of the almost-empty cavity opens up close to the midpoint (the usual weak-coupling laser limit). Figure 21(b) was taken with the pump wavelength at the first transmission minimum above the stop band. Reduction in transmission without reduction in splitting is also seen when the pump wavelength is coincident with either one of the original peaks or midway between them. Of course, the power dependence is different for each of the wavelengths, and limiting or optical bistability of the pump can occur by quasiequilibrium nonlinear effects not treated here. Citrin and Norris (1997) suggest the use of an NMC microcavity for high-speed switching: a pump into one peak controls the transmission through the other peak, simplifying cascading.

Loss of oscillator strength dominated the first nonlinear NMC experiments because structural-disorder-induced inhomogeneous broadening masked carrier-density-dependent excitonic broadening. In the experiment of Fig. 21 loss of oscillator strength certainly

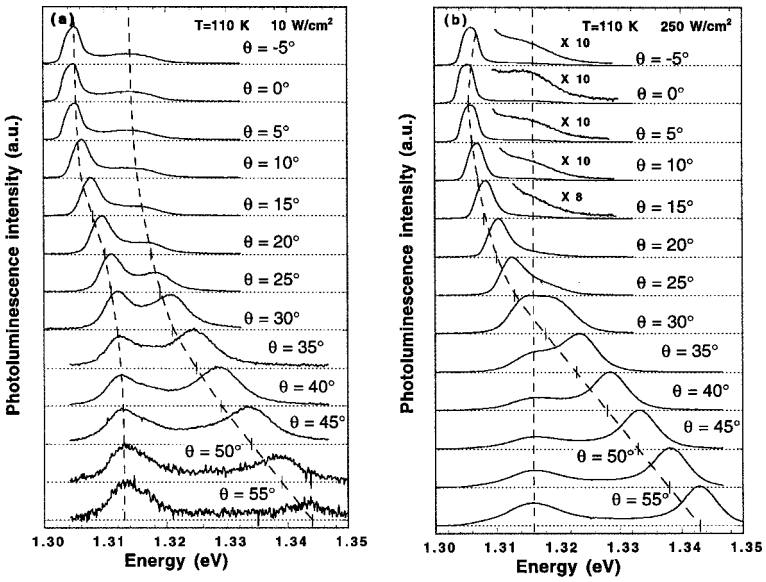

FIG. 22. Angle-resolved photoluminescence under (a) low and (b) high excitation. Dashed lines are a guide to the eye to follow the respective anticrossing and crossing behaviors of the dispersion curves. From Houdré *et al.*, 1995.

occurred, but predominantly in the transition from normal-mode to weak coupling at densities above the regime where transmission goes down with little change in splitting. The collapse of normal-mode coupling accompanying loss of oscillator strength has been studied by femtosecond spectroscopy (see Sec. III.C.3) and by photoluminescence by Houdré *et al.* (1995). The latter mapped out the NMC photoluminescence peaks as a function of angle of observation. For low-intensity quasi-cw excitation into the continuum of the bulk GaAs spacer around the InGaAs quantum wells, there is the usual nonperturbative anticrossing, as shown in Fig. 22(a) [like Fig. 5(b)]. But for high-intensity excitation the levels cross, indicating weak coupling [Fig. 22(b), like the dashed curves in Fig. 5(b)]. The anticrossing and crossing occur at the same angle because band-gap renormalization just compensates for the decrease in the exciton binding energy (Schmitt-Rink and Ell, 1985), i.e., the resonance condition is always fulfilled during the bleaching process. From carrier-density-dependent photoluminescence data (Fig. 23) the oscillator strength was found o to saturate as $1/(1+n/n_s)$ with $n_s=4.3\times10^{11}$ e-h pairs/cm^2 at 100 K. No further broadening of the NMC peaks was observed up to the complete loss of NMC transmission. These findings are consistent with the experimental results in Fig. 21.

What is the evidence that present-day NMC experiments can be described semiclassically? Semiclassical and quantum electrodynamic theories predict the same splitting for very weak probes, so one must perform nonlinear experiments to determine how close one is to the quantum-statistical regime. Our nonlinear cw and femtosecond experiments on two-quantum well $\frac{3}{2}\lambda$ microcavities (Secs. III.B and III.C) show that the best present-day microcavities are orders of magnitude away from the strong-coupling quantum-statistical regime. One source of evidence is the agreement between nonlinear transmission data and a semiclassical transfer-matrix simulation (carrier-density-dependent linear dispersion theory). Also, the observation of stable optical bistability agrees with semiclassical theory; in the quantum-statistical limit, the system fluctuates between the two states. To see why semiclassical theory works so well, we determined the number of photons that have to be absorbed to reduce the peak exciton absorption in a

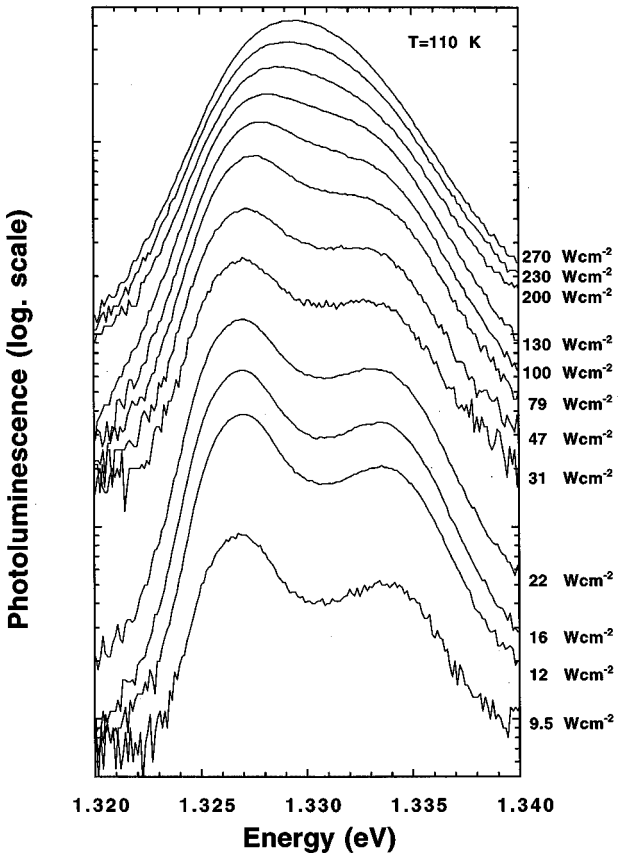

FIG. 23. Series of photoluminescence spectra (110 K) as a function of pump power showing bleaching of the strong-coupling regime. The incident power density is shown on the right axis. From Houdré *et al.*, 1995.

narrow-linewidth quantum well sample (NMC21) to one-half. This reduction in peak absorption causes the NMC peak transmissions to drop below 25% of their linear (zero-pump) values. Use of a 150-fs pulse of excitation in the continuum made a carrier lifetime measurement unnecessary. We found that a few times 10^5 photons in a 50-μm-diameter beam had to be absorbed; this can be compared to 5×10^5 from the theory presented in Fig. 20(a) for a 2500-μm^2 area. To see small changes in the NMC transmission, still many thousands of photons are necessary (Khitrova *et al.*, 1996; Nelson, Khitrova, *et al.*, 1996; Wick *et al.*, 1996). Thus present-day semiconductor microcavity experiments are at least five to six orders of magnitude away from the strong-coupling quantum-statistical regime. To emphasize that current experiments are far from the quantum-statistical limit, throughout this review we use ''nonperturbative regime'' rather than the term ''strong-coupling regime'' used in most semiconductor NMC articles. The invariance of the splitting over several orders of magnitude variation of emission intensity, considered surprising at one time (Cao, Jacobson, Björk, Pau, and Yamamoto, 1995), results from operating well below the saturation of the exciton. Earlier explanations of the appearance of new frequencies involving forbidden transitions between low rungs on a coupled boson-boson quantum ladder (Jacobson *et al.*, 1995; Hanamura *et al.*, 1995) are seen to be inappropriate.

C. Pulse propagation and nonlinear saturation

1. Time-dependent linear experiments

When a short pulse is incident on an NMC microcavity, the electric fields in both the reflected and the transmitted directions can exhibit oscillations at the NMC splitting frequency, as just shown theoretically. These normal-mode oscillations occur provided there is good overlap between the pulse spectrum and the NMC peaks, there is a reasonable splitting-to-linewidth ratio, and the pulse intensity is not high enough to destroy the normal-mode coupling.

Norris *et al.* (1993, 1994, 1995, 1996) and Rhee *et al.* (1995, 1996) performed time-resolved measurements with 80-fs pulses on the sample of Weisbuch *et al.* (1992) at 10 K. The pump beam was focused to a spot size of 160-μm diameter, with an incidence angle of 3°. By a standard upconversion technique (Shah, 1988), they time-resolved the emission, which was in the same direction as the reflected pump pulse. After the strong reflected pump at zero delay, the upconversion signal showed a fast decay, corresponding to twice the cavity lifetime, and strong beats with a period of 600 fs, close to the expected normal-mode oscillation period for $\Omega_0 = 6$ meV. Changing the detuning to obtain a splitting of 11 meV, the beats had a period of 350 fs and decayed faster. They showed that the radiation from the cavity was coherent in the direction of the reflected pump beam, consistent with the fact that the exciton dephasing time T_2 at low temperature was approximately 1 ps, which is longer than both the cavity lifetime ($T_c = 140$ fs) and the normal-mode frequency (680 fs). Due to momentum conservation, the polarization excited in the cavity by the pump pulse will coherently radiate in the direction of the reflected pump with a decay time $2T_c$. Since $T_2 \gg T_c$, most of the energy will be radiated away coherently, and almost no luminescence is observed in other directions. The decay time of the microcavity signal is much faster than that of the corresponding bare quantum wells, typically 10 ps (Devaud *et al.*, 1991).

To determine the time-dependent cavity emission and population more thoroughly, Norris *et al.* and Rhee *et al.* performed a pump-probe experiment. Both pump and probe with parallel polarizations were incident at 3° and overlapped to make them interact as much as possible with the same cavity mode. There were two contributions to the signal—one from the change in probe reflectivity induced by the pump-generated excitation in the quantum wells, and the other from light scattered in the probe beam direction by small inhomogeneities in the sample structure. If scattered light was phase coherent with the probe pulse, then the two pulses interfered on the detector, and fringes were observed as the delay was varied a fraction of a wavelength. This gave rise to the fine fringes in Fig. 24, which persist throughout the coherent reemission (unlike the case of quantum wells outside the cavity). The envelope of the fringes shows three peaks, with a period of about 700 fs, which is that expected for the observed mode splitting of 6 meV on resonance. The fringes after time zero are an unambiguous signature of the coherence of the polarization remaining in the cavity following the pump pulse.

Spectrally and temporally resolved four-wave mixing has been used to study emission from quantum wells and NMC microcavities following resonant excitation (Shah *et al.*, 1995; Wang, Shah, Damen, Jan, *et al.*, 1995; Wang, Shah, Damen, Pfeiffer, and Cunningham, 1995). Whereas oscillations in spectrally unresolved emission may arise from the interference of two fields in the detector (polarization beats), oscillations in spectrally resolved emission are interpreted as arising from two transitions sharing a common ground state (quantum beats). Oscillations seen in reflection or transmission do not prove that there is a coherent oscillation of the exciton population, since they could arise from polarization beats. The oscillations seen by Wang and co-workers in spectrally resolved four-wave mixing are interpreted as showing the creation of a coherent state between the two normal modes of the composite system and, in the time domain, the coherent energy exchange between the exciton and cavity; see also Koch (1997). Bongiovanni *et al.* (1997) show that this energy exchange is destroyed by inhomogeneous broadening: the polarization still exhibits deep oscillations, but not the exciton population; see also Pau, Björk, Cao, Hanamura, and Yamamoto (1996), and Björk *et al.* (1996).

Sermage *et al.* (1996) studied the emission from a microcavity with an AlAs $\lambda/2$ spacer using 1.5-ps pulses; thus the pulse spectral FWHM width of 1 meV was

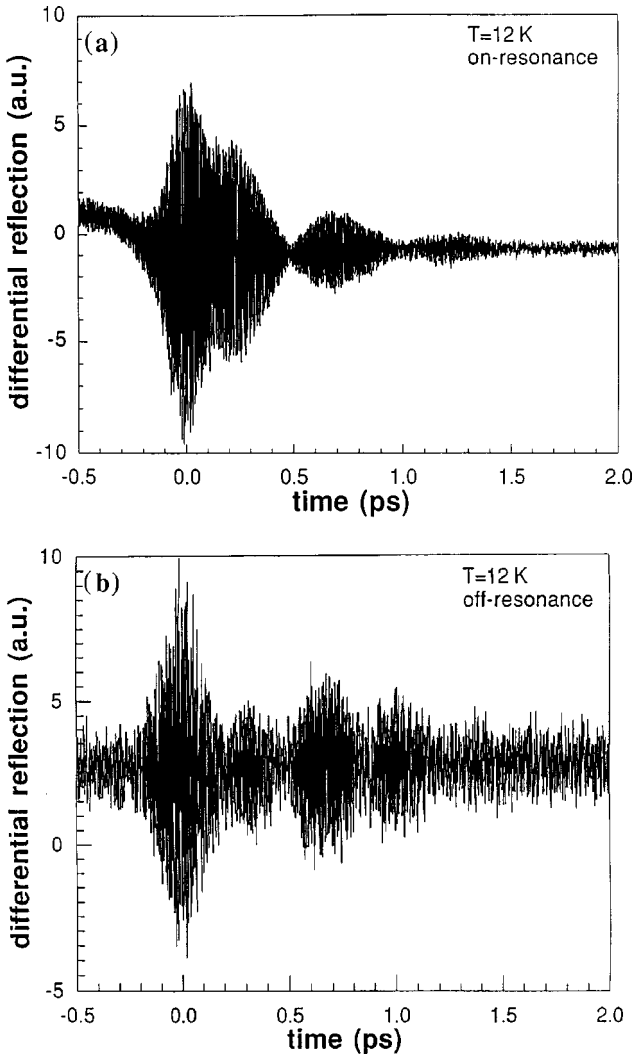

FIG. 24. Interferometric time-resolved pump-probe data for the microcavity sample, showing the envelope of the optical-frequency interference fringes: (a) resonance, and (b) cavity tuned off resonance. The ordinate axis is in arbitrary units. From Norris *et al.*, 1994.

much less than the 4.6-meV NMC splitting. For resonant excitation into either one of the two NMC peaks, the emission decay time as a function of detuning was measured and fit to a two-coupled-oscillator model. They extracted a bare-exciton decay time of 17 ps and a bare-cavity decay time of less than 3 ps, their streak-camera resolution. Whatever the detuning, the branch being excited decayed as a weighted average of bare exciton and bare cavity, determined by the detuning in the coupled-oscillator formula. For this resonant excitation, the exciton states that were populated directly were extended states with short in-plane wave vectors, that coupled directly to the cavity modes selected by the laser. Then they tuned the laser to the first blue bandpass window of the Bragg mirror and measured the rise time and decay time of emission from the lower NMC peak. For positive detunings those times were close to those measured for a cavityless quantum well (60 ps for the rise time and 400 ps for the decay), while at negative detuning the

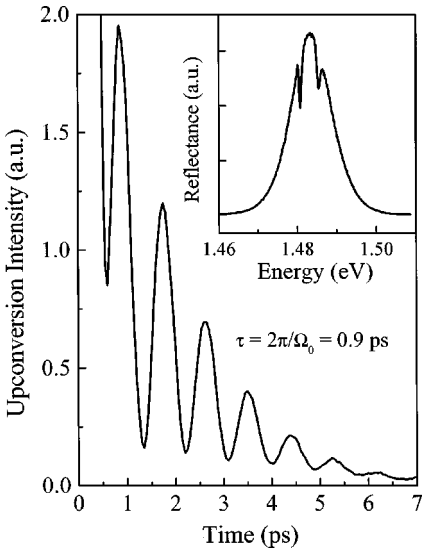

FIG. 25. Time-resolved NMC emission signal (normalized to 1000 at $t=0$ ps) close to zero detuning in the linear regime. Inset: spectrum of the reflected excitation pulse. From Berger *et al.*, 1996.

times were much shorter (less than 3 ps for the rise time and 180 ps for the decay). In this case the two-coupled-oscillator model fit gave bare times inconsistent with the measured values, indicating the need to correctly treat the complicated relaxation dynamics of carriers and excitons within a microcavity.

Of course, samples with higher splitting-to-linewidth ratios give normal-mode oscillations of higher contrast (Berger *et al.*, 1996; Lyngnes *et al.*, 1997). An example using sample NMC22 described in Sec. III.B.2 is shown in Fig. 25. Boggavarapu *et al.* (1996) report very deep oscillations using balanced homodyne detection; they use quantum state reconstruction techniques to deduce the photon statistics of the electric field directly from the phase-random quadrature probability distributions. They find that the second-order coherence function $g^{(2)}(t,t)$ remains unity wherever the NMC transmission signal is strong enough to allow for accurate measurement, characteristic of a Poisson photon distribution of laser emission, as expected for a semiclassical system.

2. Coherent nonlinear pulse propagation calculations

In the linear regime, the propagation equations developed by Jahnke, Kira, and Koch (1997) are equivalent to the transfer-matrix calculations of Sec. III.A, which are an extension of the linear dispersion theory introduced in Sec. II. Correspondingly, the system dynamics can be described by Fourier-transforming the incoming pulse and then applying the transfer-matrix method for each of its frequency components. The excitonic properties enter only through the linear time-independent susceptibility. However, this linear model is not applicable for the intense pulse propagation studied in the following. A strong excitation generates nonlinear excitonic effects that have to be treated self-consistently with the nonlinear pulse propagation problem.

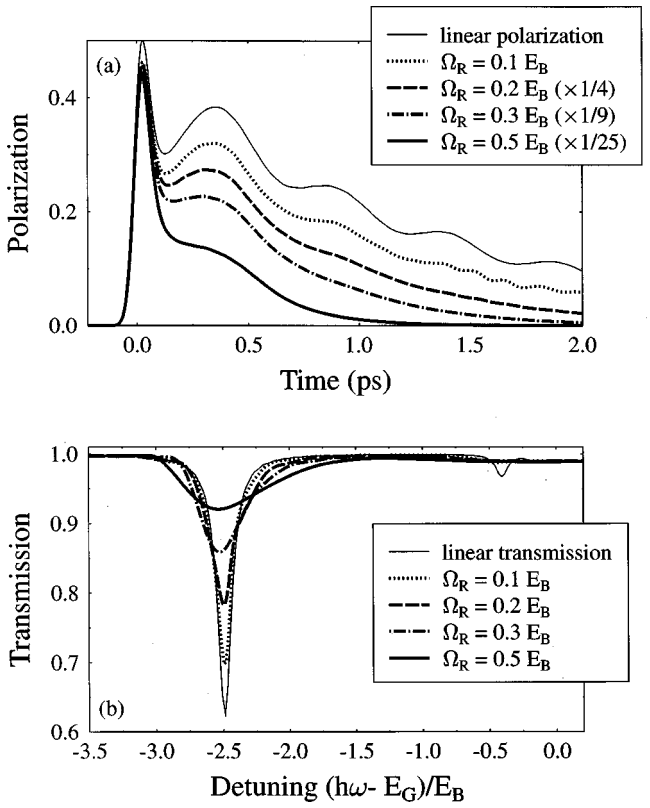

FIG. 26. Compound quantum-well polarization and transmission as a function of resonant pump Rabi energy: (a) Time-resolved quantum-well polarization $|P_{QW}(t)|$ for increasing Rabi energy Ω_R of the external 100-fs laser pulse. The linear result is obtained for $\Omega_R = 10^{-3} E_B$ where the curve has been scaled by a factor 10^{-4}. (b) Corresponding quantum well transmission spectra for increasing Rabi energy. From Jahnke, Kira, and Koch, 1997.

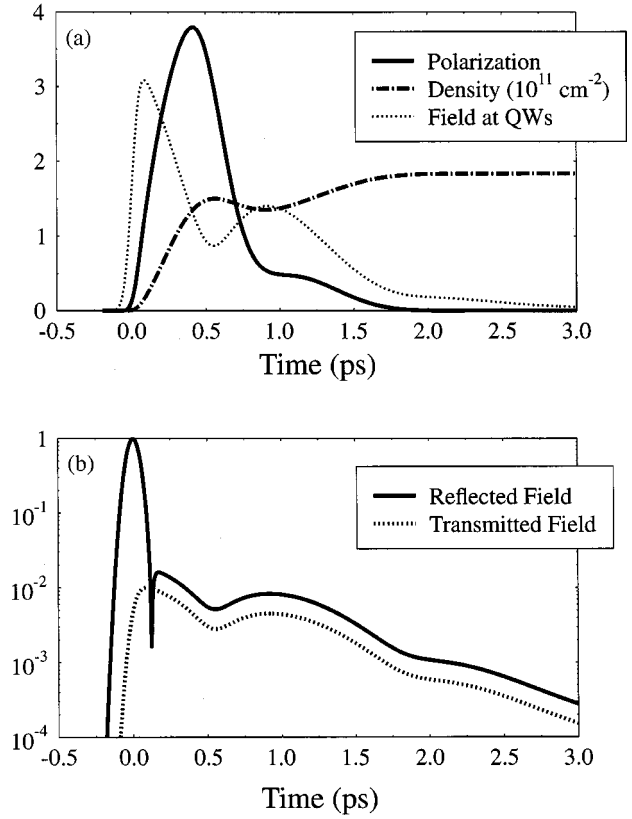

FIG. 27. Computed time dependence following femtosecond excitation: (a) Temporal evolution of a quantum well; solid line, polarization; dot-dashed line, excitation density; dotted line, cavity field at the quantum well position for a microcavity with two quantum wells and excitation with an intense 100-fs laser pulse. All quantities are the same for both quantum wells; (b) corresponding reflected and transmitted fields. Time-resolved reflected signal (solid line) and transmitted signal (dotted line) of a VCSEL. From Jahnke, Kira, and Koch, 1997.

To demonstrate the saturation of quantum well excitons, we study the propagation of an intense laser pulse through a single quantum well. The results are part of the nonlinear saturation physics of normal-mode oscillations discussed in the next section (III.C.3). In the nonlinear regime, the dynamic equation for the quantum well polarization, Eq. (43), alone is not sufficient to determine the excitation dynamics, since the carrier occupation also becomes an independent dynamic quantity. The general form of the coupled polarization and occupation equations including correlation contributions, is discussed in Appendix A. The pulse-excited quantum well polarization follows from Eqs. (A33)–(A35), (A40), and (A41), whereas the excitation-induced occupation can be determined with Eqs. (A36)–(A39). The nonlinear pulse propagation problem has been treated by Jahnke, Kira, and Koch (1997); the quantum well polarization follows from Eq. (A10).

For the propagation of a 100-fs laser pulse through a single 8-nm GaAs quantum well, the time evolution of the excited quantum well polarization is shown in Fig. 26(a). Using a small Rabi energy, $\Omega_R = \mathbf{d}_{cv}\mathbf{E}$, of an externally applied pulse, the solution remains in the linear regime and the polarization decay is governed by the background damping. At elevated pulse energies, enhanced polarization decay is obtained from increased efficiency of carrier and polarization scattering. The calculated spectra of the transmitted pulses are shown in Fig. 26(b). Similar to the case of quasiequilibrium excitation in Sec. III.B, bleaching of the exciton transmission occurs basically without any shift of the 1*s*-exciton resonance. The spectral position of the 1*s* exciton results from the interplay of a reduced exciton binding energy and the increasing band-gap shift. Both effects are calculated including the above-discussed dynamic renormalization contributions.

3. Nonlinear saturation of time-resolved normal-mode oscillations

Using nonlinear theory, we have also studied the saturation of excitonic normal-mode coupling. For the above-discussed microcavity design with two quantum wells, we have calculated the propagation of an intense 100-fs pulse ($\Omega_R = 1 E_B$) through the Bragg mirrors. Figure 27 shows that the normal-mode oscillations are strongly damped. Due to increased dephasing, the quantum well polarization (solid line in Fig. 27) rapidly van-

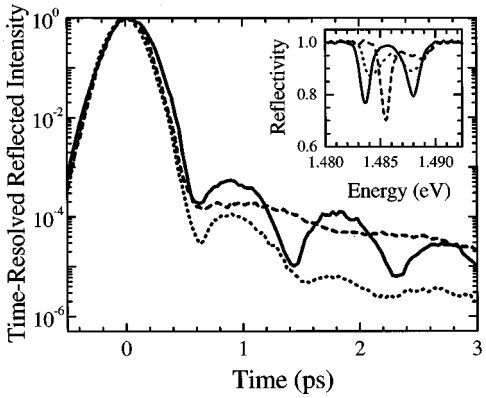

FIG. 28. Experimental time-resolved reflected intensity (normalized to 1 at $t=0$ ps) after 100-fs pulse excitation of a microcavity with two quantum wells: solid line, with a photon flux 1.4×10^{11} photons/cm^2; dotted line, 5.5×10^{12} photons/cm^2; dashed line, 1.1×10^{13} photons/cm^2. Inset: the corresponding spectra of the reflected signal divided by the spectrum of the incident pulse. From Lyngnes *et al.*, 1997.

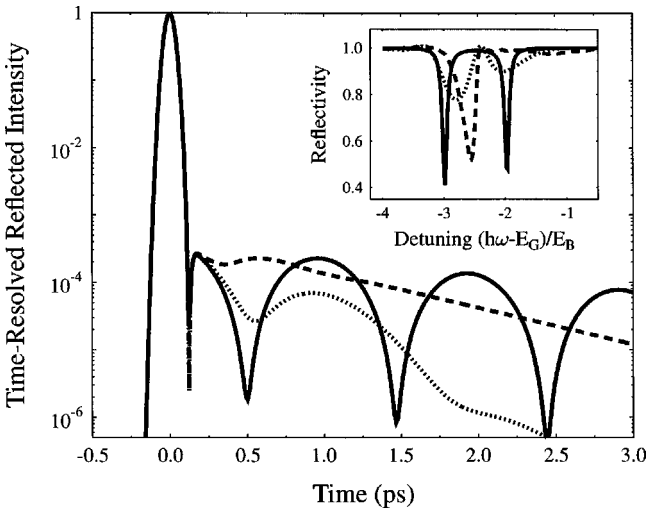

FIG. 29. Calculated time-resolved reflected intensity of a microcavity after 100-fs pulse excitation: solid line, with $\Omega_R=0.01E_B$; dotted line, $\Omega_R=1E_B$; dashed line, $\Omega_R=2E_B$. The inset shows the Fourier spectrum of the reflected signal divided by the Fourier spectrum of the incident pulse. From Lyngnes *et al.*, 1997.

ishes. Since normal-mode oscillations originate from the periodic energy exchange between the quantum well and the cavity field, the rapid polarization decay reduces the reemission of the field by the quantum wells. Hence the cavity field at the quantum wells (dotted line in Fig. 27) decays much faster than in the low-intensity case. The discussed behavior leads to strongly damped normal-mode oscillations and a fast decay of the transmitted and reflected field.

Figure 28 shows the measured time-resolved reflection of the sample (on a logarithmic scale) for different incident pulse intensities. The corresponding measured reflection spectra are shown in the inset. A rich dynamic behavior is observed: As the incident pulse intensity increases, the modulation depth of the NMC oscillations decreases, accompanied by a reduction and broadening of the dips in the reflection spectra. However, the oscillation period stays approximately constant as the pulse intensity increases, consistent with the observed near-constant splitting in the reflection spectra. Nonlinear effects strongly influence the interaction-induced decay of the time-resolved signal. When the pulse intensity is increased from a low to an intermediate value (solid line and dotted line in Fig. 28, respectively) the decay becomes faster. For a very large pulse intensity (dashed line in Fig. 28), the NMC oscillations are strongly damped out, due to fast-exciton saturation, and the decay is slowed down approaching the empty-cavity decay rate.

The corresponding calculations of the time-resolved reflected signal for increasing intensity of the applied 100-fs pulse, using the above discussed microscopic theory, are shown in Fig. 29. We find quantitative agreement with the experimental results (Fig. 28) regarding the decay behavior and the reduction in modulation depth. Note that the limited time resolution in the experimental setup increases the width of the $t=0$ peak in Fig. 28. Furthermore the reflected pulse spectrum, displayed in the inset, reproduces the experimentally observed features.

Nonlinear transmission was also studied by time-integrated detection of the throughput of 100-fs laser pulses (Gibbs *et al.*, 1997). Again loss of transmission with little reduction in splitting was seen just as in the cw case (Fig. 21). With increasing excitation, the oscillations damped out more rapidly, but the oscillation frequency hardly changed. This is the time-resolved equivalent of the cw reduced transmission without a reduction in splitting. The decay rate increased linearly with carrier density, corresponding to broadening of the exciton absorption in the cw case.

As the carrier density increased, carrier and polarization scattering increased the dephasing rate of the exciton, broadening the excitonic transition without decreasing the oscillator strength [Figs. 30 and 26(b)]. Similar behavior has been reported for bulk GaAs (Fehrenbach *et al.*, 1982; Wang *et al.*, 1993). The broadening increased the absorption at the wavelength of the reflectance dips, thus reducing the depth of the reflectance dips and broadening them. This translates in the time domain to a reduction of the modulation depth of the NMC oscillations. However, since the oscillator strength is conserved by scattering processes, the NMC splitting and oscillation period stay constant. Phase-space filling and Coulomb screening do eventually reduce the oscillator strength and collapse the NMC splitting, as described next, but not until the NMC reflectance dips and oscillations are almost completely gone. Then the bare-cavity reflectance dip appears, signaling the transition to the perturbative regime.

Rhee *et al.* (1995, 1996) and Norris *et al.* (1995) recorded the time-integrated spectra of 80-fs pulses reflected from a microcavity with a 6-meV splitting. Ad-

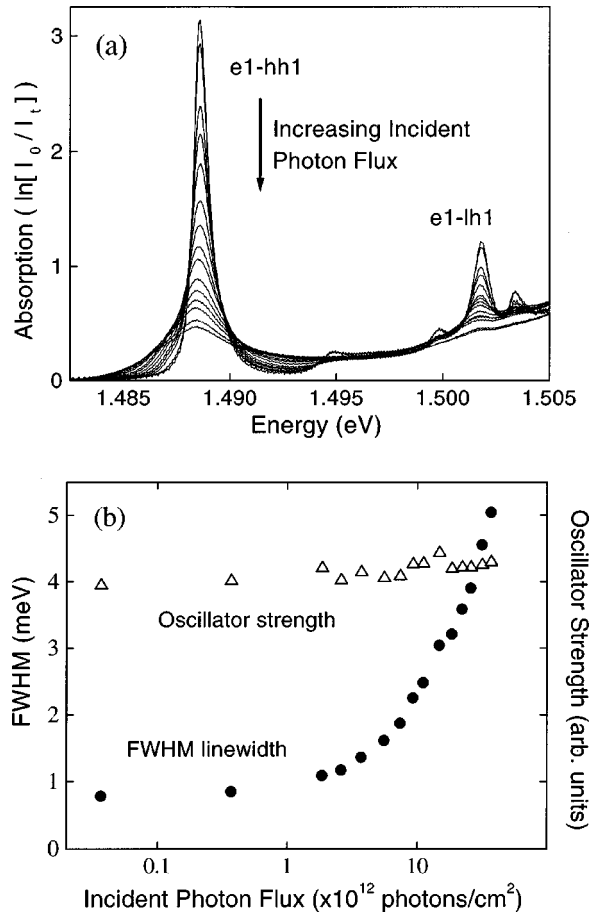

FIG. 30. Measured exciton absorption, linewidth, and relative oscillator strength as a function of resonant excitation: (a) Exciton absorption of a 20-quantum well sample measured by the transmission of 100-fs pulses. (b) FWHM linewidth and relative oscillator strength as a function of incident photon flux estimated from (a). From Lyngnes *et al.*, 1997.

justing the tuning for equal reflectivity dips, they observed no change in splitting over two orders of magnitude and then a gradual decrease in splitting as shown in Fig. 31. They attribute this reduction to loss of quantum well oscillator strength as $1/(1+n/n_s)$ with $n_s=6.6\times10^{10}$ excitons/cm^2. They note that for their sample the NMC splitting was not sensitive to pure linewidth broadening due to the exciton-exciton interaction in the relatively-low-excitation regime. As can be seen in Fig. 31, their reflectivity dips are barely resolved in spite of the large splitting. Consequently inhomogeneous broadening completely masked the broadening effects on transmission described above, just as it did in the cw carrier-density-dependent experiments of Houdré *et al.* (1995), discussed in Sec. III.B.2, and in other transient observations of the reduction in NMC splitting with increased excitation (Wang, Shah, Damen, Jan, *et al.*, 1995; Wang, Shah, Damen, Pfeiffer, and Cunningham, 1995).

When the resonant excitation is pulsed, then the equilibrium carrier-density-dependent linear dispersion theory extension of Sec. II fails because the time dynamical response of quantum well carriers within a microcavity can be quite different from that of cavityless quantum well carriers. Thus one does not know what carrier distributions to use at a given instant of time. One must self-consistently solve for the time dynamics of the coupled system of carrier distributions and polarizations and the intracavity optical fields as treated above.

IV. NONLINEAR MICROCAVITY LUMINESCENCE

The semiclassical theory developed in Sec. III and Appendix A describes both the pump and the probe beams classically. Its detailed agreement with experiments might suggest that a quantum treatment of light brings only minor corrections to the classical calculations. However, this is usually true only as long as the classical fields exceed the vacuum fluctuations, which are almost always much smaller than the weakest probe beam. Photoluminescence is an important phenomenon, which cannot be explained semiclassically. It was shown in Sec. III.C that without an external driving field the polarization and the coherent microcavity field $\langle E\rangle$ decay away typically on a ps time scale after the excitation pulse. However, in many cases a substantial number of incoherent electrons and holes remain excited in the system. The system can then reach its ground state via nonradiative electron-hole recombination or radiatively through spontaneous emission leading to photoluminescence out of the quantum well.

New and valuable information on the interplay of field and quantum well properties can be extracted from this luminescence. For example, suppressed or enhanced spontaneous emission (Kleppner, 1981; Yablonovitch, 1987) in semiconductor microcavities has been observed (Yamamoto, Machida, Horikoshi, and Igeta, 1991; Deppe and Lei, 1992; Huffaker *et al.*, 1992; Tanaka *et al.*, 1995).

A quantum treatment of light is desired to describe photoluminescence because the field has nonclassical properties, e.g., $\langle E\rangle=0$ but $\langle EE\rangle\neq0$. Alternatively to a fully quantum-mechanical theory, the analysis of photoluminescence properties is at the level of a Langevin approach using the generalized dissipation-fluctuation theorem (Louisell, 1974). However, in a strongly interacting nonlinear system with both quantum correlations in the material and light degrees of freedom, such a Langevin-type approach offers no significant simplification over the quantum theory, which is the more general approach anyhow.

The fully quantum-mechanical analysis of the interacting photon-semiconductor electron-hole system poses a considerable challenge to current theories. In the semiclassical calculations presented in Sec. III, the major difficulties arise from the consistent inclusion of carrier-carrier Coulomb interaction effects. To describe the quantum properties of light an alternative set of approximations is used frequently in which the light field is quantized, but the full electron-hole Coulomb interaction in the many-body Hamiltonian is approximated by

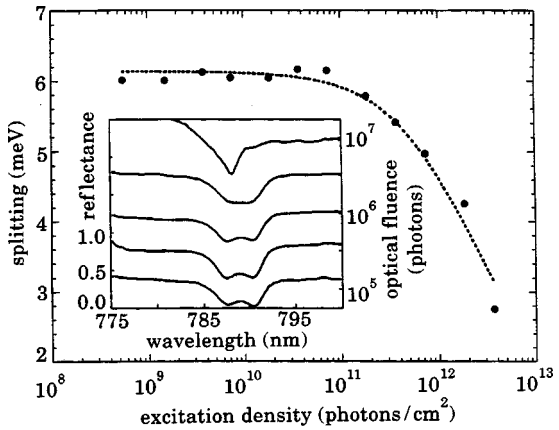

FIG. 31. Normal-mode splitting vs optical fluence for on-resonance excitation, extracted from normalized reflectance spectra as shown in the inset. The pump laser is resonant with the exciton-cavity resonance. $T=10$ K. From Norris *et al.*, 1995.

introducing exciton operators having bosonic character.[4] As already discussed in earlier sections, such calculations yield the correct linear results in the semiclassical regime, but they include only a subset of the carrier Coulomb correlation effects, and corrections become important even in the weakly nonlinear regime. Furthermore, it has been shown (Savasta and Girlanda, 1995) that the Bosonic approach does not lead to the correct quantum correlations even for very low densities.

In this section, we present a fully quantum-mechanical theory for the interacting carrier-photon system, in which electrons and holes are treated as fermions (Kira, Jahnke, and Koch, 1998; Kira *et al.*, 1999). Excitonic effects enter through the consistent inclusion of the Coulomb interaction between the carriers. On this level, investigations can be extended to the nonlinear regime and one can estimate when the Bosonic approximation breaks down.

A. Microscopic description of luminescence dynamics

For a quantum description, both light and matter properties have to be treated at the operator level. For this purpose, we introduce a bosonic photon operator b_q corresponding to a light mode having momentum q; for more details, see Appendix B. We also define the microscopic polarization operator $\hat{P}_{\mathbf{k}}=v_{\mathbf{k}}^{\dagger}c_{\mathbf{k}}$ and carrier occupation operators $\hat{n}_{\mathbf{k}}^{c}=c_{\mathbf{k}}^{\dagger}c_{\mathbf{k}}$ and $\hat{n}_{\mathbf{k}}^{v}=v_{\mathbf{k}}^{\dagger}v_{\mathbf{k}}$, for the conduction and valence-band electrons, respectively. Their quantum-mechanical expectation values, $P_{\mathbf{k}}=\langle\hat{P}_{\mathbf{k}}\rangle$, $f_{\mathbf{k}}^{e}=\langle c_{\mathbf{k}}^{\dagger}c_{\mathbf{k}}\rangle$, and $f_{\mathbf{k}}^{h}=1-\langle v_{\mathbf{k}}^{\dagger}v_{\mathbf{k}}\rangle$, relate the operators to the dynamical variables used previously in Sec. III in the semiclassical treatment.

In the following, we focus on the analysis of photoluminescence experiments where carriers are nonresonantly generated in the quantum well by cw or pulsed optical excitation high above the semiconductor band edge. Hence there is no coherent field or intraband polarization generated in the vicinity of the exciton resonances and we can use

$$\langle\hat{P}_{\mathbf{k}}(t_0=0)\rangle=0,\quad \langle b_q(t_0=0)\rangle=0. \tag{47}$$

After their generation, the carriers rapidly relax into quasiequilibrium Fermi-Dirac distributions within their respective bands (Collet *et al.*, 1986; Osman and Ferry, 1987; Pelouch *et al.*, 1992; Jahnke and Koch, 1993, 1995). Starting from the initial condition (47), the equations of motion discussed in Appendix B show that, for $t>t_0$,

$$\langle\hat{P}_{\mathbf{k}}\rangle=\langle b_q\rangle=\langle\hat{n}_{\mathbf{k}}^{c,v}b_q\rangle=\langle b_q\hat{P}_{\mathbf{k}}\rangle=0. \tag{48}$$

Hence we have to determine the incoherent field dynamics from second-order correlations like $\langle b_q^{\dagger}b_q\rangle$ and $\langle b_q^{\dagger}\hat{P}_{\mathbf{k}}\rangle$. These correlations are generated via spontaneous emission, which is genuinely a quantum phenomenon. The equation of motion for $\langle b_q^{\dagger}b_{q'}\rangle$ is obtained from the equation of motion for the photon operators, Eq. (B26),

$$i\hbar\frac{\partial}{\partial t}\langle b_q^{\dagger}b_{q'}\rangle=\hbar(\omega_{q'}-\omega_q)\langle b_q^{\dagger}b_{q'}\rangle+i\mathcal{E}_q\tilde{u}_q\langle b_{q'}\hat{P}\rangle+i\mathcal{E}_{q'}\tilde{u}_{q'}^{*}\langle b_q^{\dagger}\hat{P}\rangle, \tag{49}$$

where $\mathcal{E}_q$ is the vacuum field amplitude, $\hat{P}=\Sigma_{\mathbf{k}}d_{cv}\hat{P}_{\mathbf{k}}+\text{H.c.}$, and $\tilde{u}_q$ is the effective mode strength at the quantum well. The equations of motion for $\langle b_q^{\dagger}\hat{P}_{\mathbf{k}}\rangle$ and $f_{\mathbf{k}}^{e,h}$ can be derived from the quantum operator equations (B26)–(B28) combined with the dynamic decoupling (B33) and condition (48), yielding

$$i\hbar\frac{\partial}{\partial t}\langle b_q^{\dagger}\hat{P}_{\mathbf{k}}\rangle=\left(\epsilon_{\mathbf{k}}^{e}+\epsilon_{\mathbf{k}}^{h}-\hbar\omega_q-\frac{1}{S}\sum_{\mathbf{k}'}V_{\mathbf{k}-\mathbf{k}'}(f_{\mathbf{k}'}^{e}+f_{\mathbf{k}'}^{h})\right)\times\langle b_q^{\dagger}\hat{P}_{\mathbf{k}}\rangle+(f_{\mathbf{k}}^{e}+f_{\mathbf{k}}^{h}-1)\Omega(\mathbf{k},q)+f_{\mathbf{k}}^{e}f_{\mathbf{k}}^{h}\Omega_{SE}(\mathbf{k},q), \tag{50}$$

$$i\hbar\frac{\partial}{\partial t}f_{\mathbf{k}}^{e(h)}=-2i\sum_{q}\text{Im}[d_{cv}^{*}i\mathcal{E}_q\tilde{u}_q^{*}\langle b_q^{\dagger}\hat{P}_{\mathbf{k}}\rangle]. \tag{51}$$

Equations (49)–(51) give a closed set of semiconductor luminescence equations with the renormalized stimulated-emission/absorption term

$$\Omega(\mathbf{k},q)=d_{cv}\langle b_q^{\dagger}\hat{E}_{QW}\rangle+\frac{1}{S}\sum_{\mathbf{k}'}V_{\mathbf{k}-\mathbf{k}'}\langle b_q^{\dagger}\hat{P}_{\mathbf{k}'}\rangle, \tag{52}$$

similar to the renormalized Rabi energy of a classical field discussed in Appendix A. Using Eq. (B30) we can write

[4]See, for example, Andreani *et al.*, 1994; Citrin, 1994b; Savona *et al.*, 1994, 1995; Hanamura *et al.*, 1995; Pau, Björk, Jacobson, Cao, and Yamamoto, 1995a, 1995b; Pau, Björk, Jacobson, and Yamamoto, 1995; Savona and Tassone, 1995; Pau, Björk, Cao, Hanamura, and Yamamoto, 1996; Savasta and Girlanda, 1996a, 1996b.

$$\Omega(\mathbf{k},q)=d_{cv}\Bigg(\sum_{q'} i\mathcal{E}_{q'}\tilde{u}_{q'}\langle b_q^\dagger b_{q'}\rangle - \frac{\int dz|\xi(z)|^4}{\epsilon_0 n^2 S}\sum_{\mathbf{k}'} d_{cv}^*\langle b_q^\dagger \hat{P}_{\mathbf{k}'}\rangle\Bigg) + \sum_{\mathbf{k}'} V_{\mathbf{k}-\mathbf{k}'}\langle b_q^\dagger \hat{P}_{\mathbf{k}'}\rangle, \tag{53}$$

where the first term is the driving contribution due to field correlations and the second and third terms describe its renormalization due to the dipole self-energy and the Coulomb interaction, respectively. In Eq. (50) the rate of spontaneous emission is given by

$$\Omega_{SE}(\mathbf{k},q)=i\mathcal{E}_q\tilde{u}_q d_{cv} \tag{54}$$

in terms of the dipole matrix element d_{cv} of the transition multiplied by the effective mode strength $i\mathcal{E}_q\tilde{u}_q$ at the quantum well position.

The correlation $\langle b_q^\dagger \hat{P}_{\mathbf{k}}\rangle=\langle b_q^\dagger v_{\mathbf{k}}^\dagger c_{\mathbf{k}}\rangle$ gives the amplitude of a process in which an electron-hole pair with zero center-of-mass momentum recombines by emitting a photon with vanishing in-plane momentum, $\mathbf{q}_\parallel=0$. Even if the field-particle and the field-field correlations are initially taken to be zero, correlations start to build up because of the term $f_{\mathbf{k}}^e f_{\mathbf{k}}^h \Omega_{SE}(\mathbf{k},q)$ entering Eq. (50). This driving term is directly associated with spontaneous emission triggering the recombination process. According to the factor $f_{\mathbf{k}}^e f_{\mathbf{k}}^h$, the spontaneous recombination takes place only if an electron and hole are present simultaneously.

Together with the field correlations, the stimulated emission/absorption $\Omega(\mathbf{k},q)$ strongly influences the photoluminescence spectrum. The observed photoluminescence is a result of the interplay of the field-field and field-particle correlations affected by the elementary processes of spontaneous emission and stimulated emission or absorption. The electron-hole recombination nature of the luminescence is seen in the most transparent manner by investigating the carrier and the photon number dynamics of the system. The total change in photon and carrier number is obtained from Eqs. (49) and (51),

$$\frac{\partial}{\partial t}\sum_q \langle b_q^\dagger b_q\rangle = -\frac{\partial}{\partial t}\sum_{\mathbf{k}} f_{\mathbf{k}}^{e,h}, \tag{55}$$

which means that each time one electron-hole pair is recombined, a photon is created.

The semiconductor luminescence equations partially resemble the semiconductor Bloch Eqs. (A33) and (A36) describing the interaction of classical fields with the semiconductor. The semiclassical calculation introduces screening and dephasing due to carrier-carrier scattering and polarization scattering, which are beyond the Hartree-Fock approximation. Such a fully microscopic calculation of photoluminescence remains a major challenge for the future. A solid starting point for such an investigation might be the operator equations (B26)–(B28) because they contain all possible quantum correlations. However, since the full quantum theory can be reduced to semiclassical calculation, these effects can be described relatively well, at least for cw pumping and incoherent excitation, using a screened Coulomb potential and a dephasing rate extracted from an independent quantum-kinetic calculation. This simplifies the quantum calculations considerably, still allowing us to determine the properties of quantized light correlated with matter polarization in great detail. In practice, we replace the bare Coulomb potential of the semiconductor luminescence equations by a screened one. In the dephasing rate approximation, we add to Eq. (50) an additional term $(\Delta E_g - i\gamma)\langle b_q^\dagger \hat{P}_{\mathbf{k}}\rangle$, where $\Delta E_g=\Sigma_{\mathbf{k}}[W_{\mathbf{k}}-V_{\mathbf{k}}]$ is the Coulomb hole energy renormalization and γ is the effective dephasing rate. In practice, the dephasing constant is determined by computing the excitonic absorption spectrum using the Hartree-Fock computation and the full quantum-kinetic method; the dephasing in the Hartree-Fock computation is required to make the excitonic absorption half-width equal to that of the quantum-kinetic approach.

B. Quantum well and microcavity photoluminescence calculations

The field modes $u_q(z)$ entering in a luminescence calculation can be obtained from the transfer-matrix technique discussed in Sec. III.A. These field modes determine whether the electron-hole-pair decay is enhanced or inhibited due to the environment. For the following calculations of luminescence spectra, we use up to 180 discretization points for different q modes for both propagating and counterpropagating modes and 100 k points to describe the many-body dynamics of the carrier system. Numerically, this computation corresponds to solving over 100 time-dependent semiconductor Bloch equations simultaneously, which makes the calculation numerically rather demanding. The dephasing constant is separately determined from the quantum-kinetic calculations of Sec. III.B for each carrier density. For the situation discussed below, the dephasing changes from $\gamma=0.05E_B-0.24E_B$ as the carrier density is increased.

In an experiment, the luminescence spectrum is measured with a detector placed on one side of the microcavity. Therefore our microcavity mode basis is transformed into a detector basis, which relates the detector photon number $\langle d_q^\dagger d_q\rangle$ to $\langle b_q^\dagger b_q\rangle$ via a matrix transformation. For highly symmetrical mirrors, the photon number is practically equal to $\langle b_q^\dagger b_q\rangle$. Since the measured luminescence for stationary emission is proportional to the incoming photon flux, the luminescence intensity spectrum is given by

$$I_{LUM}(q)\propto\frac{\partial}{\partial t}\langle d_q^\dagger d_q\rangle. \tag{56}$$

For a similar definition, see Lindberg and Koch (1989).

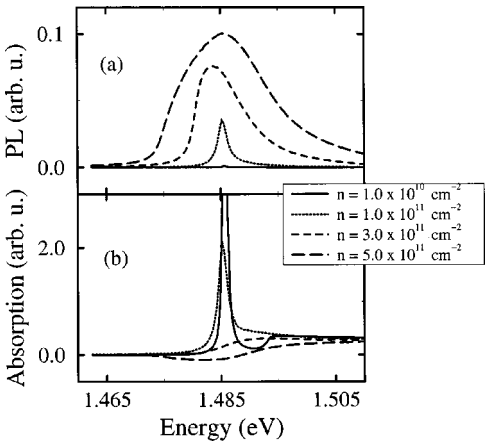

FIG. 32. Calculated luminescence (a) and absorption (b) for a single 8-nm GaAs quantum well and various carrier densities.

In the computations, we start from a situation in which all correlations are initially zero. We numerically evolve Eqs. (49) and (50) to steady state to obtain the cw photoluminescence spectrum. For the carrier distributions we take constant-temperature Fermi-Dirac functions, which must be the steady-state solutions. Then we do not have to treat the carrier occupations dynamically, but we still get the correct steady-state result; however, the approach to equilibrium cannot be used.

As discussed in Sec. IV.A, the stimulated and spontaneous contributions influence the photoluminescence spectrum. The stimulated contribution increases as the mode confinement improves. In the bare-well limit, the stimulated emission/absorption is negligible, since all photons emitted by the quantum well escape the quantum well region rapidly, preventing any back action. Consequently, the bare-well luminescence is obtained from Eqs. (49) and (50) by setting the mode function to its free-space value, $|u_q^0|=1$. Figure 32 shows the steady-state luminescence spectra of a single 8-nm quantum well for various carrier densities, in direct comparison with the corresponding absorption spectra. The photoluminescence spectra have their maxima close to the excitonic absorption peak. Furthermore, the luminescence stays peaked for much higher carrier densities than the excitonic absorption. As the exciton resonance vanishes from the absorption, the quantum well luminescence becomes strongly asymmetric.

The quantum theory presented here provides a consistent interpretation for the photoluminescence which is attributed to quantum-correlated electron-hole recombination processes. The amplitude of a single photon-assisted electron-hole recombination process is determined by $\langle b_q^\dagger v_{\mathbf{k}}^\dagger c_{\mathbf{k}}\rangle$. These events are driven simultaneously by spontaneous emission and stimulated emission or reabsorption of photons. The Coulomb interaction strongly correlates the microscopic recombination processes; at low carrier densities this leads to excitonic resonance enhancements in macroscopic carrier quantities like $\Sigma_{\mathbf{k}} d_{cv}\langle b_q^\dagger \hat{P}_{\mathbf{k}}\rangle$. For high carrier densities, stimulated emission introduces gain to the system, leading to laser operation.

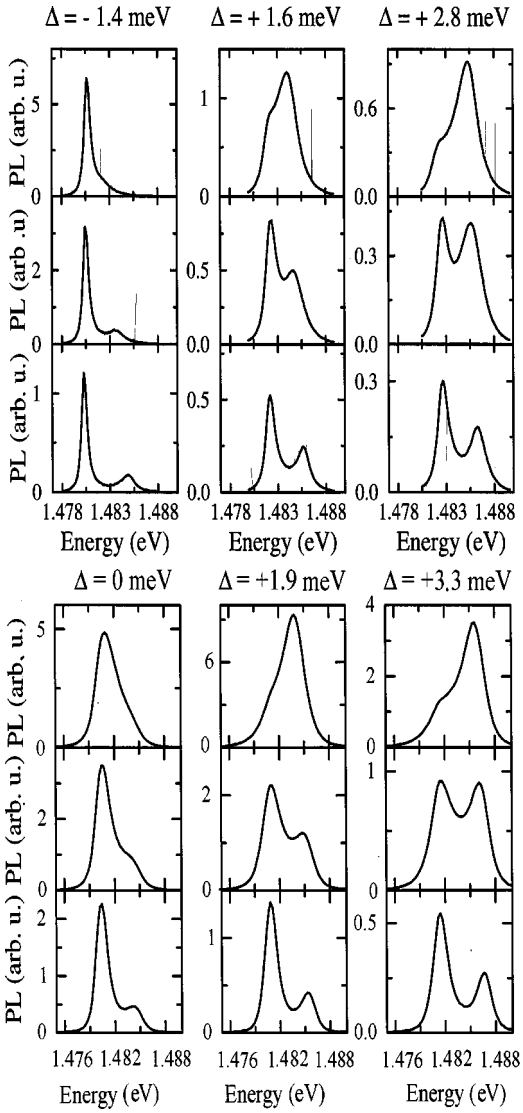

FIG. 33. Photoluminescence spectra for three cavity-exciton detunings Δ: (upper) computed for carrier densities 2.1, 1.7, and $1.25\times10^{11}\,\mathrm{cm}^{-2}$ (from top to bottom), and (lower) measured for different detunings but showing the same behavior.

C. Transitions from normal-mode luminescence to weak-coupling luminescence and onto lasing

In this section, we compare the microscopic calculations to experimental results (Kira, Jahnke, Koch, *et al.*, 1997, 1998). The pump Ti:sapphire laser beam is incident at a 15° angle from normal and focused to a 100-μm-diameter spot on the microcavity sample NMC22. The laser beam is chopped by an acousto-optic modulator into 0.5-μs pulses with a 10% duty cycle to avoid heating the sample, which is kept close to 4 K. Photoluminescence is collected in the normal direction from a small solid angle, $\sim 4\pi\times10^{-3}$ sr, and imaged onto an aperture of area an order of magnitude smaller than the image of the photoluminescence spot. The computed and measured photoluminescence spectra are shown in Fig. 33 for three different carrier densities and cavity-exciton detunings. For a low carrier density (n

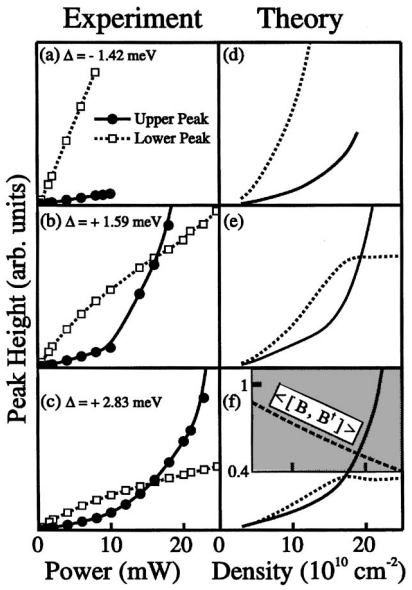

FIG. 34. NMC photoluminescence peak intensities as a function of carrier density. Measured (a)–(c) and calculated (d)–(f) microcavity emission peak intensity vs excitation for different cavity-exciton detunings Δ. The shaded inset in (f) shows the computed average Bosonic commutator.

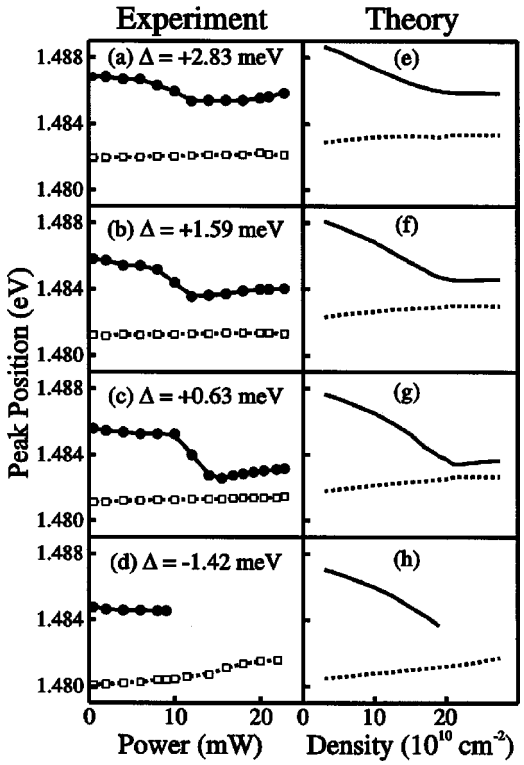

FIG. 35. Microcavity photoluminescence peak energies vs continuous-wave excitation intensity: solid line, for the high-energy peak; dotted line, for the low-energy peak corresponding to Fig. 34.

$=10^{11}\,\mathrm{cm}^{-2}$), all detunings show two normal-mode peaks such that the high-energy peak has a lower intensity. If the detuning is negative, the high-energy peak vanishes as the carrier density is increased. For positive detunings, a transitionlike behavior is observed for elevated excitations; the high-energy peak intensity overtakes the low-energy intensity. Note that the transition carrier densities are still below lasing. Examples of this crossover behavior are shown in Fig. 34. For positive detunings, the low-energy peak height clamps, whereas the high-energy peak grows strongly for elevated carrier densities. For larger detunings, the peak heights cross already for lower excitation levels.

To obtain further insight into the excitation-dependent microcavity photoluminescence, we show in Fig. 35 the energetic positions of the two emission peaks in experiments and theory. For low excitation, all spectra show large NMC splittings that are only weakly detuning dependent. For all positive detunings, the high-energy peak shifts toward the lower-energy peak, whereas the energetic position of the low-energy peak remains nearly constant. As in Fig. 34, the high-energy peak vanishes for negative detuning at higher excitation levels. For positive detunings, the energetic splitting between both peaks decreases before it reaches a basically constant value, which is determined by the cavity-exciton detuning; a strong detuning dependence is observed. This suggests that a transition to the perturbative regime takes place even if the photoluminescence stays double peaked. This might seem contradictory at first, but such a double-peaked emission can result even for a classical emitter in a cavity for detuned emission frequency and cavity resonance. The transition from normal-mode coupling to the weak-coupling regime takes place roughly when the peak heights cross in Fig. 34.

The remarkable crossover of the photoluminescence peak intensities, just explained as electron-hole pairs emitting in an NMC microcavity, was first attributed to ''Boser action'' (Pau, Cao, *et al.*, 1996; Pau, Jacobson, Björk, and Yamamoto, 1996; Yamamoto *et al.*, 1996; Ram *et al.*, 1996; Cao, Pau, Tassone, *et al.*, 1997). A series of theoretical papers (Ram and Imamoglu, 1996; Imamoglu *et al.*, 1996; Imamoglu and Ram, 1996) had argued that if excitons behave as bosons then Bose condensation could occur to the upper branch polaritons, i.e., providing a source for coherent emission from the higher-energy NMC peak. Quoting Ram and Imamoglu (1996): ''The excitons in the boser are generated by an off-resonant, circularly-polarized optical field which creates spin-polarized electron-hole pairs. These subsequently form excitons with large center-of-mass momenta that relax by acoustic phonon emission to populate the [zero center-of-mass in-plane momentum] excitonic state. It is this phonon emission rate into the exciton ground state that is enhanced by final-state stimulation. In an ideal quantum well, only those ground state excitons are able to annihilate by spontaneously emitting photons.'' It was hoped that this condensation would result in coherent light emission at densities lower than those required for conventional laser emission by an electron-hole plasma.

An important component of the ''Boser action'' interpretation is the presence of double peaks in photolumi-

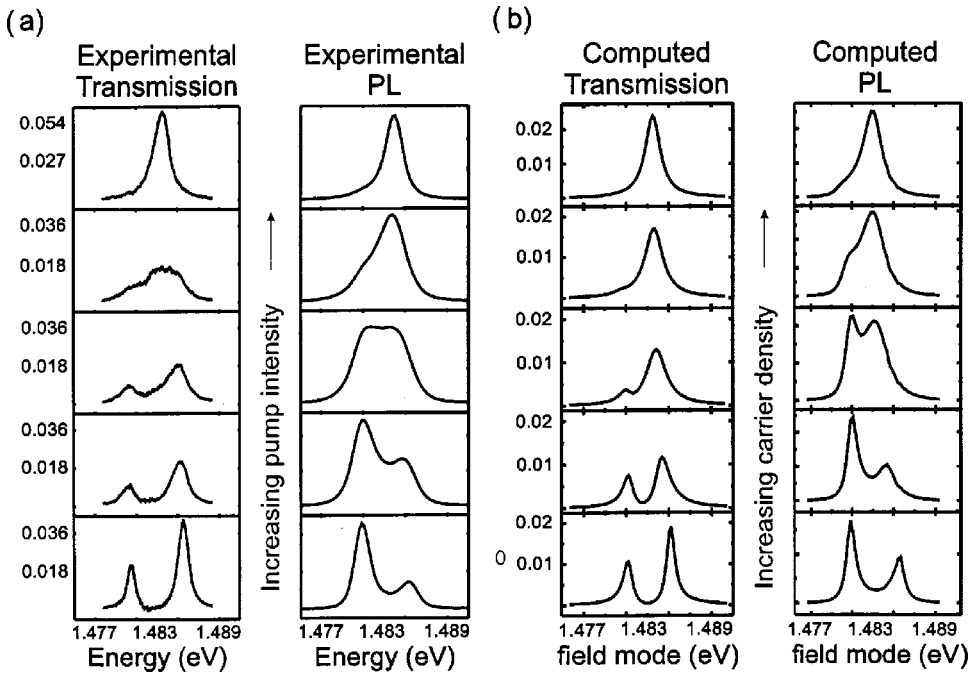

FIG. 36. Transmission and photoluminescence spectra for sample NMC22 and cavity-exciton detuning $\Delta = 1.9$ meV: (a) measured; (b) computed.

nescence, indicating that nonperturbative coupling still exists, when the upper photoluminescence peak overtakes the lower one for increasing carrier density. It was pointed out (Pau, Cao, *et al.*, 1996), however, that the splitting is less than the zero-density value, suggesting that the crossover transition occurs as normal-mode coupling starts to collapse. Both cw and fs experiments (Gibbs *et al.*, 1997; Khitrova *et al.*, 1998; Kira, Jahnke, Koch, *et al.*, 1997; Fan *et al.*, 1997; Cao, Pau, Jacobson, *et al.*, 1997) were performed over a wide range of excitations from very low densities to well above the lasing threshold. Those experiments reproduced the main features of the earlier data leading to the ''Boser'' interpretation and established several facts about the operating range of the ''Boser action.'' Particularly revealing were simultaneous measurements of cw transmission and photoluminescence spectra as a function of excitation level (Nelson, Lindmark, *et al.*, 1996). Examples of the results are shown in Fig. 36. Clearly, the NMC splittings are roughly the same in transmission and photoluminescence, but the peak-height ratios are quite different. Furthermore, the transmission spectra do not show the crossover in peak heights observed in photoluminescence spectra. However, as the upper photoluminescence peak overtakes the lower, the transmission becomes single-peaked. This indicates that the density at crossover is so high that the exciton absorption is largely gone, causing the two transmission peaks in the NMC regime to collapse to a single peak. This is consistent with the fact that the crossover occurs at a density that is only about a factor of 2 lower than the usual electron-hole-plasma lasing threshold density, as shown in Fig. 37. It is also consistent with the density dependence of the splitting shown in Fig. 35; the splitting hardly changes above the crossover density. In fact, lasing finally occurs very close to the frequency of the upper peak emission at crossover.

Compare Fig. 38, the time-integrated photoluminescence after pulsed excitation, with Fig. 36(a), the photoluminescence with cw excitation. One sees that the high-density pulsed data are double-peaked simply because the photoluminescence spectra are time integrated over the decay of the carrier density (Fan *et al.*, 1997). Clearly, for densities below the crossover density, this averaging contributes predominantly to the lower-energy photoluminescence peak. The presence of pronounced double peaks in the pulsed photoluminescence spectra throughout the ''Boser action'' regime, an important part of the argument that nonperturbative coupling still exists (Pau, Cao, *et al.*, 1996), can be seen to be an artifact of the pulsed measurement. Nonetheless the cw measurements show that the photoluminescence spectra can be double peaked even after the transmission becomes single peaked, as discussed above, but the range above crossover is much smaller than for the pulsed data.

Fan *et al.* (1997) suggest that the double-peaked emission after loss of normal-mode coupling can result from the inclusion in the signal of photoluminescence from

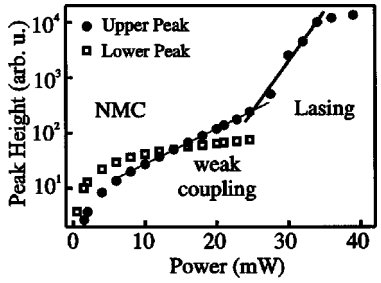

FIG. 37. Peak photoluminescence intensity vs pump power for $\Delta = 4.2$ meV detuning and 100-fs pulse excitation above the cavity stop band. From Kira, Jahnke, Koch, Berger, Wick, Nelson, Khitrova, and Gibbs, 1997.

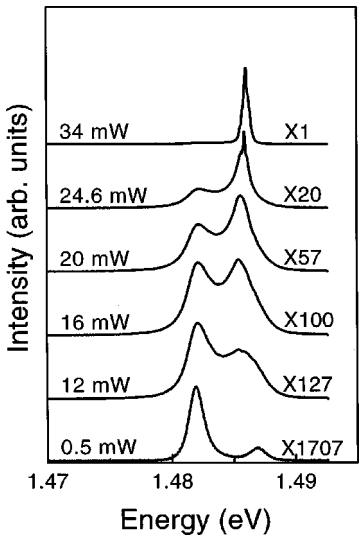

FIG. 38. Time-integrated microcavity photoluminescence spectra for increasing pump power following 100-fs excitation above the cavity stop band with the cavity mode 2.83 meV above the exciton. From Khitrova *et al.*, 1998.

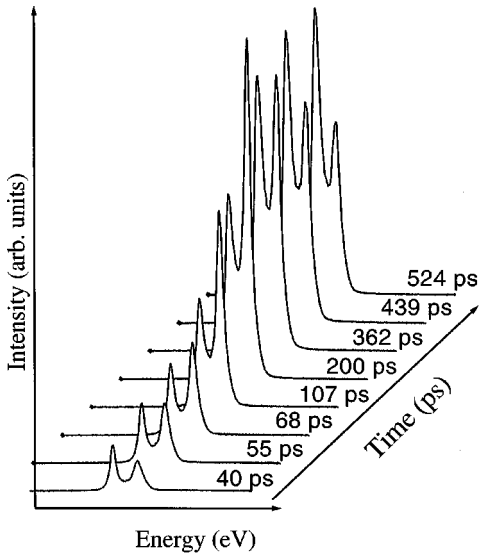

FIG. 39. Time-resolved magnetoexciton NMC photoluminescence spectra at 14 T magnetic field, following femtosecond above-stop band excitation for 1.05-meV positive detuning.

spatial regions of lower carrier density; i.e., a spatial averaging much like the temporal averaging in the pulsed data. Khitrova *et al.* (1998) imaged the photoluminescence output collected within a small solid angle ($4\pi \times 10^{-3}$ sr) onto an aperture that passed only the uniform-excitation 10% central part of the photoluminescence. Without the aperture the double-peaked cw emission did extend to slightly higher excitations; in the data of Figs. 33–37 such effects were avoided by aperturing.

The crossover occurs twice in time-resolved photoluminescence after pulsed excitation (Fig. 39). The intensities cross first as the carriers cool and increase the distribution in the vicinity of the NMC peaks. They cross again as the carriers decay away, and the density drops below the crossover value.

To estimate the validity of the condensation hypothesis let us check the basic assumption of bosonic theories claiming that a fermionic electron and hole form an exciton which can be described with a bosonic operator. The commutator of $1s$-boson operators $[\hat{B}_{00},\hat{B}_{00}^{\dagger}]$ is itself an operator, if one uses Eq. (58). However, the expectation value of the commutator $\langle[\hat{B}_{00},\hat{B}_{00}^{\dagger}]\rangle$ can be determined. This value should be close to unity if the Bosonic approximation is valid. Calculated values for $\langle[\hat{B}_{00},\hat{B}_{00}^{\dagger}]\rangle$ as a function of the carrier density are shown in the inset to Fig. 34 for the same conditions as the photoluminescence spectra. We see that for the elevated carrier densities at which the NMC peaks cross, the commutator varies between 0.7 and 0.4, i.e., far below the ideal bosonic value 1. Hence we conclude that the Bosonic approximation is not valid anymore and that the transition observed in Fig. 34 cannot be attributed to Bosonic properties of electron-hole pairs. Furthermore, both the theoretical and the experimental data show that the collapse of normal-mode coupling to the weak-coupling regime occurs right in the middle of the "Boser action" regime, so that there are no excitons present that could Bose condense.

These thorough theoretical and experimental investigations do not support a Bosonic interpretation. In fact, that explanation for the observed behavior has been retracted (Cao, Pau, Jacobson, *et al.*, 1997). The experimental observations can be explained by the fermionic carrier nonlinearities (phase-space filling, absorption saturation) and cavity effects (see Kira, Jahnke, Koch, Berger, *et al.*, 1997, 1998). The roles of stimulated and spontaneous emission can be separated by performing a computation in which stimulated emission/absorption is switched off, as described in Sec. IV. B. In this case, the computation corresponds to effective decoupling of photoluminescence and normal-mode coupling since the stimulated emission is not present. The computed full and artificial spectra for detuning $\Delta = +3$ meV are plotted in Fig. 40. Without normal-mode coupling, the effect of spontaneous emission is basically that of a classical emitter inside a detuned cavity. Increasing the emission intensity leads to a dramatic increase in the emission at the cavity mode, but only to a weak increase of the emission at the frequency of the detuned emitter. When the term $\langle b_q^{\dagger}\hat{E}_{QW}\rangle$ is switched on, the stimulated term establishes a strong reabsorption of photons for the low-carrier-density case. The reabsorption is much higher for the high-energy peak because it is closer to the empty-cavity mode, which forces the light modes to propagate many roundtrips in the absorbing material. The reabsorption at the high-energy peak is enhanced further because it is energetically closer to the unrenormalized continuum states. For higher carrier densities, the semiconductor absorption is gradually bleached (Fig. 40), reducing the suppression of the high-energy luminescence. As a consequence, the high-energy peak becomes larger

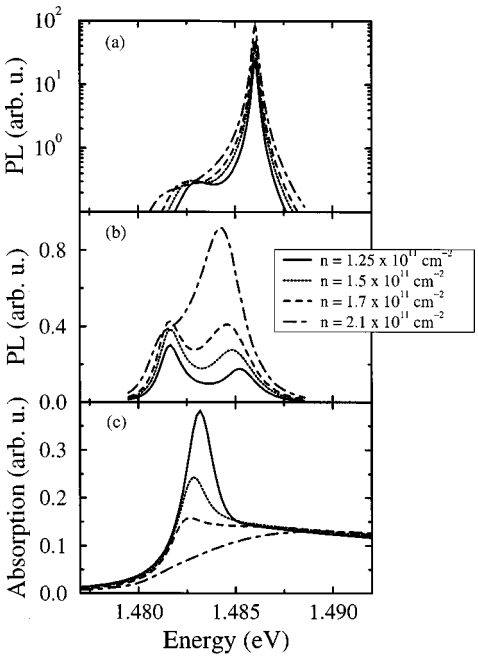

FIG. 40. Photoluminescence spectra for various excitation densities for the detuning $\Delta=3$ meV: (a) from a calculation without the stimulated emission/absorption term causing normal-mode coupling (on a logarithmic scale); (b) from the full calculation; (c) the corresponding excitonic absorption.

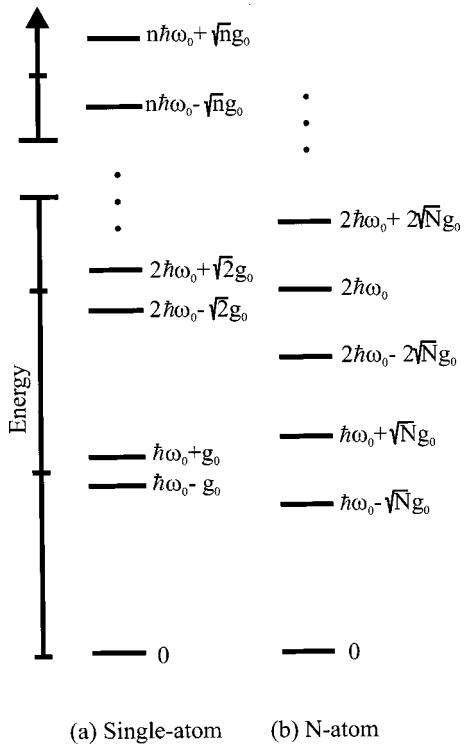

FIG. 41. The first few rungs of the light interaction quantum ladder for (a) a single atom and (b) N atoms.

than the low-energy peak. The bleaching of the exciton also means that the exciton vanishes at the peak height crossing. Thus the system has reached the perturbative regime even before the "Boser" transition. These observations are verified by comparison of transmission and photoluminescence experiments. For positive detunings, the upper branch transmission peak goes continuously from the NMC regime to the perturbative regime, enabling its emission to grow continuously with increased carrier density. In contrast the transmission of the lower branch is attenuated rapidly when normal-mode coupling disappears, inhibiting lower-branch photoluminescence; the increase in carrier density is offset by the increased difficulty of emission.

For very low cw-excitation powers, Senellart and Bloch (1999) have observed another transition in the low-energy photoluminescence intensity when the exciton-cavity detuning is strongly negative. They suggest that the phenomenon can be explained by a Bosonic model that includes phonon-assisted relaxation stimulated by polariton final-state population. However, according to our calculations these results can be explained within the framework of our fermionic quantum theory. The observed transition arises as a consequence of the nonlinear relationship between pump power and generated carrier density under stationary conditions, which can be reproduced by model calculations. Dang *et al.* (1998) offer stimulation of cavity polaritons as one possible explanation for a low-power threshold on the high-energy side of the lower branch in an NMC microcavity containing 16 CdTe quantum wells; our Fermionic quantum theory has not yet been applied to that case.

V. CONCLUSIONS AND FUTURE DIRECTIONS

A. Quantum-statistical limit

Since strong light-matter coupling effects are important in microcavity systems, we briefly outline in this section some aspects of the quantum-statistical limit known from atomic physics. In the field of experimental atomic cavity quantum electrodynamics it was an important goal for some time to observe the second rung of the Jaynes-Cummings ladder (Jaynes and Cummings, 1963) for the single-atom strong-coupling regime. This was seen in 1996 by Haroche's group (Brune *et al.*, 1996).

For a single two-level-atom system, the Jaynes-Cummings interaction Hamiltonian is

$$H_{atom}=g_0(b_q\sigma^+ + b_q^\dagger\sigma^-), \tag{57}$$

where the vacuum field amplitude $\mathcal{E}_{vac}=\sqrt{\hbar\omega/2\varepsilon_0 V}$ and dipole matrix element d determine the coupling constant $g_0=d\mathcal{E}_{vac}$. Here, σ^+ raises the atom from the ground state $|g\rangle$ to the excited state $|e\rangle$, and σ^- lowers it from the excited state $|e\rangle$ to the ground state $|g\rangle$. The system dynamics takes place within the states $|n\rangle|e\rangle$ and $|n+1\rangle|g\rangle$, where $|n\rangle$ is a photon number state. If the atom and the cavity systems are in resonance, a wave-function solution $|\psi\rangle=C_n(t)|n\rangle|e\rangle+C_{n+1}(t)|n+1\rangle|g\rangle$ leads to two discrete energy levels with energy difference $\Omega_n=2\sqrt{n+1}g_0$. The energetic level structure of such a system is often called a single-atom quantum ladder; see Fig. 41(a).

If the coupling g_0 of a single atom exceeds the cavity

damping and the dipole dephasing rates, then vacuum field Rabi splitting can be seen with a single atom. This is the regime of strong coupling in which a single photon can change the transmission of the coupled cavity-atom system. If a large number N of identical atoms all interact with a single mode of a cavity, then they give rise to a splitting $2\sqrt{N}g_0$; this is the regime of nonperturbative normal-mode coupling [Fig. 41(b); Haroche, 1984, 1992; Kimble, 1994; Raimond and Haroche, 1995]. The first excited rungs on the single-atom and many-atom ladders look alike in that both consist of two states (split by $2g_0$ and $2\sqrt{N}g_0$, respectively). The second rung on the single-atom ladder consists of two states split by $2\sqrt{2}g_0$, so that transitions from the first and second rungs differ from those from the zeroth (ground) to the first rungs. In contrast, the second rung of the many-atom ladder consists of three states with energies $2\hbar\omega_0$ and $2\hbar\omega_0 \pm 2\sqrt{N}g_0$. As a result the transition energies are the same from the first and second as from the zeroth to the first. Thus no new frequencies appear in the spectrum to help determine how high one is on the many-atom quantum ladder. It has been shown (Carmichael *et al.*, 1994) that the many-atom case (described by a semiclassical theory) and the single-atom case (described by the Jaynes-Cummings model) give the same doublet splitting (multiplied by $\sqrt{N}$ for N atoms) for a weak probe field. In both cases the equations resemble those of two coupled oscillators, i.e., semiclassical calculations give correct answers. To see the difference between the semiclassical behavior of a many-atom system and the genuine quantum behavior of a single-atom system, one has to perform nonlinear experiments. Only for the quantum system will one obtain ''ladder effects.'' So the goals were clear, though difficult to achieve, for the atomic world. At least they had distinguishable ladders.

Life is much more complicated for the semiconductor community. Whereas for the atom-light interaction problem the Jaynes-Cummings Hamiltonian was easy to diagonalize, yielding the dressed states, i.e., the new eigenstates with the atom-light interaction, we saw in Secs. III and IV that because of the Coulomb interaction the diagonalization of an interacting electron system in a semiconductor is not possible. This Coulomb many-body problem is an essential part of semiconductor physics.

In the past, a simplified treatment was often used based on the approximation of the full semiconductor electron-hole Hamiltonian by a boson Hamiltonian, to which high-density effects were added phenomenologically. This Hamiltonian led to results similar to the Jaynes-Cummings model. To obtain this Hamiltonian, electron-hole-pair operators were replaced by exciton operators $B^\dagger_{\nu,\mathbf{K}}$,

$$B^\dagger_{\nu,\mathbf{K}} = \sum_{\mathbf{k}} \psi_\nu(\mathbf{k}) c^\dagger_{\mathbf{k}+\mathbf{K}/2} v_{\mathbf{k}-\mathbf{K}/2}, \tag{58}$$

where $\psi_\nu(\mathbf{k})$ is the relative motion exciton wave function with quantum number ν, and $c^\dagger_{\mathbf{k}} v_{\mathbf{k}'}$ describes the creation of a conduction-band electron and annihilation of a valence-band electron (Haug and Koch, 1994). Thus the operators $B^\dagger_{\nu,\mathbf{K}}$ represent the creation of an exciton with center-of-mass momentum $\mathbf{K}$. Starting from a first-principles Hamiltonian in the electron hole picture, as discussed in Appendixes A and B, one can introduce exciton operators without approximations only in the light-matter-interaction Hamiltonian and a simplified Coulomb Hamiltonian. However, the reduction of the Coulomb interaction between carriers to bosonic excitons represents only a subset of possible processes in the nonlinear regime. Important fermionic effects like phase-space filling, screening, and dephasing are poorly approximated. Also a description of the interplay between excitons and free carriers is no longer possible. Experimentally it is difficult to avoid the excitation of free carriers, even for excitation at the exciton resonance, due to various interaction processes. On the other hand, excitonic luminescence is not an unambiguous signature of bound excitons but equally possible due to recombination of Coulomb correlated carriers of an electron-hole plasma (Kira, Jahnke, and Koch, 1998), as discussed in Sec. IV.

Since the bosonic Hamiltonian is strictly valid only in the linear regime, its predictions are not reliable in the nonlinear regime, where quantum ladder effects occur. Hence quantum effects of the nonlinear exciton system usually cannot simply be handled by models of the Jaynes-Cummings type. Clearly it is mathematically correct to expand all pair wave functions into an exciton basis. However, important nondiagonal coupling elements occur which cannot be approximated simply by keeping only the first bound-exciton contribution. The proper inclusion of screening effects, fermionic phase-space filling, interaction-induced dephasing, etc., in the exciton description remains a challenging problem for the future.

In Sec. III.B.2 evidence was given that present-day NMC microcavities are far from the quantum-statistical limit. Even if through clever techniques the semiconductor quantum limit is achieved one day, it is at least currently not well understood what its genuine signatures and quantum effects will be. Nonetheless, note that the quantum-statistical regime of true strong coupling, where a single pump photon already changes the optical properties for a probe photon, is conceivable with a single quantum dot in a transversely confined microcavity. Consider a nanocavity with cavity-mode volume of $1\lambda^3$ (Huffaker *et al.*, 1998); already Gutbrod *et al.* (1998) report a 2-meV NMC splitting for a quantum well in a 1.2-μm-diameter ''photon dot.'' Assume that the quantum dot comes from a monolayer fluctuation (Gammon *et al.*, 1996a); Bonadeo *et al.* (1998) have performed nonlinear optical experiments on such a dot and concluded that it behaves like an atom with dephasing dominated by radiative decay. The parameters of Gammon *et al.* (1996b) yield a single-oscillator NMC splitting of $2g_0 = 140\,\mu$eV, i.e., larger than the NMC FWHM linewidth $(\gamma + \delta_c) = (11.5 + 55)\,\mu\text{eV} \approx 66\,\mu\text{eV}$ for a mirror reflectivity of 0.998. This quantum-dot nanocavity Q needed for $\delta_c \leq g_0$ is much smaller than that for a single Cs atom (Hood *et al.*, 1998; Kimble, 1998) because both

the dipole moment and the vacuum field are $\approx 12\times$ larger. It will be exciting if quantum features, such as entanglement, and the quantum-classical boundary (Haroche and Raimond, 1996; Haroche, 1998) can be observed and studied with a quantum-dot nanocavity.

B. Directional dependence of microcavity emission

Experimental observations show that one may have more than two peaks under normal-mode-coupling conditions. These peaks occur in the vicinity of zero detuning for both single-pulse and pump-probe transmission experiments.

According to our current understanding, the occurrence of a three- or more-peaked NMC spectrum can be attributed to the coupling of the fundamental cavity mode to guided or leaky modes of the microcavity. The fundamental cavity mode, which on its own results in the usual double-peaked NMC spectrum, therefore acquires contributions particularly from those guided or leaky modes that have a high amplitude at the quantum-well position. Therefore the resulting spectra are not only determined by the fundamental mode, but contain information about the complex 3D mode structure of the cavity by showing additional signatures. This mode coupling can be mediated either by static disorder in the quantum well or by higher-order quantum correlations; currently both mechanisms are under investigation.

Since the full 3D mode structure influences the light-matter coupling, it will be interesting to study structures in which the optical modes are controlled in more than one dimension (Björk *et al.*, 1993; Bloch *et al.*, 1997; Ohnesorge *et al.*, 1997; Gutbrod *et al.*, 1998). Noteworthy developments in this context are the so-called photonic band-gap materials (Yablonovitch, 1987; 1993; Labilloy *et al.*, 1997) which may also be fabricated around semiconductor microcavities. The study of NMC effects in such systems promises to be an interesting research field in the near future.

C. What other questions remain open?

In Ell *et al.* (1998) it was shown that the reflectivity, which was calculated using linear dispersion (transfer-matrix) theory and the experimentally reconstructed quantum well susceptibility, agrees well with the measured linear reflectivity of an NMC microcavity; see also Ell *et al.* (1999). So-called motional narrowing, i.e., wave-function averaging over the structural disorder, is not enhanced by microcavity effects in presently investigated samples [as suggested by Whittaker *et al.* (1996) and Savona *et al.* (1997) and retracted by Whittaker (1998)]. The NMC linewidth puzzles that led to this suggestion, namely, that the lower branch linewidth is always smaller than that of the upper branch and often less than the mean of the cavity and total exciton linewidths, as expected for a homogeneously broadened oscillator, turned out to be explicable as the effect of disorder-induced quantum-well line-shape asymmetry much like the example of Fig. 7. However, the possibility that linewidth averaging is improved and dephasing processes reduced within a microcavity continues to be a subject of intense investigations (Baumberg *et al.*, 1998) with relevance to the open problem of excitonic Bose condensation in semiconductors. There is no question that ideally light propagation and all interactions within the quantum wells should be included on an equal footing (simultaneously). Clearly, nonlinear pulse propagation modeling requires the full solution of the coupled light-matter equations. Model calculations for NMC in strongly disordered structures show signatures, such as the three-peak spectrum mentioned above, which cannot be explained using linear dispersion theory (Grote *et al.*, 1999).

Interesting recent experimental observations include the following: selective resonant tunneling into a microcavity exciton-polariton state (Klimovitch *et al.*, 1997; Cao, Klimovitch, Björk, and Yamamoto, 1995a, 1995b); the claim of a transition from NMC to the ac Stark triplet (Quochi *et al.*, 1997, 1998); time-resolved four-wave mixing (Koch, 1997; Koch *et al.*, 1998) and spectral interferometry (Huang *et al.*, 1997) to determine the phase of microcavity coherent reemission; the use of phase-controlled pulses for coherent control (Lee *et al.*, 1998); strong polarization dependences of degenerate four-wave mixing and transient pump-probe experiments (Kuwata-Gonokami *et al.*, 1997; Fan *et al.*, 1998); NMC studies on materials with large exciton binding energies, such as II-VI semiconductors (Kelkar *et al.*, 1997; Bleuse *et al.*, 1998); studies in which radiative coupling effects (super radiance) dominate the behavior of both quantum wells spaced by half wavelengths (Bragg structures) and NMC microcavities;[5] and resonant Raman scattering (Fainstein *et al.*, 1997; Savasta *et al.*, 1997; Tribe *et al.*, 1997). It remains to be seen if and to what degree of accuracy these experimental observations can be explained by current theories or if additional microscopic effects have to be included.

In conclusion, this article reviews detailed experiments and a comprehensive theoretical analysis of light-semiconductor interaction effects. Both linear and nonlinear NMC behaviors have been described on the basis of the fermionic many-body theory. The comparison of experiments and theory clearly shows that nonclassical effects, i.e., truly quantum-statistical or quantum-mechanical light correlation effects, have not yet been observed in state-of-the-art semiconductor microcavity systems. Neither has pure exciton lasing been observed, nor has an example been found in the linear regime where light propagation effects significantly modify microscopic interactions affecting only the carriers in the quantum well. Even though answers have been given herein to many of the questions posed in the first section of this article, many interesting and challenging prob-

[5]Numerous publications include those of Andreani *et al.*, 1991; Ivchenko, 1991; Andreani, 1994, 1995a; Björk *et al.*, 1994, 1995, 1996; Ivchenko *et al.*, 1994b; Haas *et al.*, 1998; Hubner *et al.*, 1998.

lems still await a final answer. Hence the subfield of semiconductor microcavity optics can be expected to yield many new results in the future.

ACKNOWLEDGMENTS

The Tucson group thanks AFOSR/DARPA, NSF (AMOP, DMR, and ECS/EPDT), DARPA/ARO, and JSOP (AFOSR and ARO) for support and Claudia Ell for multiple contributions. The Marburg group acknowledges support through the Leibniz prize (S.W.K.) and the Heisenberg program (F.J.) from the Deutsche Forschungsgemeinschaft, and a grant for CPU time at the Forschungszentrum Jülich. M.K. acknowledges an EC fellowship.

APPENDIX A: EXCITATION DYNAMICS IN QUANTUM WELLS

For a semiclassical treatment of the light-matter interaction in quantum wells one has to determine the linear or nonlinear quantum well polarization which enters in the wave equation for the optical field. In this appendix we outline calculation schemes based on a microscopic semiconductor theory. Starting from the Hamiltonian of the interacting electron-hole system, we derive equations of motion for the density-matrix elements in a quantum well Bloch basis.

For the weak-field regime, the theory yields the field-independent optical quantum well susceptibility used in Secs. III.A.2 and III.A.3. As a next step, the density-dependent exciton saturation for increasing incoherent plasma excitation, discussed in Sec. III.B, is included in the calculation of the optical susceptibility. For a treatment of field-induced nonlinearities in Sec. III.C, the theory is further extended to include the coupled dynamics of the semiconductor density-matrix elements.

1. Semiconductor density matrix

The excitation dynamics of semiconductor quantum wells can be treated in terms of a single-particle density matrix,

$$\rho(\mathbf{r},\mathbf{r}',t)=\langle\Psi^{\dagger}(\mathbf{r},t)\Psi(\mathbf{r}',t)\rangle, \tag{A1}$$

with the Heisenberg picture field operators $\Psi^{\dagger}(\mathbf{r},t)$ and $\Psi(\mathbf{r},t)$ creating and annihilating a semiconductor electron at position $\mathbf{r}$ and time t, respectively. In a Bloch basis, the field operators are expanded according to

$$\Psi(\mathbf{r},t)=\sum_{\nu,\mathbf{k}} a_{\nu}(\mathbf{k},t)\,\phi_{\nu,\mathbf{k}}(\mathbf{r}), \tag{A2}$$

where $a_{\nu}(\mathbf{k},t)$ is the annihilation operator of an electron in the state $\mathbf{k},\nu$. The wave functions of quantum well electrons can be given in an envelope function approximation (Bastard, 1988):

$$\phi_{\nu,\mathbf{k}}(\mathbf{r})=\xi_{\nu}(z)\,\frac{1}{\sqrt{S}}e^{i\mathbf{k}\cdot\boldsymbol{\rho}}u_{\lambda}(\mathbf{r}), \tag{A3}$$

describing a free motion within the quantum well plane, with the momentum $\mathbf{k}$ and carrier confinement in the direction of growth in terms of the envelope function $\xi_{\nu}(z)$. The Bloch wave functions are normalized with respect to the area S of the well, and $\boldsymbol{\rho}=(x,y)$ is the space vector in the quantum well plane. The additional quantum number $\nu=(\lambda,n)$ includes the band index $\lambda=c,v$ and the quantum well subband index n. $u_{\lambda}(\mathbf{r})$ is the lattice-periodic Bloch function.

The macroscopic polarization, which acts as a sink or source for light propagation through the quantum well is given by the dipole density

$$\mathbf{P}(t)=\frac{1}{SL}\int d^3r\,\rho(\mathbf{r},\mathbf{r},t)e\mathbf{r}, \tag{A4}$$

where L is the thickness of the quantum well. To formulate the macroscopic polarization in the Bloch basis, we use Eqs. (A1)–(A3) and rewrite the integral in Eq. (A4) as a sum of integrals over the crystal unit cells (Haug and Koch, 1994). The resulting polarization,

$$\mathbf{P}(t)=\frac{1}{S}\sum_{\mathbf{k}}\sum_{\nu,\nu'}\mathbf{d}_{\lambda,\lambda'}\langle a_{\nu}^{\dagger}(\mathbf{k},t)a_{\nu'}(\mathbf{k},t)\rangle\,\frac{1}{L}\times\int dz\,\xi_{\nu}^{*}(z)\xi_{\nu'}(z), \tag{A5}$$

contains all allowed interband dipole transitions for various $\mathbf{k}$ states. With the Bloch functions u, we can introduce the dipole matrix element,

$$\mathbf{d}_{\lambda,\lambda'}=\frac{1}{V_i}\int_{V_i}d^3r\,u_{\lambda}^{*}(\mathbf{r})e\mathbf{r}u_{\lambda'}(\mathbf{r}), \tag{A6}$$

where the integral has to be extended over the volume V_i of a crystal unit cell. Since for GaAs-like materials the Bloch functions are *s*-like and *p*-like for conduction and valence band states near the band edge, respectively, the dipole coupling involves only interband transitions and $\mathbf{d}_{cc}=\mathbf{d}_{vv}=0$. Possible transitions between the corresponding subbands are selected by the integral over envelope functions in Eq. (A5). The transition probabilities are described by expectation values of creation and annihilation operators with different band indexes. In a similar way, the excitation density $n_{\nu}(t)$ in the band/subband ν,

$$n_{\nu}(t)=\frac{1}{S}\sum_{\mathbf{k}}\langle a_{\nu}^{\dagger}(\mathbf{k},t)a_{\nu}(\mathbf{k},t)\rangle, \tag{A7}$$

can be traced back to band-diagonal expectation values of Bloch operators. Restricting our analysis to the lowest quantum well subband $n=1$, we find that the density matrix in the Bloch representation reduces to a 2×2 matrix in the band index $\lambda=c,v$. We introduce the simplified notation

$$a_{c,n}(\mathbf{k})=c_{\mathbf{k}},\quad a_{v,n}(\mathbf{k})=v_{\mathbf{k}} \tag{A8}$$

to distinguish the two band from the general multiband version of the theory, where we use $a_{\nu}(\mathbf{k})$, from the two-band version with the annihilation operators

$c_{\mathbf{k}}$ ($v_{\mathbf{k}}$) for conduction (valence) band electrons. Then we obtain for the two-band density matrix

$$\begin{pmatrix} \langle c_{\mathbf{k}}^{\dagger}(t)\ c_{\mathbf{k}}(t)\rangle & \langle v_{\mathbf{k}}^{\dagger}(t)\ c_{\mathbf{k}}(t)\rangle \\ \langle c_{\mathbf{k}}^{\dagger}(t)\ v_{\mathbf{k}}(t)\rangle & \langle v_{\mathbf{k}}^{\dagger}(t)\ v_{\mathbf{k}}(t)\rangle \end{pmatrix} = \begin{pmatrix} f_{\mathbf{k}}^{e}(t) & P_{\mathbf{k}}(t) \\ P_{\mathbf{k}}^{*}(t) & 1-f_{\mathbf{k}}^{h}(t) \end{pmatrix}, \tag{A9}$$

with the momentum-dependent electron and hole distribution functions $f_{\mathbf{k}}^{e,h}$ and the coherent interband polarization $P_{\mathbf{k}}$. In terms of these density-matrix elements, the quantum well polarization is given by

$$\mathbf{P}_{QW}(t)=\frac{1}{S}\sum_{\mathbf{k}}\mathbf{d}_{vc}P_{\mathbf{k}}(t)+\text{c.c.}, \tag{A10}$$

with $\mathbf{P}_{QW}(z,t)=\mathbf{P}_{QW}(t)|\xi(z)|^2$, and the excitation density follows from

$$n_a(t)=\frac{1}{S}\sum_{\mathbf{k}} f_{\mathbf{k}}^{a}(t). \tag{A11}$$

2. Hamiltonian

Equations of motion for the density-matrix elements can be derived from the Hamiltonian of the interacting carrier system,

$$H=H_0+H_{coul}+H_{light}. \tag{A12}$$

The free motion of carriers in the periodic lattice potential V_G follows from

$$H_0=\int d^3r\,\Psi^{\dagger}(\mathbf{r},t)\left[\frac{\hbar^2}{2m}\Delta+V_G(\mathbf{r})\right]\Psi(\mathbf{r},t). \tag{A13}$$

In transverse or Coulomb gauge, the Coulomb interaction between carriers,

$$H_{coul}=\frac{1}{2}\int d^3r\,d^3r'\,\Psi^{\dagger}(\mathbf{r},t)\Psi^{\dagger}(\mathbf{r}',t)v(\mathbf{r}-\mathbf{r}') \times\Psi(\mathbf{r}',t)\Psi(\mathbf{r},t), \tag{A14}$$

with the bare Coulomb potential $v(\mathbf{r})=(e^2/4\pi\epsilon_0)(1/|\mathbf{r}|)$ represents the contribution of the longitudinal electromagnetic field. The interaction of carriers with the transverse part of the electromagnetic field is described by the dipole Hamiltonian

$$H_{light}=\int d^3r\,\Psi^{\dagger}(\mathbf{r},t)[-e\mathbf{r}]\cdot\mathbf{E}(\mathbf{r},t)\Psi(\mathbf{r},t). \tag{A15}$$

In this appendix and in Sec. III we treat the light field in semiclassical approximation, whereas in Appendix B and Sec. IV a quantized light field will be introduced. Using Eqs. (A2) and (A3), we can reformulate the Hamiltonian in the Bloch basis. Then in the free-carrier Hamiltonian,

$$H_0=\sum_{\nu,\mathbf{k}}\epsilon_{\mathbf{k}}^{\nu}a_{\nu}^{\dagger}(\mathbf{k},t)a_{\nu}(\mathbf{k},t), \tag{A16}$$

we find the single-particle energies $\epsilon_{\mathbf{k}}^{c,n}=\epsilon_{\mathbf{k}}^{e,n}$ and $\epsilon_{\mathbf{k}}^{v,n}=-\epsilon_{\mathbf{k}}^{h,n}$ for electrons and holes, respectively. Correspondingly, the Coulomb Hamiltonian becomes

$$H_{coul}=\sum_{\nu_1,\ldots,\nu_4}\sum_{\mathbf{k}',\mathbf{k}'',\boldsymbol{\kappa}} a_{\nu_1}^{\dagger}(\mathbf{k}',t)a_{\nu_2}^{\dagger}(\mathbf{k}'',t)a_{\nu_3}(\mathbf{k}''-\boldsymbol{\kappa},t) \times a_{\nu_4}(\mathbf{k}'+\boldsymbol{\kappa},t)v_{\nu_1,\ldots,\nu_4}(\kappa). \tag{A17}$$

Here

$$v_{\nu_1,\ldots,\nu_4}(\kappa)=\delta_{\lambda_1,\lambda_4}\delta_{\lambda_2,\lambda_3}\int dz\,dz'\,\xi_{\nu_1}(z)\xi_{\nu_2}(z') \times\frac{e^2}{2\epsilon_0\kappa}e^{-\kappa|z-z'|}\xi_{\nu_3}(z')\xi_{\nu_4}(z) \tag{A18}$$

is the quantum well Coulomb matrix element, and $(e^2/2\epsilon_0\kappa)e^{-\kappa|z-z'|}$ is the 2D Fourier transform of the bare Coulomb potential $v(\mathbf{r}-\mathbf{r}')$. For the Hamiltonian of the carrier-light interaction we obtain

$$H_{light}=\sum_{\nu\neq\nu'}\sum_{\mathbf{k},\mathbf{q}} a_{\nu}^{\dagger}(\mathbf{k},t)a_{\nu'}(\mathbf{k}-\mathbf{q}_{\parallel},t)\mathbf{d}_{\lambda,\lambda'}\mathbf{E}_{\nu,\nu'}(\mathbf{q},t), \tag{A19}$$

where $\mathbf{d}_{\lambda,\lambda'}$ is the dipole matrix element. The quantum well matrix element of the field,

$$\mathbf{E}_{\nu,\nu'}(\mathbf{q},t)=\int dz\,\xi_{\nu}^{*}(z)\xi_{\nu'}(z)\mathbf{E}(\mathbf{q}_{\parallel},z,t), \tag{A20}$$

contains the 2D Fourier transform of the field $\mathbf{E}(\mathbf{q}_{\parallel},z,t)$ which is defined through

$$\mathbf{E}(\mathbf{r},t)=\mathbf{E}(\boldsymbol{\rho},z,t)=\frac{1}{S}\sum_{\mathbf{q}_{\parallel}}e^{i\mathbf{q}_{\parallel}\cdot\boldsymbol{\rho}}\mathbf{E}(\mathbf{q}_{\parallel},z,t), \tag{A21}$$

with the in-plane photon momentum $\mathbf{q}_{\parallel}$ both outside and inside the medium. As an important result of the introduction of the quantum well Bloch basis, the overlap integral of the field with the carrier confinement wave functions determines the interaction of the light field with the corresponding bands and subbands. Similarly, the carrier-carrier interaction is determined by quantum well matrix elements of the Coulomb potential.

In the following, we restrict our analysis to the case of normal incidence of the external field, i.e., vanishing in-plane photon momentum $\mathbf{q}_{\parallel}$ (cf. Sec. III.A). In the limit of strong carrier confinement (narrow quantum wells with large subband spacing), we assume that the laser field is only resonant with the lowest quantum well subband. For excitation close to the band edge, the corresponding free-carrier energies will be used in parabolic approximation,

$$\epsilon_{\mathbf{k}}^{a,n}=\frac{E_G}{2}+\frac{\hbar^2}{2m_a}k^2+E_n, \tag{A22}$$

with the electron-hole index $a=e,h$ and reduced mass m_a; E_G and E_n are the band-gap energy and the subband confinement energy, respectively. The inclusion of band-mixing effects in the theory presented here is discussed, for example, by Girndt *et al.* (1997).

3. Equations of motion

Equations of motion for the density-matrix elements (A9) can be directly derived using the Heisenberg equations of motion for the carrier annihilation and creation operators,

$$i\hbar \frac{\partial}{\partial t} a_\nu(\mathbf{k}) = [a_\nu(\mathbf{k}), H]. \tag{A23}$$

From the free-carrier Hamiltonian H_0 as well as the Hamiltonian for the carrier-light interaction H_{light}, we obtain on the operator level

$$i\hbar \frac{\partial}{\partial t} v_{\mathbf{k}}^\dagger c_{\mathbf{k}} = (\varepsilon_{\mathbf{k}}^e - \varepsilon_{\mathbf{k}}^v) v_{\mathbf{k}}^\dagger c_{\mathbf{k}} - \mathbf{d}_{cv} \mathbf{E}_{QW} (c_{\mathbf{k}}^\dagger c_{\mathbf{k}} - v_{\mathbf{k}}^\dagger v_{\mathbf{k}}), \tag{A24}$$

$$i\hbar \frac{\partial}{\partial t} c_{\mathbf{k}}^\dagger c_{\mathbf{k}} = \mathbf{d}_{cv}^* \mathbf{E}_{QW} v_{\mathbf{k}}^\dagger c_{\mathbf{k}} - \text{H.c.} \tag{A25}$$

Since H_0 and H_{light} are single-particle operators, these equations of motion for bilinear operators contain only bilinear operators on the right side. Taking the expectation value of Eqs. (A24) and (A25) leads to a closed set of equations for the density-matrix elements. Using the electron-hole picture, we obtain optical Bloch equations for the interband polarization $P_{\mathbf{k}} = \langle v_{\mathbf{k}}^\dagger c_{\mathbf{k}} \rangle$,

$$\left[i\hbar \frac{\partial}{\partial t} - \varepsilon_{\mathbf{k}}^e(t) - \varepsilon_{\mathbf{k}}^h(t) \right] P_{\mathbf{k}}(t) + [1 - f_{\mathbf{k}}^e(t) - f_{\mathbf{k}}^h(t)] \Omega_{\mathbf{k}}(t) = 0, \tag{A26}$$

and for the occupation probabilities of electrons $f_{\mathbf{k}}^e = \langle c_{\mathbf{k}}^\dagger c_{\mathbf{k}} \rangle$ and holes $f_{\mathbf{k}}^h = 1 - \langle v_{\mathbf{k}}^\dagger v_{\mathbf{k}} \rangle$,

$$i\hbar \frac{\partial}{\partial t} f_{\mathbf{k}}^a(t) + \Omega_{\mathbf{k}}(t) P_{\mathbf{k}}^*(t) - \Omega_{\mathbf{k}}^*(t) P_{\mathbf{k}}(t) = 0, \tag{A27}$$

with the electron-hole index $a = e,h$. Equations (A26) and (A27) resemble the conventional atomic density-matrix equations. Every $\mathbf{k}$ state corresponds to a two-level system in which the transition energy $\varepsilon_{\mathbf{k}}^a(t) = \epsilon_{\mathbf{k}}^a$ is optically driven by the Rabi energy $\Omega_{\mathbf{k}}(t) = \mathbf{d}_{cv} \mathbf{E}_{QW}(t)$. Dephasing of the interband polarization (off-diagonal density-matrix elements) and nonradiative depletion of the occupation (diagonal density-matrix elements) are not included on this level. In atomic systems, dissipation is often introduced by coupling the two-level system to a reservoir. In semiconductors, a large number of two-level transitions corresponding to various $\mathbf{k}$ states is mutually coupled by the Coulomb interaction. A microscopic description of this interaction provides both dephasing of the interband polarization and redistribution of carriers between various $\mathbf{k}$ states. However, dephasing and scattering follow only from a treatment of the Coulomb interaction beyond the mean-field approximation, to be discussed in Secs. A.4 and A.5 of this appendix.

The Coulomb Hamiltonian H_{coul} is a two-particle operator and its inclusion leads to the hierarchy problem. From the Heisenberg equation of motion and H_{coul} we obtain

$$\begin{aligned} \left[i\hbar \frac{\partial}{\partial t} v_{\mathbf{k}}^\dagger c_{\mathbf{k}} \right]_{coul} = \frac{1}{S} \sum_{\mathbf{k}',\mathbf{k}''} V_{\mathbf{k}-\mathbf{k}'} [& v_{\mathbf{k}}^\dagger (c_{\mathbf{k}'+\mathbf{k}''-\mathbf{k}}^\dagger c_{\mathbf{k}''} \\ & + v_{\mathbf{k}'+\mathbf{k}''-\mathbf{k}}^\dagger v_{\mathbf{k}''}) c_{\mathbf{k}'} - v_{\mathbf{k}'}^\dagger (c_{\mathbf{k}''}^\dagger c_{\mathbf{k}'+\mathbf{k}''-\mathbf{k}} \\ & + v_{\mathbf{k}''}^\dagger v_{\mathbf{k}'+\mathbf{k}''-\mathbf{k}}) c_{\mathbf{k}}], \end{aligned} \tag{A28}$$

$$\begin{aligned} \left[i\hbar \frac{\partial}{\partial t} c_{\mathbf{k}}^\dagger c_{\mathbf{k}} \right]_{coul} = \frac{1}{S} \sum_{\mathbf{k}',\mathbf{k}''} V_{\mathbf{k}-\mathbf{k}'} & c_{\mathbf{k}'}^\dagger (c_{\mathbf{k}''}^\dagger c_{\mathbf{k}'+\mathbf{k}''-\mathbf{k}} \\ & + v_{\mathbf{k}''}^\dagger v_{\mathbf{k}'+\mathbf{k}''-\mathbf{k}}) c_{\mathbf{k}} - \text{H.c.}, \end{aligned} \tag{A29}$$

where $V_{\mathbf{k}}$ is the Coulomb matrix element of the lowest quantum well subband. Taking the expectation value of Eqs. (A28) and (A29), we see that the contribution of the Coulomb interaction to the density-matrix equations is described by expectation values containing four carrier operators. Without further approximation, there is no closed equation for the single-particle density-matrix elements, since the equation of motion for an expectation value with n carrier Bloch operators contains expectation values with $n+2$ Bloch operators. The lowest-order (mean-field, Hartree-Fock) approximation corresponds to a factorization of four-operator expectation values in the equation of motion for the single-particle density-matrix elements,

$$\begin{aligned} \langle a_{\nu_1}^\dagger(\mathbf{k}_1) a_{\nu_2}^\dagger(\mathbf{k}_2) a_{\nu_3}(\mathbf{k}_3) a_{\nu_4}(\mathbf{k}_4) \rangle & \\ \simeq \langle a_{\nu_1}^\dagger(\mathbf{k}_1) a_{\nu_4}(\mathbf{k}_4) \rangle \langle a_{\nu_2}^\dagger(\mathbf{k}_2) a_{\nu_3}(\mathbf{k}_3) \rangle \delta_{\mathbf{k}_1,\mathbf{k}_4} \delta_{\mathbf{k}_2,\mathbf{k}_3} & \\ - \langle a_{\nu_1}^\dagger(\mathbf{k}_1) a_{\nu_3}(\mathbf{k}_3) \rangle \langle a_{\nu_2}^\dagger(\mathbf{k}_2) a_{\nu_4}(\mathbf{k}_4) \rangle \delta_{\mathbf{k}_1,\mathbf{k}_3} \delta_{\mathbf{k}_2,\mathbf{k}_4}. & \end{aligned} \tag{A30}$$

On this level, the coupling of the individual $\mathbf{k}$ states via the Coulomb potential can be expressed in terms of renormalized single-particle energies,

$$\varepsilon_{\mathbf{k}}^a(t) = \epsilon_{\mathbf{k}}^a - \frac{1}{S} \sum_{\mathbf{k}'} V_{\mathbf{k}-\mathbf{k}'} f_{\mathbf{k}'}^a(t), \tag{A31}$$

and a renormalized optical Rabi energy,

$$\Omega_{\mathbf{k}}(t) = \mathbf{d}_{cv} \mathbf{E}_{QW}(t) + \frac{1}{S} \sum_{\mathbf{k}'} V_{\mathbf{k}-\mathbf{k}'} P_{\mathbf{k}'}(t), \tag{A32}$$

in Eqs. (A26) and (A27). These corrections, linear in the bare Coulomb potential, couple different semiconductor $\mathbf{k}$ states and, together with the phase-space filling term in Eq. (A26), $1 - f_{\mathbf{k}}^e(t) - f_{\mathbf{k}}^h(t)$, introduce nonlinearities into the light-matter interaction.

The density-matrix equations in the Bloch basis, Eqs. (A26) and (A27), together with the Hartree-Fock renormalizations, Eqs. (A31) and (A32), are often called semiconductor Bloch equations (Schmitt-Rink and Chemla, 1986; Linberg and Koch, 1988). They have been successfully used in the past to describe coherent excitonic nonlinearities in the optical Stark effect (Koch, Peyghambarian, and Lindberg, 1988; Schmitt-Rink, Chemla, and Haug, 1988; Binder *et al.*, 1991) and in four-wave mixing signals (Lindberg *et al.*, 1992; Schäfer *et al.*, 1993).

For a realistic description of high-excitation conditions, a microscopic treatment of polarization dephasing (damping) and carrier scattering due to Coulomb interaction is necessary. Furthermore, under high-excitation conditions, screening of the Coulomb interaction has to be included. A systematic way to treat these effects is the nonequilibrium Green's-function technique

(Keldysh, 1965; Korenman, 1966; DuBois, 1967) that has been applied in the past to highly excited semiconductors in both the coherent and the incoherent regime (Haug, 1985; Schäfer and Treusch, 1986; Henneberger, 1988). However, the interacting system of crystal electrons, plasmons, and phonons, their interplay with the band structure, and the short-time dynamics are so complicated that a first-principles solution of the problem is currently not possible. Various authors have focused in the past on selected problems. The treatment of Coulomb correlations can be limited to terms up to quadratic order in the screened Coulomb interaction which is often called the second Born approximation. On this level, the contributions of carrier scattering and polarization interactions in the equations of motion for the carrier occupation and interband polarization, Eqs. (A26) and (A27), can be obtained.[6] While these models are well suited for the description of plasma-carrier correlations, some of the excitonic correlations are lost. The theory includes the coherent exciton dynamics, but incoherent exciton collisions or biexcitonic effects are missing. While a generalization of the factorization scheme (A30) leads only to equations containing the unscreened Coulomb potential, the functional-derivative technique (DuBois, 1967) allows the inclusion of screening. For practical calculations often simplified screening models have been used. The Lindhard formula for the longitudinal dielectric function again treats only screening due to plasma carriers (see below). Recently attention has been paid to the carrier dynamics on very short time scales where the Markov approximation becomes invalid (Zimmermann, 1990; Hartmann and Schäfer, 1992; Haug, 1992; Zimmermann, 1992; Bányai *et al.*, 1996; Schäfer, 1996). Equations of motion without Markov approximation have been denoted as quantum kinetics. To describe the dynamics of screening, especially the build-up on an ultrafast time scale, equations of motion for plasmons have been formulated and numerically solved for simple systems (Hartmann *et al.*, 1990; El Sayed *et al.*, 1994; Manzke *et al.*, 1995). An alternative method for including correlation contributions in the carrier and polarization dynamics is the dynamic truncation scheme (Axt and Stahl, 1994; Lindberg *et al.*, 1994; Schäfer *et al.*, 1996), in which expectation values of more than two carrier operators are classified in terms of powers of the electric field. This method is well suited for the description of coherent effects on a short time scale and allows, for example, the inclusion of biexcitonic effects or non-Markovian effects. It is not easy to use, however, for the description of incoherent excitations, e.g., when a prepulse excites an electron-hole plasma or when the coherent excitation dephases into incoherent states. This list is certainly incomplete and much work remains to be done for a microscopic description of carrier correlations and their dynamics in semiconductors.

In the following we review a theory for carrier correlations up to quadratic order in the screened Coulomb potential that includes the nonlinear carrier and polarization interaction. The time dynamics have been treated in the Markov approximation and screening has been included in a quasistatic approximation. Details of the theoretical framework are discussed by Jahnke, Kira, and Koch (1997). The numerical calculations on this level exhaust the possibilities of currently available supercomputers.

4. Correlation contributions for quasiequilibrium plasma nonlinearities

In the weak-field regime, the equations of motion for the density-matrix elements, Eqs. (A26) and (A27), and the inclusion of correlation contributions can be simplified. We can restrict the analysis to terms linear in the effective quantum well field $\mathbf{E}_{QW}(t)$ which enters in the theory via Eq. (A32). Since changes of the occupation probabilities $f_{\mathbf{k}}^{a}(t)$, described by Eq. (A27), are at least of quadratic order in $\mathbf{E}_{QW}$ ($P_{\mathbf{k}}$ and $\Omega_{\mathbf{k}}$ are at least linear in $\mathbf{E}_{QW}$), there are no contributions of a weak field to the carrier occupation. Hence linear contributions to the carrier momentum-dependent polarization $P_{\mathbf{k}}(t)$ can be obtained using field-independent (incoherent) carrier occupation probabilities $f_{\mathbf{k}}^{a}$. The equation of motion for $P_{\mathbf{k}}(t)$ including correlation contributions on the discussed level has the form

$$\left[i\hbar\frac{\partial}{\partial t}-\varepsilon_{\mathbf{k}}^{e}(t)-\varepsilon_{\mathbf{k}}^{h}(t)\right]P_{\mathbf{k}}(t)+[1-f_{\mathbf{k}}^{e}-f_{\mathbf{k}}^{h}]\Omega_{\mathbf{k}}(t)$$
$$=-i\tilde{\Gamma}_{\mathbf{k}}P_{\mathbf{k}}(t)+i\sum_{\mathbf{k}'}\tilde{\Gamma}_{\mathbf{k},\mathbf{k}'}P_{\mathbf{k}+\mathbf{k}'}(t). \tag{A33}$$

The right-hand side can be obtained, for example, from a Green's-function treatment (Jahnke, Kira, and Koch, 1997) and contains complex self-energies that are either diagonal or off-diagonal with respect to their carrier-momentum dependence. The real part of $\tilde{\Gamma}_{\mathbf{k}}$ describes polarization dephasing. In the weak-field regime, it is given by the sum of in-and out-scattering rates for carrier collisions; see Eqs. (A37) and (A38) below. Its Kramers-Kronig transform, the imaginary part of $\tilde{\Gamma}_{\mathbf{k}}$, describes the corresponding energy renormalization beyond the Hartree-Fock level. For the complex rate we obtain

$$\tilde{\Gamma}_{\mathbf{k}}=\frac{1}{S^2}\sum_{\mathbf{k}',\mathbf{k}''}\sum_{a,b=e,h}g(\varepsilon_{\mathbf{k}}^{a}+\varepsilon_{\mathbf{k}'+\mathbf{k}''}^{b}-\varepsilon_{\mathbf{k}''}^{b}-\varepsilon_{\mathbf{k}'+\mathbf{k}}^{a})$$
$$\times[2W_{\mathbf{k}'}^{2}-\delta_{ab}W_{\mathbf{k}'}W_{\mathbf{k}-\mathbf{k}''}][(1-f_{\mathbf{k}'+\mathbf{k}''}^{b})f_{\mathbf{k}''}^{b}f_{\mathbf{k}'+\mathbf{k}}^{a}$$
$$+f_{\mathbf{k}'+\mathbf{k}''}^{b}(1-f_{\mathbf{k}''}^{b})(1-f_{\mathbf{k}'+\mathbf{k}}^{a})]. \tag{A34}$$

A complex delta function $g(\varepsilon)=\pi\delta(\varepsilon)+i(\mathcal{P}/\varepsilon)$ has been introduced where $\mathcal{P}$ denotes that the principal value of the corresponding integral has to be taken. Terms up to quadratic order in the screened Coulomb

[6]See, for example, Lindberg and Koch, 1988; Tran Thoai and Haug, 1993; Kuhn, 1994; Rappen *et al.*, 1994; Rossi *et al.*, 1994; Schäfer *et al.*, 1994; Schäfer, 1996; Jahnke, Kira, and Koch, 1997.

potential $W_{\mathbf{k}}$ have been retained, which corresponds to a restriction to two-particle collisions. From the second term on the right-hand side of Eq. (A33),

$$\tilde{\Gamma}_{\mathbf{k},\mathbf{k}'}=\frac{1}{S^2}\sum_{\mathbf{k}''}\sum_{a,b=e,h} g(-\varepsilon^a_{\mathbf{k}}-\varepsilon^b_{\mathbf{k}'+\mathbf{k}''}+\varepsilon^b_{\mathbf{k}''}+\varepsilon^a_{\mathbf{k}'+\mathbf{k}}) \times[2W^2_{\mathbf{k}'}-\delta_{ab}W_{\mathbf{k}'}W_{\mathbf{k}-\mathbf{k}''}] \times[(1-f^a_{\mathbf{k}})(1-f^b_{\mathbf{k}'+\mathbf{k}''})f^b_{\mathbf{k}''}+f^a_{\mathbf{k}}f^b_{\mathbf{k}'+\mathbf{k}''}(1-f^b_{\mathbf{k}''})], \tag{A35}$$

we obtain diagonal contributions (with respect to the carrier momentum) for $\mathbf{k}'=0$ as well as off-diagonal contributions for $\mathbf{k}'\neq 0$. It turns out that the contributions of $\tilde{\Gamma}_{\mathbf{k},\mathbf{k}'=0}$ partially compensate $\tilde{\Gamma}_{\mathbf{k}}$. This leads to reduced dephasing and reduced band-gap renormalization. The off-diagonal contributions can be viewed as higher-order corrections to the renormalized Rabi energy.

In Eqs. (A34) and (A35), the δ function describes energy conservation; the conservation of the in-plane carrier momentum has been included already in the $\mathbf{k}$ arguments. The z dependence of the carrier confinement wave functions enters in the quantum well matrix element of the screened Coulomb potential $W_{\mathbf{k}}$. We find direct (RPA) contributions, $\propto W^2_{\mathbf{k}'}$, as well as exchange (vertex) contributions, $\propto W_{\mathbf{k}'}W_{\mathbf{k}-\mathbf{k}''}$. In the quasistatic approximation for $W_{\mathbf{k}}(\omega=0,t)$, dependence on the frequency or on two independent time arguments is neglected. This is usually a good approximation for carrier-plasma excitation, even though the results might weakly depend on the screening model.

5. Nonequilibrium carrier dynamics and nonlinear correlations

When the interband polarization $P_{\mathbf{k}}$ has a nonlinear field dependence and/or when the momentum-dependent carrier occupation probability $f^{e,h}_{\mathbf{k}}$ deviates from quasiequilibrium Fermi-Dirac functions, $f^{e,h}_{\mathbf{k}}$ becomes a dynamical quantity that describes the redistribution of carriers due to carrier and polarization interaction. The kinetic equation of carriers including correlation effects has the form

$$i\hbar\frac{\partial}{\partial t}f^a_{\mathbf{k}}(t)+\Omega_{\mathbf{k}}(t)P^*_{\mathbf{k}}(t)-\Omega^*_{\mathbf{k}}(t)P_{\mathbf{k}}(t) =i\{\Sigma^{in,a}_{\mathbf{k}}(t)[1-f^a_{\mathbf{k}}(t)]-\Sigma^{out,a}_{\mathbf{k}}(t)f^a_{\mathbf{k}}(t)+\Sigma^{pol,a}_{\mathbf{k}}(t)\}. \tag{A36}$$

The probability for carrier scattering into a $\mathbf{k}$ state depends on the nonoccupation of this state $(1-f^a_{\mathbf{k}})$ and the inverse scattering time $\Sigma^{in,a}_{\mathbf{k}}$; the out-scattering probability is determined by the occupation $f^a_{\mathbf{k}}$ and $\Sigma^{out,a}_{\mathbf{k}}$. The self-energies for carrier Coulomb scattering (including terms up to quadratic order in the screened Coulomb potential) are given by

$$\Sigma^{in,a}_{\mathbf{k}}=\frac{2\pi}{S^2}\sum_{\mathbf{k}',\mathbf{k}''}\sum_{b=e,h}[2W^2_{\mathbf{k}'}-\delta_{ab}W_{\mathbf{k}'}W_{\mathbf{k}-\mathbf{k}''}] \times\delta(\varepsilon^a_{\mathbf{k}}+\varepsilon^b_{\mathbf{k}'+\mathbf{k}''}-\varepsilon^b_{\mathbf{k}''}-\varepsilon^a_{\mathbf{k}'+\mathbf{k}})(1-f^b_{\mathbf{k}'+\mathbf{k}''})f^b_{\mathbf{k}''}f^a_{\mathbf{k}'+\mathbf{k}}, \tag{A37}$$

$$\Sigma^{out,a}_{\mathbf{k}}=\frac{2\pi}{S^2}\sum_{\mathbf{k}',\mathbf{k}''}\sum_{b=e,h}[2W^2_{\mathbf{k}'}-\delta_{ab}W_{\mathbf{k}'}W_{\mathbf{k}-\mathbf{k}''}] \times\delta(\varepsilon^a_{\mathbf{k}}+\varepsilon^b_{\mathbf{k}'+\mathbf{k}''}-\varepsilon^b_{\mathbf{k}''}-\varepsilon^a_{\mathbf{k}'+\mathbf{k}}) \times f^b_{\mathbf{k}'+\mathbf{k}''}(1-f^b_{\mathbf{k}''})(1-f^a_{\mathbf{k}'+\mathbf{k}}). \tag{A38}$$

In Eqs. (A33)–(A35) $f^a_{\mathbf{k}}$ becomes explicitly time dependent. Since the screened Coulomb potential $W_{\mathbf{k}}$ is self-consistently computed from the occupation of the carrier system (see below), it also "follows" the changes of $f^a_{\mathbf{k}}$.

For a strong optical field $\mathbf{E}_{QW}$, the occupation probability contains odd powers and the interband polarization includes even powers of $\mathbf{E}_{QW}$. Via the $f^{e,h}_{\mathbf{k}}(t)\Omega_{\mathbf{k}}(t)$ driving term in Eq. (A33) and the $\Omega_{\mathbf{k}}(t)P^*_{\mathbf{k}}(t)$ driving term in Eq. (A36) arbitrarily high powers of the field $\mathbf{E}_{QW}$ can appear. Correlation contributions describing the nonlinear polarization interaction in Eq. (A36) are given by

$$\Sigma^{pol,a}_{\mathbf{k}}=\frac{1}{S^2}\sum_{\mathbf{k}',\mathbf{k}''}\sum_{b=e,h}[2W^2_{\mathbf{k}'}-\delta_{ab}W_{\mathbf{k}'}W_{\mathbf{k}-\mathbf{k}''}] \times\{g(\varepsilon^a_{\mathbf{k}}+\varepsilon^b_{\mathbf{k}'+\mathbf{k}''}-\varepsilon^b_{\mathbf{k}''}-\varepsilon^a_{\mathbf{k}'+\mathbf{k}}) \times[(f^a_{\mathbf{k}}-f^a_{\mathbf{k}'+\mathbf{k}})P_{\mathbf{k}'+\mathbf{k}''}P^*_{\mathbf{k}''}+\text{c.c.}] +g(\varepsilon^{\bar{a}}_{\mathbf{k}}+\varepsilon^b_{\mathbf{k}'+\mathbf{k}''}-\varepsilon^b_{\mathbf{k}''}-\varepsilon^{\bar{a}}_{\mathbf{k}'+\mathbf{k}}) \times[(f^b_{\mathbf{k}''}-f^b_{\mathbf{k}'+\mathbf{k}''})P_{\mathbf{k}}P^*_{\mathbf{k}'+\mathbf{k}}+\text{c.c.}]\}. \tag{A39}$$

Similarly, the nonlinear polarization interaction contributions in Eq. (A33), which have to be added to $\tilde{\Gamma}$, are given by

$$\tilde{\tilde{\Gamma}}_{\mathbf{k}}=-\frac{1}{S^2}\sum_{\mathbf{k}',\mathbf{k}''}\sum_{a,b=e,h}[2W^2_{\mathbf{k}'}-\delta_{ab}W_{\mathbf{k}'}W_{\mathbf{k}-\mathbf{k}''}] \times g(\varepsilon^a_{\mathbf{k}}+\varepsilon^b_{\mathbf{k}'+\mathbf{k}''}-\varepsilon^b_{\mathbf{k}''}-\varepsilon^a_{\mathbf{k}'+\mathbf{k}})P_{\mathbf{k}'+\mathbf{k}''}P^*_{\mathbf{k}''}, \tag{A40}$$

$$\tilde{\tilde{\Gamma}}_{\mathbf{k},\mathbf{k}'}=-\frac{1}{S^2}\sum_{\mathbf{k}''}\sum_{a,b=e,h}[2W^2_{\mathbf{k}'}-\delta_{ab}W_{\mathbf{k}'}W_{\mathbf{k}-\mathbf{k}''}] \times g(-\varepsilon^a_{\mathbf{k}}-\varepsilon^b_{\mathbf{k}'+\mathbf{k}''}+\varepsilon^b_{\mathbf{k}''}+\varepsilon^a_{\mathbf{k}'+\mathbf{k}})P^*_{\mathbf{k}'+\mathbf{k}''}P_{\mathbf{k}''}. \tag{A41}$$

For notational simplicity, we have omitted additional vertex contributions, which usually represent only small corrections; they are discussed by Jahnke, Kira, and Koch (1997).

We should like to point out that terms in Eqs. (A39)–(A41) are *not* restricted to quadratic or cubic field nonlinearities, since every polarization function $P_{\mathbf{k}}$ itself can have a nonlinear field dependence. The number of polarization functions in the correlation contributions de-

pends on the order of the diagrammatic expansion of the self-energy in terms of the Coulomb interaction. Higher-order expansions can be obtained from a T-matrix formulation of the self-energies; see, for example, Morawetz and Roepke (1995).

We explicitly note here that Eqs. (A33)–(A41) provide the simplest consistent form for a description of correlations in the carrier and polarization dynamics up to quadratic order in the screened Coulomb interaction. On an ultrafast time scale, energy conservation can be violated and non-Markovian effects have to be considered. Furthermore, for time intervals of the inverse plasma frequency the buildup of screening is incomplete. The consistent inclusion of these effects in the carrier and polarization dynamics presents, however, a challenge to current theories.

Screening of the Coulomb interaction due to free electrons and holes can be described in a manner similar to the electron-gas theory (Mahan, 1990). From a longitudinal dielectric function in the random-phase approximation, the Lindhard dielectric function can be derived in the Markov approximation, which has become a standard tool for the description of electron-hole-plasma screening in semiconductors. By omitting the Markov approximation, the theory has been further developed towards a kinetic modeling of screening in terms of carrier-plasmon interaction (El Sayed *et al.*, 1994; Manzke *et al.*, 1995). Only a few attempts have been made to properly describe screening due to excitons (Röpke and Der, 1979; Haug and Schmitt-Rink, 1984; Schäfer, 1988). For excitons in the presence of free carriers, one usually neglects the excitonic screening contribution due to the small induced charge density of the almost neutral exciton complex. A proper description of coexisting bound and free carriers is especially missed for the understanding of group-II–VI semiconductors or group-III nitrides, in which strong excitonic effects have been observed even at and above room temperature (Nurmikko and Gunshor, 1993). For the present analysis, we restrict ourselves to the Lindhard formula,

$$\epsilon(\mathbf{k},\omega,t)=1-v(\mathbf{k})\frac{1}{S}\sum_{a,\mathbf{k}'}\frac{f^a_{\mathbf{k}'-\mathbf{k}}(t)-f^a_{\mathbf{k}'}(t)}{\hbar\omega+\epsilon^a_{\mathbf{k}'-\mathbf{k}}(t)-\epsilon^a_{\mathbf{k}'}(t)+i\gamma}, \tag{A42}$$

which has been extensively discussed in the literature (Mahan, 1990) and will be used in the quasistatic approximation $W_{\mathbf{k}}(t)=\epsilon^{-1}(\mathbf{k},\omega=0,t)V_{\mathbf{k}}$.

APPENDIX B: QUANTUM THEORY OF THE COUPLED CARRIER-PHOTON SYSTEM

In this appendix, we outline a treatment of the quantized electromagnetic field in the framework of a semiconductor many-body theory. The Hamiltonian for the interaction of carriers with a quantized light field is derived to replace its semiclassical counterpart used in Appendix A. On the operator level, we can formulate the analog to the semiconductor Bloch equations extended to a quantum description of light. In Sec. IV.A these operator equations are used to derive semiconductor luminescence equations. To distinguish between the classical and quantum-mechanical treatments of the transverse field, classical quantities are denoted by $\mathbf{A}$, $\mathbf{E}$ and their quantum operators by $\hat{\mathbf{A}},\hat{\mathbf{E}}$.

1. Field quantization

A standard approach is to perform the field quantization for the vector potential $\hat{\mathbf{A}}$ using the Coulomb gauge, $\nabla\cdot\hat{\mathbf{A}}=0$ (Cohen-Tannoudji *et al.*, 1989). The field quantization is formulated first for a microcavity without active material. In the sourceless case, both the classical and the quantized vector potential obey the wave equation

$$\left[\nabla^2-\frac{n_B^2(z)}{c_0^2}\frac{\partial^2}{\partial t^2}\right]\hat{\mathbf{A}}(\mathbf{r},t)=\mathbf{0}, \tag{B1}$$

where $n_B(z)$ describes the refractive index profile across the microcavity structure. The vector potential determines the transverse electric field $\hat{\mathbf{E}}=-\partial\hat{\mathbf{A}}/\partial t$ and the magnetic field $\hat{\mathbf{B}}=\nabla\times\hat{\mathbf{A}}$.

The wave equation has the stationary solutions $\mathbf{U}_{\mathbf{q}\sigma}(\mathbf{r})\exp(-i\omega_{\mathbf{q}}t)$ where $\omega_{\mathbf{q}}=c_0|\mathbf{q}|$ is the frequency and σ denotes the two polarization directions of the field perpendicular to the propagation direction $\mathbf{q}$. For simplicity, we restrict the following analysis to photoluminescence in the normal direction. Then $\mathbf{q}=q\mathbf{e}_z$, and $\mathbf{U}_{\mathbf{q}\sigma}(\mathbf{r})=u_q(z)\mathbf{e}_\sigma$ contains the polarization directions $\sigma=x,y$. By inserting the stationary solution into Eq. (B1) we obtain

$$\left[\frac{\partial^2}{\partial z^2}+q^2n_B^2(z)\right]u_q(z)=0. \tag{B2}$$

The solutions of Eq. (B2) form a complete set of functions, which can be orthonormalized via

$$\frac{1}{SL}\int d^3r\,u_q^*(z)u_{q'}(z)=\delta_{q,q'}. \tag{B3}$$

For the quantization volume we choose a large cylinder around the microcavity. The length L of the quantization volume is much longer than the microcavity and the cross-section area S is the same as that of the microcavity (see Fig. 1). For our analysis we choose a cylinder diameter substantially larger than the wavelength of light. Light properties inside such a large system are described by a mode basis computed for an infinite-diameter system.

Studying light propagation effects in small-diameter microcavities (Burak and Binder, 1997) one finds that the effects of cylinder boundaries do not have to be included when the diameter exceeds 10 μm. The derived quantum theory is also formally valid for small-diameter systems. However, the computation of three-dimensional small-diameter mode functions is far from trivial. For a large quantization volume, one can evaluate the mode functions using the transfer-matrix techniques discussed in Sec. III.A.

The vector potential can be expanded in terms of eigenmodes,

$$\hat{\mathbf{A}}(z)=\sum_{q,\sigma}\mathcal{A}_q[u_q(z)b_{q,\sigma}+\text{H.c.}]\mathbf{e}_\sigma, \tag{B4}$$

where $\mathcal{A}_q$ is a real number and b_q is the operator for the quantum field. Since the modes have only two possible q-independent polarization directions, the vector potential is determined by a scalar operator,

$$\hat{A}_\sigma(z)=\sum_{q}\mathcal{A}_q[u_q(z)b_{q\sigma}+\text{H.c.}], \tag{B5}$$

where $\hat{\mathbf{A}}=\Sigma_\sigma\hat{A}_\sigma\mathbf{e}_\sigma$. The quantization for the field (consult Cohen-Tannoudji *et al.*, 1989 for details) determines a boson commutation relation for each field mode,

$$[b_{q\sigma},b_{q'\sigma'}]=[b^\dagger_{q\sigma},b^\dagger_{q'\sigma'}]=0,$$
$$[b_{q\sigma},b^\dagger_{q'\sigma'}]=\delta_{q,q'}\delta_{\sigma,\sigma'}. \tag{B6}$$

Since operators with different σ are independent, we investigate the quantum dynamics of a given polarization direction and omit the σ index.

The coefficients in Eqs. (B4) and (B5) are often called vacuum field amplitudes. Using

$$\mathcal{A}_q=\sqrt{\frac{\hbar}{2\epsilon_0\omega_q SL}} \tag{B7}$$

within Eq. (B5) as well as the normalization (B3) and the commutator relations (B6) we obtain from the operator of the transverse field energy

$$H_F=\frac{1}{2}\int d^3r\,\epsilon_0[n_B^2(z)\hat{\mathbf{E}}^2(z,t)+c^2\hat{\mathbf{B}}^2(z,t)] \tag{B8}$$

the empty cavity Hamiltonian

$$H_F=\sum_q\hbar\omega_q\left(b^\dagger_q b_q+\frac{1}{2}\right). \tag{B9}$$

We point out that this Hamiltonian is diagonal only because we use eigenmodes of the microcavity system described by the wave equation (B2). For example, a plane-wave basis inevitably gives a nondiagonal Hamiltonian H_F.

2. Interaction of quantum well carriers with a quantum field

The fully quantized interaction between light and matter can be obtained from the minimal substitution Hamiltonian

$$H_{light}=\int d^3r\,\psi^\dagger(\mathbf{r},t)\left[-\frac{e}{m_a}\hat{\mathbf{A}}(z)\cdot\mathbf{p}+\frac{e^2}{2m_a}\hat{\mathbf{A}}^2(z)\right]\psi(\mathbf{r},t). \tag{B10}$$

To eliminate complications resulting from the $\hat{\mathbf{A}}^2$ term in Eq. (B10), we apply a unitary gauge transformation (Cohen-Tannoudji *et al.*, 1989), which leads in the dipole approximation to

$$H_{light}=H_D+H_{dip}, \tag{B11}$$

with

$$H_D=-\int d^3r\,\Psi^\dagger(\mathbf{r})e\mathbf{r}\cdot\hat{\mathbf{D}}(\mathbf{r})\Psi(\mathbf{r}), \tag{B12}$$

$$H_{dip}=\frac{1}{2\epsilon_0}\int\int d^3r\,d^3r'\,\Psi^\dagger(\mathbf{r})\Psi^\dagger(\mathbf{r}')\times\sum_{q\sigma}[e\mathbf{r}\cdot\mathbf{U}_{q\sigma}(\mathbf{r})][e\mathbf{r}\cdot\mathbf{U}^\star_{q\sigma}(\mathbf{r}')]\Psi(\mathbf{r}')\Psi(\mathbf{r}). \tag{B13}$$

As a result of the transformation (i) the $\hat{\mathbf{A}}^2$ term is removed, (ii) the additional dipole self-energy term H_{dip} occurs, and (iii) the operator of transverse electric field $\hat{\mathbf{E}}$ is replaced by the electric displacement $\hat{\mathbf{D}}$, which after the transformation becomes

$$\hat{\mathbf{D}}(z)=\sum_{q\sigma}i\mathcal{E}_q[u_q(z)b_{q\sigma}-\text{H.c.}]\mathbf{e}_\sigma, \tag{B14}$$

with $\mathcal{E}_q=\omega_q\mathcal{A}_q$. As for $\hat{\mathbf{A}}$, a scalar operator for $\hat{\mathbf{D}}$ is defined by

$$\hat{D}(z)=\sum_q i\mathcal{E}_q[u_q(z)b_q-\text{H.c.}]. \tag{B15}$$

The dipole Hamiltonian H_D with the transformed displacement $\hat{\mathbf{D}}$ resembles the semiclassical Hamiltonian (A15). In the quantum well Bloch basis, we obtain with Eqs. (A2), (A6), and (B14)

$$H_D=-\sum_{q,\mathbf{k}}i\mathcal{E}_q\tilde{u}_q b_q[d_{cv}c^\dagger_{\mathbf{k}}v_{\mathbf{k}}+d^\star_{cv}v^\dagger_{\mathbf{k}}c_{\mathbf{k}}]+\text{H.c.}$$
$$=-\hat{D}_{QW}S\hat{P}, \tag{B16}$$

where we have defined the operator form of the macroscopic polarization

$$\hat{P}=\frac{1}{S}\sum_{\mathbf{k}}d^\star_{cv}v^\dagger_{\mathbf{k}}c_{\mathbf{k}}+\text{H.c.} \tag{B17}$$

Similar to the classical case, the interaction involves the matrix element of the optical field

$$\hat{D}_{QW}=\int dz|\xi(z)|^2\hat{D}(z), \tag{B18}$$

where we again have restricted the analysis to the lowest quantum well subband. However, instead of the local electric field E_{QW} occurring for the semiclassical case, the quantum treatment involves the electric displacement at the quantum well position in the transformed picture. Using Eq. (B15), we find that the quantum well matrix element contains the overlap of the mode function with the confinement wave function

$$\tilde{u}_q=\int dz|\xi(z)|^2u_q(z). \tag{B19}$$

The dipole self-energy has the form of a two-particle interaction. With the help of the definition (B17), Eq. (B13) can be written as

$$H_{dip}=\frac{\int dz|\xi(z)|^4}{2\epsilon_0 n_{B^2}} S\{\hat{P}\hat{P}\}_N, \tag{B20}$$

where N denotes normal ordering of the carriers operators. The fully quantized Hamiltonian of the complete photon-carrier system is given by Eq. (A12) provided that the photon Hamiltonian (B9) is added to H_0 and the semiclassical interaction Hamiltonian is replaced by Eq. (B11).

3. Operator dynamics of a fully quantized system

The field operators commute with the particle operators for a noninteracting field-matter system. Similarly, a straightforward calculation, starting from Hamiltonians (B16) and (B20) and Heisenberg equations of motion for commutators like $[c_{\mathbf{k}},b_q^\dagger]$, confirms that these commutation relations also hold for an interacting system. For example, the electric displacement is a pure field operator and the polarization a pure matter operator. However, since we want to see the analogy of our full quantum theory with a corresponding semiclassical treatment, we use the electric field rather than the displacement field. From the Heisenberg equations of motion, we obtain the electric field operator as

$$\hat{E}(z)=-\frac{\partial\hat{A}(z)}{\partial t}=-\frac{1}{i\hbar}[\hat{A}(z),H]$$
$$=\hat{D}(z)-\frac{1}{\epsilon_0 n_{B^2}}\hat{P}_{QW}(z), \tag{B21}$$

where the right-hand side contains the transverse part of the quantum well polarization. For the case of normal incidence studied here, the quantum well polarization is purely transverse, and as in the semiclassical case we can write

$$\hat{P}_{QW}(z)=|\xi(z)|^2\hat{P}. \tag{B22}$$

Using Eqs. (B17) and (B18), we find the explicit form of the electric field,

$$\hat{E}(z)=\sum_q i\mathcal{E}_q u_q(z)b_q-\frac{|\xi(z)|^2}{\epsilon_0 n_{B^2}S}\sum_{\mathbf{k}} d_{cv}^\star(\mathbf{k})v_{\mathbf{k}}^\dagger c_{\mathbf{k}}+\text{H.c.} \tag{B23}$$

In the derivation of these expressions, we used the completeness relation of the mode function basis. A distinctive property of the dipole interaction picture is that the electric field contains both field and particle operators (Cohen-Tannoudji *et al.*, 1989). Relation (B21) implies that $\hat{E}$ equals the electric displacement minus the matter polarization, as in the classical case.

To formulate the wave equation for the interacting case, we take a time derivative of Eq. (B21). The time derivative of $\hat{\mathbf{D}}$ is computed using the Heisenberg equation of motion $i\hbar\partial/\partial t\hat{\mathbf{D}}=[\hat{\mathbf{D}},H]$. Since $\hat{\mathbf{D}}$ commutes with all other parts of the Hamiltonian except H_F, this term leads to the empty-cavity part of the wave equation. Together with the time derivative of $\hat{P}_{QW}$ we obtain

$$\left[\frac{\partial^2}{\partial z^2}-\frac{n_{B^2}(z)}{c_0^2}\frac{\partial^2}{\partial t^2}\right]\hat{A}_\sigma(z)=-\mu_0\frac{\partial}{\partial t}\hat{P}_{QW}(z), \tag{B24}$$

$$\left[\frac{\partial^2}{\partial z^2}-\frac{n_{B^2}(z)}{c_0^2}\frac{\partial^2}{\partial t^2}\right]\hat{E}(z)=\mu_0\frac{\partial^2}{\partial t^2}\hat{P}_{QW}(z). \tag{B25}$$

Equations (B24) and (B25) are exactly the same as those obtained from Maxwell's equations for classical fields, which confirms the consistency of the interaction Hamiltonian (B11). On the other hand, Eqs. (B24) and (B25) describe the operator dynamics, whereas we are interested in correlation functions of the field. Equation (B24) has been used by Jahnke and Koch (1995) to define a photon Green's function for a semiconductor laser theory that includes a quantized treatment of the light field as well as a many-body treatment of the interacting carrier system.

An alternative method for the description of quantum dynamics is to derive Heisenberg equations of motion for photon operators from the Hamiltonian of the interacting system,

$$i\hbar\frac{\partial}{\partial t}b_q^\dagger=-\hbar w_q b_q^\dagger+i\mathcal{E}_q\tilde{u}_q\sum_{\mathbf{k}}(d_{cv}^\star v_{\mathbf{k}}^\dagger c_{\mathbf{k}}+d_{cv}c_{\mathbf{k}}^\dagger v_{\mathbf{k}}). \tag{B26}$$

Clearly the evolution of the photon operator depends on the electron-hole pair transition operator in the Bloch basis $\hat{P}_{\mathbf{k}}=v_{\mathbf{k}}^\dagger c_{\mathbf{k}}$. The Heisenberg equations of motion for $\hat{P}_{\mathbf{k}}$ and for the carrier momentum-dependent occupation operators $\hat{n}_{\mathbf{k}}^c=c_{\mathbf{k}}^\dagger c_{\mathbf{k}}$ and $\hat{n}_{\mathbf{k}}^v=v_{\mathbf{k}}^\dagger v_{\mathbf{k}}$ are

$$i\hbar\frac{\partial}{\partial t}v_{\mathbf{k}}^\dagger c_{\mathbf{k}}=(\epsilon_{\mathbf{k}}^c-\epsilon_{\mathbf{k}}^v)v_{\mathbf{k}}^\dagger c_{\mathbf{k}}+d_{cv}[c_{\mathbf{k}}^\dagger\hat{E}_{QW}c_{\mathbf{k}}-v_{\mathbf{k}}^\dagger\hat{E}_{QW}v_{\mathbf{k}}]$$
$$+\frac{1}{S}\sum_{\mathbf{k}',\mathbf{k}''}V_{\mathbf{k}'-\mathbf{k}}[v_{\mathbf{k}}^\dagger(c_{\mathbf{k}'+\mathbf{k}''-\mathbf{k}}^\dagger c_{\mathbf{k}''}$$
$$+v_{\mathbf{k}'+\mathbf{k}''-\mathbf{k}}^\dagger v_{\mathbf{k}''})c_{\mathbf{k}'}-v_{\mathbf{k}'}^\dagger(c_{\mathbf{k}''}^\dagger c_{\mathbf{k}'+\mathbf{k}''-\mathbf{k}}$$
$$+v_{\mathbf{k}''}^\dagger v_{\mathbf{k}'+\mathbf{k}''-\mathbf{k}})c_{\mathbf{k}}], \tag{B27}$$

$$i\hbar\frac{\partial}{\partial t}c_{\mathbf{k}}^\dagger c_{\mathbf{k}}=\Bigg[d_{cv}^\star v_{\mathbf{k}}^\dagger\hat{E}_{QW}c_{\mathbf{k}}-\frac{1}{S}\sum_{\mathbf{k}',\mathbf{k}''}V_{\mathbf{k}'-\mathbf{k}}c_{\mathbf{k}'}^\dagger(c_{\mathbf{k}''}^\dagger c_{\mathbf{k}'+\mathbf{k}''-\mathbf{k}}$$
$$+v_{\mathbf{k}''}^\dagger v_{\mathbf{k}'+\mathbf{k}''-\mathbf{k}})c_{\mathbf{k}}\Bigg]-\text{H.c.} \tag{B28}$$

The equation for $(\partial/\partial t)\hat{n}_{\mathbf{k}}^v$ is obtained from Eq. (B28) by the replacement $c(v)\rightarrow v(c)$. Equations (B27) and (B28) contain the operator of the transverse electric field evaluated at the quantum well position

$$\hat{E}_{QW}=\int dz|\xi(z)|^2\hat{E}(z), \tag{B29}$$

which can be written explicitly with help of Eqs. (B19) and (B23):

$$\hat{E}_{QW}=\sum_q i\mathcal{E}_q\tilde{u}_q b_q-\frac{\int dz|\xi(z)|^4}{\epsilon_0 n_{B^2}S}\sum_{\mathbf{k}} d_{cv}^\star v_{\mathbf{k}}^\dagger c_{\mathbf{k}}+\text{H.c.} \tag{B30}$$

Equations (B27) and (B28) are formally equivalent to

the semiclassical equations (A24), (A25), (A28), and (A29). However, for the case of a quantized light field, the ordering of $\hat{E}_{QW}$ and the carrier operators is crucial in Eqs. (B27) and (B28), since $\hat{E}_{QW}$ contains field and particle operators, as can be seen from Eq. (B30). Both types of operators are normally ordered in Eq. (B27), which means that $\hat{E}_{QW}$ is sandwiched between $c_{\mathbf{k}}^{\dagger}$ and $c_{\mathbf{k}}$, for instance. We point out that the field dynamics could equivalently be computed from the wave equation (B25). In the context of excitonic luminescence, it is more convenient to use the dynamic equation (B26)–(B28) as a general starting point of quantum correlation investigations.

The generalization of Eqs. (B26)–(B28) to modes that do not propagate normal to the microcavity surface is straightforward. In that case, both the mode functions $\mathbf{U}_{\mathbf{q}\sigma}$ and the polarization have the in-plane dependency $e^{i\mathbf{q}_{\parallel}\cdot\rho}$, where $\rho=(x,y)$. If the system consists only of heavy-hole excitons of the lowest quantum well subband, the modes can be classified as transverse electric (TE) or transverse magnetic (TM) fields. The introduction of scalar operators like Eqs. (B5), (B15), and (B21) becomes more complicated. However, the resulting operator equations have a similar form to that of Eqs. (B26)–(B28).

To check the consistency of Eqs. (B26)–(B28) we consider the semiclassical limit where the b_q operators are treated as c numbers. The simplest application of Eqs. (B26)–(B28) is to describe the field-induced polarization and population dynamics. The relevant expectation values are $\langle P_{\mathbf{k}}\rangle$, $\langle\hat{E}\rangle$, and the electron and hole populations $f_{\mathbf{k}}^{e}$ and $f_{\mathbf{k}}^{h}$, respectively. In the semiclassical limit, the pure field operators like $\hat{\mathbf{D}}$ are complex numbers and can be taken out from the expectation values. For example, the second term on the right side of Eq. (B27) becomes

$$\begin{aligned}\langle c_{\mathbf{k}}^{\dagger}\hat{E}_{QW}c_{\mathbf{k}}\rangle&=\langle c_{\mathbf{k}}^{\dagger}\hat{D}_{QW}c_{\mathbf{k}}\rangle\\&\quad-\frac{\int dz|\xi(z)|^4}{\epsilon_0 n_{B^2}S}\sum_{\mathbf{k}'}\left(d_{cv}^{\star}\langle c_{\mathbf{k}}^{\dagger}v_{\mathbf{k}'}^{\dagger}c_{\mathbf{k}'}c_{\mathbf{k}}\rangle\right.\\&\quad\left.+d_{cv}\langle c_{\mathbf{k}}^{\dagger}c_{\mathbf{k}'}^{\dagger}v_{\mathbf{k}'}c_{\mathbf{k}}\rangle\right)\\&=\langle f_{\mathbf{k}}^{e}\rangle\left[\langle\hat{D}_{QW}\rangle-\frac{\int dz|\xi(z)|^4}{\epsilon_0 n_{B^2}}\right.\\&\quad\left.\times\left(\frac{1}{S}\sum_{\mathbf{k}'\neq\mathbf{k}}d_{cv}^{\star}\langle P_{\mathbf{k}'}\rangle+\text{H.c.}\right)\right]\\&=\langle f_{\mathbf{k}}^{e}\rangle\langle\hat{E}_{QW}\rangle,\end{aligned}\tag{B31}$$

where we have used the factorization (A30) and the definition (A9) for $f_{\mathbf{k}}^{e}=\langle c_{\mathbf{k}}^{\dagger}c_{\mathbf{k}}\rangle$. From this procedure we obtain as the semiclassical limit of Eqs. (B26)–(B28) the Hartree-Fock semiconductor Bloch equations (A26) and (A27). Note that, in order to obtain this agreement, it was indeed necessary to include the dipole-dipole interaction in the Hamiltonian (B11).

When equations of motion for expectation values are derived using the operator equations (B26)–(B28), we are again confronted with the problem that the nonlinear Coulomb terms lead to an infinite hierarchy of equations. Sophisticated truncation schemes have been discussed for the semiclassical case in Sec. III. For the quantum calculations of this section, these high-order procedures lead to equations that are beyond current numerical capabilities. Therefore we limit ourselves here to the Hartree-Fock approximation (A30) as the simplest truncation scheme.

In the photoluminescence application, it is important to retain field-particle correlations in terms like $\langle a_{\mathbf{1}}^{\dagger}a_{\mathbf{2}}^{\dagger}\hat{O}_F a_{\mathbf{3}}a_{\mathbf{4}}\rangle$, where $\hat{O}_F$ is a single photon operator. To get some insight into the applied truncation scheme we formally integrate Eq. (B26),

$$b_q^{\dagger}(t)=b_q^{\dagger}(0)e^{i\omega_q t}+\frac{\mathcal{E}_q\tilde{u}_q}{\hbar}S\int_0^t dt'\hat{P}(t')e^{i\omega_q(t-t')},\tag{B32}$$

which shows that $b_q^{\dagger}(t)$ corresponds formally to a two-particle operator $v_{\mathbf{k}}^{\dagger}c_{\mathbf{k}}$. Thus $\langle a_{\mathbf{1}}^{\dagger}a_{\mathbf{2}}^{\dagger}\hat{O}_F a_{\mathbf{3}}a_{\mathbf{4}}\rangle$ corresponds to a six-particle expectation value. The Hartree Fock approximation for such a term can be written as

$$\begin{aligned}&\langle a_{\mathbf{1}}^{\dagger}a_{\mathbf{2}}^{\dagger}\hat{O}_F a_{\mathbf{3}}a_{\mathbf{4}}\rangle|_{HF}\\&\quad=\langle\hat{O}_F\rangle\langle a_{\mathbf{1}}^{\dagger}a_{\mathbf{2}}^{\dagger}a_{\mathbf{3}}a_{\mathbf{4}}\rangle|_{HF}+(\langle a_{\mathbf{1}}^{\dagger}\hat{O}_F a_{\mathbf{4}}\rangle\langle a_{\mathbf{2}}^{\dagger}a_{\mathbf{3}}\rangle\\&\qquad-\langle a_{\mathbf{1}}^{\dagger}\hat{O}_F a_{\mathbf{3}}\rangle\langle a_{\mathbf{2}}^{\dagger}a_{\mathbf{4}}\rangle-\langle\hat{O}_F\rangle\langle a_{\mathbf{1}}^{\dagger}a_{\mathbf{2}}^{\dagger}a_{\mathbf{3}}a_{\mathbf{4}}\rangle|_{HF})\\&\qquad+(\langle a_{\mathbf{1}}^{\dagger}a_{\mathbf{4}}\rangle\langle a_{\mathbf{2}}^{\dagger}\hat{O}_F a_{\mathbf{3}}\rangle-\langle a_{\mathbf{1}}^{\dagger}a_{\mathbf{3}}\rangle\langle a_{\mathbf{2}}^{\dagger}\hat{O}_F a_{\mathbf{4}}\rangle\\&\qquad-\langle\hat{O}_F\rangle\langle a_{\mathbf{1}}^{\dagger}a_{\mathbf{2}}^{\dagger}a_{\mathbf{3}}a_{\mathbf{4}}\rangle|_{HF}).\end{aligned}\tag{B33}$$

Furthermore, we can use

$$\begin{aligned}&\langle c_{\mathbf{k}}^{\dagger}c_{\mathbf{k}'}\hat{O}_F\rangle=\sigma_{\mathbf{k},\mathbf{k}'}\langle\hat{n}_{\mathbf{k}}^{c}\rangle\langle\hat{O}_F\rangle;\\&\langle v_{\mathbf{k}}^{\dagger}v_{\mathbf{k}'}\hat{O}_F\rangle=\delta_{\mathbf{k},\mathbf{k}'}\langle\hat{n}_{\mathbf{k}}^{v}\rangle\langle\hat{O}_F\rangle\end{aligned}\tag{B34}$$

since the optical field does not introduce intraband transitions.

REFERENCES

Abraham, E., and S. D. Smith, 1982, Rep. Prog. Phys. **45**, 815.

Abram, I., S. Iung, R. Kuszelewicz, G. L. Roux, C. Licoppe, J. L. Oudar, E. V. K. Rao, J. I. Bloch, R. Planel, and V. Thierry-Mieg, 1994, Appl. Phys. Lett. **65**, 2516.

Agarwal, G. S., 1984, Phys. Rev. Lett. **53**, 1732.

Agranovich, V. M., and O. A. Dubovskii, 1966, JETP Lett. **3**, 223.

Andreani, L. C., 1994, Phys. Lett. A **192**, 99.

Andreani, L. C., 1995a, in *Confined Electrons and Photons: New Physics and Applications*, edited by E. Burstein, and C. Weisbuch (Plenum, New York), p. 57.

Andreani, L. C., 1995b, Phys. Status Solidi B **188**, 29.

Andreani, L. C., and F. Bassani, 1990, Phys. Rev. B **41**, 7536.

Andreani, L. C., and G. Panzarini, 1995, Nuovo Cimento D **17**, 1211.
Andreani, L. C., F. Tassone, and F. Bassani, 1991, Solid State Commun. **77**, 641.
Andreani, L. C., G. Panzarini, A. V. Kavokin, and M. R. Vladimirova, 1998, Phys. Rev. B **57**, 4670.
Andreani, L. C., V. Savona, P. Schwendimann, and A. Quattropani, 1994, Superlattices Microstruct. **15**, 453.
Armitage, A., *et al.*, 1998, Phys. Rev. B **57**, 14877.
Axt, V. M., and A. Stahl, 1994, Z. Phys. B **93**, 195 and 205.
Bányai, L., and S. W. Koch, 1986, Z. Phys. B **63**, 283.
Bányai, L., E. Reitsamer, D. B. Tran Thoai, and H. Haug, 1996, J. Opt. Soc. Am. B **13**, 1278.
Bastard, G., 1988, *Wave Mechanics Applied to Semiconductor Heterostructures* (Les Editions de Physique, Paris).
Baumberg, J. J., A. Armitage, M. S. Skolnick, and J. S. Roberts, 1998, Phys. Rev. Lett. **81**, 661.
Berger, J. D., O. Lyngnes, H. M. Gibbs, G. Khitrova, T. R. Nelson Jr., E. K. Lindmark, A. V. Kavokin, M. A. Kaliteevski, and V. Zapasskii, 1996, Phys. Rev. B **54**, 1975.
Berman, P. R., 1994, *Cavity Quantum Electrodynamics* (Academic, Boston).
Binder, R., S. W. Koch, M. Lindberg, W. Schäfer, and F. Jahnke, 1991, Phys. Rev. B **43**, 6520.
Björk, G., H. Heitmann, and Y. Yamamoto, 1993, Phys. Rev. A **47**, 4451.
Björk, G., S. Pau, J. Jacobson, and Y. Yamamoto, 1994, Phys. Rev. B **50**, 17 336.
Björk, G., S. Pau, J. M. Jacobson, H. Cao, and Y. Yamamoto, 1995, Phys. Rev. B **52**, 17 310.
Björk, G., S. Pau, J. M. Jacobson, H. Cao, and Y. Yamamoto, 1996, J. Opt. Soc. Am. B **13**, 1069.
Bleuse, J., F. Kany, A. P. de Boer, P. C. M. Christianen, R. Andre, and H. Ulmer-Tuffigo, 1998, J. Cryst. Growth **185**, 750.
Bloch, J., R. Planel, V. Thierry-Mieg, J. M. Gerard, D. Barrier, J. Y. Marzin, and E. Costard, 1997, Superlattices Microstruct. **22**, 371.
Boggavarapu, D., D. McAlister, M. Anderson, M. Munroe, M. G. Raymer, G. Khitrova, and H. M. Gibbs, 1996, in *International Quantum Electronics Conference* (Optical Society of America, Washington, D.C.), p. ML5.
Bonadeo, N. H., G. Chen, D. Gammon, D. S. Katzer, D. Park, and D. G. Steel, 1998, Phys. Rev. Lett. **81**, 2759.
Bongiovanni, G., A. Mura, F. Quochi, S. Gürtler, J. L. Staehli, F. Tassone, R. P. Stanley, U. Oesterle, and R. Houdré, 1997, Phys. Rev. B **55**, 7084.
Born, M., and E. Wolf, 1980, *Principles of Optics* (Pergamon, New York).
Brune, M., F. Schmidt-Kaler, A. Maali, J. Dreyer, E. Hagley, J. M. Raimond, and S. Haroche, 1996, Phys. Rev. Lett. **76**, 1800.
Burak, D., and R. Binder, 1997, IEEE J. Quantum Electron. **33**, 1205.
Burstein, E., and C. Weisbuch, 1995, Eds., *Confined Electrons and Photons: New Physics and Applications* (Plenum, New York).
Cao, H., J. Jacobson, G. Björk, S. Pau, and Y. Yamamoto, 1995, Appl. Phys. Lett. **66**, 1107.
Cao, H., G. Klimovitch, G. Björk, and Y. Yamamoto, 1995a, Phys. Rev. Lett. **75**, 1146.
Cao, H., G. Klimovitch, G. Björk, and Y. Yamamoto, 1995b, Phys. Rev. B **52**, 12 184.
Cao, H., S. Pau, J. M. Jacobson, G. Björk, Y. Yamamoto, and A. Imamoglu, 1997, Phys. Rev. A **55**, 4632.
Cao, H., S. Pau, F. Tassone, R. Huang, G. Björk, and Y. Yamamoto, 1997, in *Topical Meeting on Quantum Optoelectronics* (Optical Society of America, Washington, D.C.), p. QThB1.
Carmichael, H. J., L. Tian, W. Ren, and P. Alsing, 1994, in *Cavity Quantum Electrodynamics*, edited by P. R. Berman (Academic, Boston), p. 381.
Casperson, L. W., 1978, IEEE J. Quantum Electron. **QE-14**, 756.
Chemla, D. S., 1999, in *Semiconductors and Semimetals 58: Nonlinear Optics in Semiconductors*, edited by R. K. Willardson, and A. C. Beers (Academic, Chestnut Hill, MA), p. 175.
Chemla, D. S., D. A. B. Miller, P. W. Smith, A. C. Gossard, and W. Wiegmann, 1984, IEEE J. Quantum Electron. **QE-20**, 265.
Chen, Y., A. Tredicucci, and F. Bassani, 1993, J. Phys. IV **3**, 453.
Chen, Y., A. Tredicucci, and F. Bassani, 1995, Phys. Rev. B **52**, 1800.
Chow, W. W., P. M. Smowton, P. Blood, A. Girndt, F. Jahnke, and S. W. Koch, 1997, Appl. Phys. Lett. **71**, 157.
Citrin, D. S., 1993, Comments Condens. Matter Phys. **16**, 263.
Citrin, D. S., 1994a, Phys. Rev. B **49**, 1943.
Citrin, D. S., 1994b, IEEE J. Quantum Electron. **QE-30**, 997.
Citrin, D. S., and T. B. Norris, 1997, IEEE J. Sel. Top. Quantum Electron. **2**, 401.
Cohen-Tannoudji, C., J. Dupont-Roc, and G. Grynberg, 1989, *Photons & Atoms*, 3rd ed. (Wiley, New York).
Coldren, L. A., and S. W. Corzine, 1995, *Diode Lasers and Photonic Integrated Circuits* (Wiley, New York).
Collet, J., J. L. Oudar, and T. Amand, 1986, Phys. Rev. B **34**, 5443.
Dang, L. S., D. Heger, R. André, F. Boeuf, and R. Romestain, 1998, Phys. Rev. Lett. **81**, 3920.
Deppe, D. G., and C. Lei, 1992, Appl. Phys. Lett. **60**, 527.
Devaud, B., F. Clérot, K. S. N. Roy, B. Sermage, and D. S. Katzer, 1991, Phys. Rev. Lett. **67**, 2355.
Drexhage, K. H., 1974, in *Progress in Optics*, edited by E. Wolf (North-Holland, Amsterdam), p. 165.
DuBois, D. F., 1967, in *Lectures in Theoretical Physics*, edited by W. E. Brittin *et al.* (Gordon and Breach, New York), Vol. 9C, p. 469.
El Sayed, K., S. Schuster, H. Haug, F. Herzel, and K. Henneberger, 1994, Phys. Rev. B **49**, 7337.
Ell, C., J. Prineas, T. R. Nelson Jr., S. Park, E. S. Lee, H. M. Gibbs, G. Khitrova, and S. W. Koch, 1999, in *Advances in Laser Physics: A Festschrift in Honor of Peter Franken on His 70th Birthday*, edited by V. S. Letokhov and P. Meystre (Gordon and Breach, Reading, UK).
Ell, C., T. R. Nelson Jr., S. Park, H. M. Gibbs, G. Khitrova, S. W. Koch, and R. Houdré, 1998, Phys. Rev. Lett. **80**, 4795.
Fainstein, A., B. Jusserand, and V. Thierry-Mieg, 1997, Phys. Rev. Lett. **78**, 1576.
Fan, X., H. Wang, H. Q. Hou, and B. E. Hammons, 1997, Phys. Rev. A **56**, 3233.
Fan, X., H. Wang, H. Q. Hou, and B. E. Hammons, 1998, Phys. Rev. B **57**, R9451.
Fehrenbach, G. W., W. Schäfer, J. Treusch, and R. G. Ulbrich, 1982, Phys. Rev. Lett. **49**, 1281.

Fisher, T. A., A. M. Afshar, D. M. Whittaker, M. S. Skolnick, J. S. Roberts, G. Hill, and M. A. Pate, 1995, Phys. Rev. B **51**, 2600.
Fisher, T. A., A. M. Afshar, M. S. Skolnick, D. M. Whittaker, and J. S. Roberts, 1996, Phys. Rev. B **53**, R10 469.
Gammon, D., E. S. Snow, B. V. Shanabrook, D. S. Katzer, and D. Park, 1996a, Phys. Rev. Lett. **76**, 3005.
Gammon, D., E. S. Snow, B. V. Shanabrook, D. S. Katzer, and D. Park, 1996b, Science **273**, 87.
Gibbs, H. M., 1985, *Optical Bistability: Controlling Light with Light* (Academic, New York).
Gibbs, H. M., A. C. Gossard, S. L. McCall, A. Passner, W. Wiegmann, and T. N. C. Venkatesan, 1979, Solid State Commun. **30**, 271.
Gibbs, H. M., *et al.*, 1997, Adv. Solid State Phys. **37**, 227.
Girndt, A., F. Jahnke, A. Knorr, S. W. Koch, and W. W. Chow, 1997, Phys. Status Solidi B **202**, 725.
Goldstein, E. V., and P. Meystre, 1995, in *Spontaneous Emission and Laser Oscillation in Microcavities*, edited by H. Yokoyama and K. Ujihara (CRC, Boca Raton), p. 1.
Goobar, E., R. J. Ram, J. Ko, G. Björk, M. Oestreich, and A. Imamaglu, 1996, Appl. Phys. Lett. **69**, 3465.
Gourley, P. L., T. M. Brennan, B. E. Hammons, S. W. Corzine, R. S. Geels, R. H. Yam, J. W. Scott, and L. A. Coldren, 1989, Appl. Phys. Lett. **54**, 1397.
Graham, L. A., Q. Deng, D. G. Deppe, and D. L. Huffaker, 1997, Appl. Phys. Lett. **70**, 814.
Grote, B., *et al.*, 1999, ''Microscopic modelling of the influence of structural disorder on normal-mode coupling in semiconductor microcavities,'' manuscript in preparation.
Gutbrod, T., M. Bayer, A. Forchel, J. P. Reithmaier, T. L. Reinecke, S. Rudin, and P. A. Knipp, 1998, Phys. Rev. B **57**, 9950.
Haas, S., T. Strouken, A. Knorr, F. Jahnke, and S. W. Koch, 1997, Phys. Status Solidi A **164**, 19.
Haas, S., T. Strouken, M. Hübner, J. Kuhl, B. Grote, A. Knorr, F. Jahnke, S. W. Koch, R. Hey, and K. Ploog, 1998, Phys. Rev. B **57**, 14 860.
Hanamura, E., 1988, Phys. Rev. B **38**, 1228.
Hanamura, E., I. Inoue, and F. Yara, 1995, J. Nonlinear Opt. Phys. Mater. **4**, 13.
Haroche, S., 1984, in *Les Houches, Session XXXVIII 1982-New Trends in Atomic Physics*, edited by G. Grynberg and R. Stora (Elsevier, Oxford), p. 193.
Haroche, S., 1992, in *Fundamental Systems in Quantum Optics*, edited by J. Dalibard, J. M. Raimond, and J. Zinn-Justin (Elsevier Science, New York), p. 767.
Haroche, S., 1998, Phys. Today **51** (7), 36.
Haroche, S., and J.-M. Raimond, 1996, Phys. Today **49** (8), 51.
Hartmann, M., and W. Schäfer, 1992, Phys. Status Solidi B **173**, 165.
Hartmann, M., H. Stolz, and R. Zimmermann, 1990, Phys. Status Solidi B **159**, 35.
Haug, H., 1985, J. Lumin. **30**, 171.
Haug, H., 1992, Phys. Status Solidi B **173**, 139.
Haug, H., and D. B. Tran Thoai, 1978, Phys. Status Solidi B **85**, 561.
Haug, H., and S. Schmitt-Rink, 1984, Prog. Quantum Electron. **9**, 3.
Haug, H., and S. Schmitt-Rink, 1985, J. Opt. Soc. Am. B **2**, 1135.
Haug, H., and S. W. Koch, 1994, *Quantum Theory of the Optical and Electronic Properties of Semiconductors*, 3rd ed. (World Scientific, Singapore).
Henneberger, K., 1988, Physica A **150**, 419.
Hood, C. J., M. S. Chapman, T. W. Lynn, and H. J. Kimble, 1998, Phys. Rev. Lett. **80**, 4157.
Hopfield, J. J., 1958, Phys. Rev. **112**, 1555.
Hopfield, J. J., and D. J. Thomas, 1965, Phys. Rev. Lett. **15**, 22.
Houdré, R., J. L. Gibernon, P. Pellandini, R. P. Stanley, U. Oesterle, C. Weisbuch, J. O'Gorman, B. Roycroft, and M. Ilegems, 1995, Phys. Rev. B **52**, 7810.
Houdré, R., R. P. Stanley, and M. Ilegems, 1996, Phys. Rev. A **53**, 2711.
Houdré, R., R. P. Stanley, U. Oesterle, M. Ilegems, and C. Weisbuch, 1993, J. Phys. IV **3**, 51.
Houdré, R., R. P. Stanley, U. Oesterle, M. Ilegems, and C. Weisbuch, 1994, Phys. Rev. B **49**, 16 761.
Houdré, R., C. Weisbuch, R. P. Stanley, U. Oesterle, P. Pellandini, M. Ilegems, and 1994, Phys. Rev. Lett. **73**, 2043.
Hu, Y. Z., R. Binder, S. W. Koch, S. T. Cundiff, H. Wang, and D. Steele, 1994, Phys. Rev. B **49**, 14 382.
Huang, R., H. Cao, and Y. Yamamoto, 1997, Phys. Rev. B **56**, 9217.
Hübner, M., J. Kuhl, B. Grote, T. Stroucken, S. Haas, A. Knorr, S. W. Koch, G. Khitrova, and H. M. Gibbs, 1998, Phys. Status Solidi B **206**, 333.
Hübner, M., J. Kuhl, T. Stroucken, A. Knorr, S. W. Koch, R. Hey, and K. Ploog, 1996, Phys. Rev. Lett. **76**, 4199.
Huffaker, D. L., G. Park, Z. Zou, O. B. Shchekin, and D. G. Deppe, 1998, Appl. Phys. Lett. **73**, 2564.
Huffaker, D. L., Z. Huang, C. Lei, D. G. Lei, D. G. Deppe, C. J. Pinzone, and J. G. N. R. D. Dupuis, 1992, Appl. Phys. Lett. **61**, 877.
Iga, K., F. Koyanama, and S. Kinoshita, 1988, IEEE J. Quantum Electron. **24**, 1845.
Imamoglu, A., and R. J. Ram, 1996, Phys. Lett. A **214**, 193.
Imamoglu, A., R. J. Ram, S. Pau, and Y. Yamamoto, 1996, Phys. Rev. A **53**, 4250.
Ivchenko, E. L., 1991, Sov. Phys. Solid State **33**, 1344.
Ivchenko, E. L., A. I. Nesvizhskii, and S. Jorda, 1994a, Phys. Solid State **36**, 1156.
Ivchenko, E. L., A. I. Nesvizhskii, and S. Jorda, 1994b, Superlattices Microstruct. **16**, 17.
Ivchenko, E. L., M. A. Kaliteevski, A. V. Kavokin, and A. L. Nesvizhskii, 1996, J. Opt. Soc. Am. B **13**, 1061.
Jacobson, J. M., H. Cao, S. Pau, G. Björk, Y. Yamamoto, and E. Hanamura, 1995, in *Conference on Quantum Electronics and Laser Science* (Optical Society of America, Washington, D.C.), p. QThE2.
Jahnke, F., *et al.*, 1996, Phys. Rev. Lett. **77**, 5257.
Jahnke, F., and S. W. Koch, 1993, Opt. Lett. **18**, 1438.
Jahnke, F., and S. W. Koch, 1995, Phys. Rev. A **52**, 1712.
Jahnke, F., M. Kira, and S. W. Koch, 1997, Z. Phys. B **104**, 559.
Jahnke, F., M. Ruopp, M. Kira, and S. W. Koch, 1997, Adv. Solid State Phys. **37**, 191.
Jaynes, E. T., and F. W. Cummings, 1963, Proc. IEEE **51**, 89.
Jewell, J. L., J. P. Harbison, A. Scherer, Y. H. Lee, and L. T. Florez, 1991, IEEE J. Quantum Electron. **27**, 1332.
Jewell, J. L., Y. H. Lee, S. L. McCall, J. P. Harbison, and L. T. Florez, 1988, Appl. Phys. Lett. **53**, 640.
Jorda, S., 1994, Phys. Rev. B **50**, 18 690.
Kadoya, Y., K. Kameda, M. Yamanishi, T. Nishikawa, T. Kannari, T. Ishihara, and I. Ogura, 1996, Appl. Phys. Lett. **68**, 281.
Kahen, K. B., 1992, J. Appl. Phys. **71**, 4577.
Kahen, K. B., 1993, IEEE J. Quantum Electron. **29**, 368.

Kavokin, A. V., and M. A. Kaliteevski, 1995, Solid State Commun. **95**, 859.
Keldysh, L. V., 1965, Sov. Phys. JETP **20**, 1018.
Kelkar, P., V. Kozlov, H. Jeon, A. V. Nurmikko, C. C. Chu, D. C. Grille, J. Han, C. G. Hua, and R. L. Gunshor, 1995, Phys. Rev. B **52**, R5491.
Kelkar, P., V. G. Kozlov, A. V. Nurmikko, C.-C. Chu, J. Han, and R. L. Gunshor, 1997, Phys. Rev. B **56**, 7564.
Khitrova, G., *et al.*, 1996, in *International Quantum Electronics Conference* (Optical Society of America, Washington D.C.), p. TuL37.
Khitrova, G., *et al.*, 1998, Phys. Status Solidi B **206**, 3.
Kim, D. S., J. Shah, D. A. B. Miller, T. C. Damen, W. Schäfer, and L. Pfeiffer, 1993, Phys. Rev. B **48**, 17 902.
Kimble, H. J., 1994, in *Cavity Quantum Electrodynamics*, edited by P. Berman (Academic, San Diego), p. 203.
Kimble, H. J., 1998, Phys. Scr. **T76**, 127.
Kira, M., F. Jahnke, and S. W. Koch, 1997, Solid State Commun. **102**, 703.
Kira, M., F. Jahnke, and S. W. Koch, 1998, Phys. Rev. Lett. **81**, 3263.
Kira, M., F. Jahnke, S. W. Koch, J. D. Berger, D. V. Wick, T. R. Nelson Jr., G. Khitrova, and H. M. Gibbs, 1997, Phys. Rev. Lett. **79**, 5170.
Kira, M., F. Jahnke, S. W. Koch, J. D. Berger, D. V. Wick, T. R. Nelson Jr., G. Khitrova, and H. M. Gibbs, 1998, Proc. SPIE **3283**, 212.
Kira, M., F. Jahnke, W. Hoyer, and S. W. Koch, 1999, Prog. Quantum Electron. (in press).
Kleppner, D., 1981, Phys. Rev. Lett. **47**, 233.
Klimovitch, G., G. Björk, H. Cao, and Y. Yamamoto, 1997, Phys. Rev. B **55**, 7078.
Klingshirn, C., and H. Haug, 1980, Phys. Rep. **70**, 315.
Klingshirn, C. F., 1995, *Semiconductor Optics* (Springer, Berlin).
Koch, M., 1997, Adv. Solid State Phys. **37**, 169.
Koch, M., J. Shah, and T. Meier, 1998, Phys. Rev. B **57**, R2049.
Koch, S. W., F. Jahnke, and W. W. Chow, 1995, Semicond. Sci. Technol. **10**, 739.
Koch, S. W., N. Peyghambarian, and H. M. Gibbs, 1988, J. Appl. Phys. **63**, R1.
Koch, S. W., N. Peyghambarian, and M. Lindberg, 1988, J. Phys. C **21**, 5229.
Korenman, V., 1966, Ann. Phys. (N.Y.) **39**, 72.
Kuhn, T., 1994, "Ladungsträgerdynamik in Halbleitersystemen fern vom Gleichgewicht," Habilitation thesis (Universität Stuttgart).
Kuwata-Gonokami, M., S. Inouye, H. Suzuura, M. Shirane, R. Shimano, T. Someya, and H. Sakaki, 1997, Phys. Rev. Lett. **79**, 1341.
Labilloy, D., H. Benisty, C. Weisbuch, T. F. Krauss, R. M. D. L. Rue, V. Bardinal, R. Houdré, U. Oesterle, D. Cassagne, and C. Jouanin, 1997, Phys. Rev. Lett. **79**, 4147.
Lee, T.-S., T. B. Norris, D. S. Citrin, J. Prineas, G. Khitrova, and H. M. Gibbs, 1998, in *International Quantum Electronics Conference* (Optical Society of America, Washington, D.C.), p. QPD2.
Lee, Y. H., A. Chavez-Pirson, S. W. Koch, H. M. Gibbs, S. H. Park, J. Morhange, A. Jeffery, N. Peyghambarian, L. Banyai, A. C. Gossard, and W. Wiegmann, 1986, Phys. Rev. Lett. **57**, 2446.
Lindberg, M., and S. W. Koch, 1988, Phys. Rev. B **38**, 3342.
Lindberg, M., and S. W. Koch, 1989, Phys. Rev. A **40**, 4415.
Lindberg, M., R. Binder, and S. W. Koch, 1992, Phys. Rev. B **45**, 1865.
Lindberg, M., Y. Z. Hu, R. Binder, and S. W. Koch, 1994, Phys. Rev. B **50**, 18 060.
Lindmark, E. K., T. R. Nelson Jr., G. Khitrova, H. M. Gibbs, A. V. Kavokin, and M. A. Kaliteevski, 1996, Opt. Lett. **21**, 994.
Long, S., B. Sermage, I. Abram, J. Bloch, R. Planel, and V. Thierry-Mieg, 1995, Nuovo Cimento D **17**, 1601.
Loudon, R., 1973, *The Quantum Theory of Light* (Clarendon, Oxford).
Louisell, W., 1974, *Quantum Statistical Properties of Radiation* (Wiley, New York).
Lyngnes, O., J. D. Berger, J. P. Prineas, S. Park, G. Khitrova, H. M. Gibbs, F. Jahnke, M. Kira, and S. Koch, 1997, Solid State Commun. **104**, 297.
MacLeod, H. A., 1986, *Thin-Film Optical Filters*, 2nd ed. (Hilger, Bristol).
Mahan, G. D., 1990, *Many-Particle Physics*, 2nd ed. (Plenum, New York).
Mandel, P., S. D. Smith, and B. S. Wherrett, 1987, Eds., *From Optical Bistability towards Optical Computing* (North-Holland, Amsterdam).
Manzke, G., and K. Henneberger, 1998, Phys. Status Solidi B **147**, 733.
Manzke, G., K. Henneberger, J. Heeg, K. El Sayed, S. Schuster, and H. Haug, 1995, Phys. Status Solidi B **188**, 395.
Meystre, P., 1992, in *Progress in Optics*, edited by E. Wolf (Elsevier, Amsterdam), p. 261.
Miller, A., D. A. B. Miller, and S. D. Smith, 1981, Adv. Phys. **30**, 697.
Morawetz, K., and G. Roepke, 1995, Phys. Rev. E **51**, 4247.
Nelson, T. R., Jr., *et al.*, 1996, Appl. Phys. Lett. **69**, 3031.
Nelson, T. R., Jr., G. Khitrova, E. K. Lindmark, D. V. Wick, J. D. Berger, H. M. Gibbs, K. Tai, and Y. Lai, 1996, in *Conference on Nonlinear Optics: Materials, Fundamentals, and Applications* (Optical Society of America, Washington, D.C.), p. NThE15.
Nelson, T. R., Jr., E. K. Lindmark, D. V. Wick, K. Tai, G. Khitrova, and H. M. Gibbs, 1996, in *Microcavities and Photonic Bandgaps: Physics and Applications*, edited by J. Rarity, and C. Weisbuch (Kluwer, Dordrecht), p. 43.
Nishioka, K., K. Tanaka, I. Nakamura, Y. Lee, and M. Yaminishi, 1993, Appl. Phys. Lett. **63**, 2944.
Norris, T. B., J.-K. Rhee, C.-Y. Sung, Y. Arakawa, M. Nishioka, and C. Weisbuch, 1993, in *International Quantum Electronics Conference* (Optical Society of America, Washington), p. QPD19.
Norris, T. B., J.-K. Rhee, C.-Y. Sung, Y. Arakawa, M. Nishioka, and C. Weisbuch, 1994, Phys. Rev. B **50**, 14 663.
Norris, T. B., J.-K. Rhee, D. S. Citrin, M. Nishioka, and Y. Arakawa, 1995, Nuovo Cimento D **17**, 1295.
Norris, T. B., J.-K. Rhee, R. Lai, D. S. Citrin, M. Nishioka, and Y. Arakawa, 1996, Prog. Cryst. Growth Charact. Mater. **33**, 155.
Nurmikko, A. V., and R. L. Gunshor, 1993, in *Optics of Semiconductor Nanostructures*, edited by F. Henneberger, S. Schmitt-Rink, and E. O. Göbel (Akademie Berlin).
Ohnesorge, B., M. Bayer, A. Forchel, J. P. Reithmaier, N. A. Gippius, and S. G. Tikhodeev, 1997, Phys. Rev. B **56**, R4367.
Orrit, M., C. Aslangul, and P. Kottis, 1982, Phys. Rev. B **25**, 7263.
Osman, M. A., and D. K. Ferry, 1987, Phys. Rev. B **36**, 6018.

Panzarini, G., and L. C. Andreani, 1995a, Phys. Rev. B **52**, 10 780.
Panzarini, G., and L. C. Andreani, 1995b, Nuovo Cimento D **17**, 1651.
Passner, A., H. M. Gibbs, A. C. Gossard, S. L. McCall, and T. N. C. Venkatesan, 1980, IEEE J. Quantum Electron. **QE-16**, 1283.
Pau, S., G. Björk, H. Cao, E. Hanamura, and Y. Yamamoto, 1996, Solid State Commun. **98**, 781.
Pau, S., G. Björk, J. Jacobson, H. Cao, and Y. Yamamoto, 1995a, Phys. Rev. B **51**, 14 437.
Pau, S., G. Björk, J. Jacobson, H. Cao, and Y. Yamamoto, 1995b, Phys. Rev. B **51**, 7090.
Pau, S., G. Björk, J. Jacobson, and Y. Yamamoto, 1995, Nuovo Cimento D **17**, 1657.
Pau, S., H. Cao, J. Jacobson, G. Björk, Y. Yamamoto, and A. Imamoglu, 1996, Phys. Rev. A **54**, R1789.
Pau, S., J. Jacobson, G. Björk, and Y. Yamamoto, 1996, J. Opt. Soc. Am. B **13**, 1078.
Pelouch, W. S., R. J. Ellingson, P. E. Powers, C. L. Tang, D. M. Szmyd, and A. J. Nozik, 1992, Phys. Rev. B **45**, 1450.
Purcell, E. M., 1946, Phys. Rev. **69**, 681.
Quochi, F., G. Bongiovanni, A. Mura, J. L. Staehli, B. Devaud, R. P. Stanley, U. Oesterle, and R. Houdré, 1998, Phys. Rev. Lett. **80**, 4733.
Quochi, F., G. Bongiovanni, A. Mura, J. L. Staehli, R. P. Stanley, U. Oesterle, and R. Houdré, 1997, Phys. Status Solidi A **164**, 23.
Raimond, J. M., and S. Haroche, 1995, in *Confined Electrons and Photons*, edited by E. Burstein and C. Weisbuch (Plenum, New York), p. 383.
Ram, R. J., and A. Imamoglu, 1996, in *Microcavities and Photonic Bandgaps: Physics and Applications*, edited by J. Rarity and C. Weisbuch (Kluwer, Dordrecht), p. 517.
Ram, R. J., C.-K. Sun, G. Wang, E. Goobar, J. Ko, M. Oestreich, J. E. Bowers, and A. Imamoglu, 1996, in *International Quantum Electronics Conference* (Optical Society of America, Washington, D.C.), p. MF5.
Rappen, T., G. Mohs, and M. Wegener, 1993, Phys. Rev. B **47**, 9658.
Rappen, T., U. G. Peter, M. Wegener, and W. Schäfer, 1994, Phys. Rev. B **49**, 10 774.
Rarity, J., and C. Weisbuch, 1996, Eds., *Microcavities and Photonic Bandgaps: Physics and Applications* (Kluwer, Dordrecht).
Rhee, J.-K., D. S. Citrin, T. B. Norris, Y. Arakawa, and M. Nishioka, 1996, Solid State Commun. **97**, 941.
Rhee, J.-K., R. Lai, T. B. Norris, Y. Arakawa, and M. Nishioka, 1995, in *Conference on Quantum Electronics and Laser Science* (Optical Society of America, Washington, D.C.), p. QThI3.
Röpke, G., and R. Der, 1979, Phys. Status Solidi B **92**, 501.
Rossi, F., S. Haas, and T. Kuhn, 1994, Phys. Rev. Lett. **72**, 152.
Savasta, S., and R. Girlanda, 1995, Nuovo Cimento D **17**, 1705.
Savasta, S., and R. Girlanda, 1996a, Phys. Rev. A **53**, 2716.
Savasta, S., and R. Girlanda, 1996b, Phys. Rev. Lett. **77**, 4736.
Savasta, S., R. Girlanda, and G. Martino, 1997, Phys. Status Solidi A **164**, 85.
Savona, V., L. C. Andreani, P. Schwendimann, and A. Quattropani, 1995, Solid State Commun. **93**, 733.
Savona, V., Z. Hradil, A. Quattropani, and P. Schwendimann, 1994, Phys. Rev. B **49**, 8774.
Savona, V., C. Piermarocchi, A. Quattropani, F. Tassone, and P. Schwendimann, 1997, Phys. Rev. Lett. **78**, 4470.
Savona, V., and F. Tassone, 1995, Solid State Commun. **95**, 673.
Savona, V., F. Tassone, C. Piermarocchi, A. Quattropani, and P. Schwendimann, 1996, Phys. Rev. B **53**, 13 051.
Schäfer, W., 1988, in *Optical Nonlinearities and Instabilities in Semiconductors*, edited by H. Haug (Academic, New York).
Schäfer, W., 1996, J. Opt. Soc. Am. B **13**, 1291.
Schäfer, W., R. Binder, and K. H. Schuldt, 1986, J. Lumin. **38**, 282.
Schäfer, W., I. Brener, and W. Knox, 1994, in *Coherent Optical Interactions in Semiconductors*, edited by R. T. Phillips (Plenum, New York).
Schäfer, W., F. Jahnke, and S. Schmitt-Rink, 1993, Phys. Rev. B **47**, 1217.
Schäfer, W., D. S. Kim, J. Shah, T. C. Damen, J. E. Cunningham, K. W. Goossen, L. N. Pfeiffer, and K. Köhler, 1996, Phys. Rev. B **53**, 16429.
Schäfer, W., and J. Treusch, 1986, Z. Phys. B **63**, 407.
Schmitt-Rink, S., and C. Ell, 1985, J. Lumin. **30**, 585.
Schmitt-Rink, S., and D. S. Chemla, 1986, Phys. Rev. Lett. **57**, 2752.
Schmitt-Rink, S., D. S. Chemla, and D. A. B. Miller, 1989, Adv. Phys. **38**, 89.
Schmitt-Rink, S., D. S. Chemla, and H. Haug, 1988, Phys. Rev. B **37**, 941.
Senellart, P., and J. Bloch, 1999, Phys. Rev. Lett. **82**, 1233.
Sermage, B., S. Long, I. Abram, J. Y. Marzin, J. Bloch, R. Planel, and V. Thierry-Mieg, 1996, Phys. Rev. B **53**, 16 516.
Shah, J., 1988, IEEE J. Quantum Electron. **24**, 276.
Shah, J., H. Wang, T. C. Damen, W. Y. Jan, and J. E. Cunningham, 1995, in *Conference on Quantum Electronics and Laser Science* (Optical Society of America, Washington, D.C.), p. QThI5.
Shah, J., R. F. Leheny, and W. Wiegmann, 1977, Phys. Rev. B **16**, 1577.
Soda, H., K. Iga, C. Kitahara, and Y. Suematsu, 1979, Jpn. J. Appl. Phys. **18**, 2329.
Stanley, R. P., R. Houdré, C. Weisbuch, U. Oesterle, and M. Ilegems, 1996, Phys. Rev. B **53**, 10 995.
Stanley, R. P., R. Houdré, U. Oesterle, M. Gailhanou, and M. Ilegems, 1994, Appl. Phys. Lett. **65**, 1883.
Stanley, R. P., R. Houdré, U. Oesterle, M. Ilegems, and C. Weisbuch, 1994, Appl. Phys. Lett. **65**, 2093.
Steyn-Ross, M. L., and C. W. Gardiner, 1983, Phys. Rev. A **27**, 310.
Stroucken, T., A. Knorr, P. Thomas, and S. W. Koch, 1996, Phys. Rev. B **53**, 2026.
Tanaka, K., T. Nakamura, W. Takamatsu, M. Yamanishi, Y. Lee, and T. Isihara, 1995, Phys. Rev. Lett. **74**, 3380.
Tanaka, T., Z. Zhang, M. Nishioka, and Y. Arakawa, 1996, Appl. Phys. Lett. **69**, 887.
Tassone, F., F. Bassani, and L. C. Andreani, 1992, Phys. Rev. B **45**, 6023.
Thompson, R. J., G. Rempe, and H. J. Kimble, 1992, Phys. Rev. Lett. **68**, 1132.
Tignon, J., P. Voisin, C. Delalande, M. Voos, R. Houdri, U. Oesterle, and R. P. Stanley, 1995, Phys. Rev. Lett. **74**, 3967.
Tran Thoai, D. B., and H. Haug, 1993, Z. Phys. B **91**, 199.
Tredicucci, A., Y. Chen, V. Pellegrini, M. Börger, and F. Bassani, 1996, Phys. Rev. A **54**, 3493.

Tredicucci, A., Y. Chen, V. Pellegrini, M. Börger, L. Sorba, F. Beltram, and F. Bassani, 1995, Phys. Rev. Lett. **75**, 3906.
Tredicucci, A., Y. Chen, V. Pellegrini, and C. Deparis, 1995, Appl. Phys. Lett. **66**, 2388.
Tribe, W. R., D. Baxter, M. S. Skolnick, D. J. Mowbray, and T. A. Fisher, 1997, Phys. Rev. B **56**, 12 429.
Wang, H., J. Shah, T. C. Damen, L. N. Pfeiffer, and J. E. Cunningham, 1995, Phys. Status Solidi B **188**, 381.
Wang, H., J. Shah, T. C. Damen, W. Y. Jan, J. E. Cunningham, M. Hong, and J. P. Mannaerts, 1995, Phys. Rev. B **51**, 14 713.
Wang, H., K. Ferrio, D. G. Steele, Y. Z. Hu, R. Binder, and S. W. Koch, 1993, Phys. Rev. Lett. **71**, 1261.
Warren, M., S. W. Koch, and H. M. Gibbs, 1987, IEEE Comput. Sci. Eng. **20**, 68.
Weber, M., J. Feldmann, E. O. Göbel, T. Stroucken, A. Knorr, S. W. Koch, D. S. Citrin, and K. Köhler, 1996, J. Opt. Soc. Am. B **13**, 1241.
Weisbuch, C., 1994a, J. Vac. Sci. Technol. B **12**, 1191.
Weisbuch, C., 1994b, J. Cryst. Growth **138**, 776.
Weisbuch, C., R. Houdré, and R. P. Stanley, 1995, in *Spontaneous Emission and Laser Oscillation in Microcavities*, edited by H. Yokoyama, and K. Ujihara (CRC, Boca Raton), p. 109.
Weisbuch, C., M. Nishioka, A. Ishikawa, and Y. Arakawa, 1992, Phys. Rev. Lett. **69**, 3314.
Weisbuch, C., and J. G. Rarity, 1996, in *Microcavities and Photonic Bandgaps: Physics and Applications*, edited by J. Rarity, and C. Weisbuch (Kluwer, Dordrecht), p. 1.
Weisbuch, C., and B. Vinter, 1991, *Quantum Semiconductor Structures* (Academic, Boston).
Whittaker, D. M., 1998, Phys. Rev. Lett. **80**, 4791.
Whittaker, D. M., P. Kinsler, T. A. Fisher, M. S. Skolnick, A. Armitage, A. M. Afshar, M. D. Sturge, and J. S. Roberts, 1996, Phys. Rev. Lett. **77**, 4792.
Whittaker, D. M., T. A. Fisher, A. M. Asfhar, M. S. Skolnick, P. Kinsler, J. S. Roberts, G. Hill, and M. A. Pate, 1995, Nuovo Cimento D **17**, 1781.
Wick, D. V., T. R. Nelson Jr., E. K. Lindmark, H. M. Gibbs, G. Khitrova, and K. Tai, 1996, in *Physics and Simulation of Optoelectronic Devices IV*, Proc. SPIE **2693**, p. 160.
Yablonovitch, E., 1987, Phys. Rev. Lett. **58**, 2059.
Yablonovitch, E., 1993, J. Opt. Soc. Am. B **10**, 283.
Yamamoto, Y., F. Matinaga, S. Machida, A. Karlsson, J. Jacobson, G. Björk, and T. Mukai, 1993, J. Phys. IV **3**, 39.
Yamamoto, Y., J. M. Jacobson, S. Pau, H. Cao, and G. Björk, 1996, in *Microcavities and Photonic Bandgaps: Physics and Applications*, edited by J. Rarity and C. Weisbuch (Kluwer, Dordrecht), p. 457.
Yamamoto, Y., S. Machida, and G. Björk, 1991, Phys. Rev. A **44**, 657.
Yamamoto, Y., S. Machida, Y. Horikoshi, and K. Igeta, 1991, Opt. Commun. **80**, 337.
Yamanishi, M., 1995, Prog. Quantum Electron. **19**, 1.
Yariv, A., and P. Yeh, 1983, *Optical Waves in Crystals: Propagation and Control of Laser Radiation* (Wiley, New York).
Yokoyama, H., K. Nishi, T. Anan, H. Yamada, S. D. Brorson, and E. P. Ippen, 1990, Appl. Phys. Lett. **57**, 2814.
Zhang, Z. L., M. Nishioka, C. Weisbuch, and Y. Arakawa, 1994, Appl. Phys. Lett. **64**, 1068.
Zhu, Y., D. J. Gauthier, S. E. Morin, Q. Wu, H. J. Carmichael, and T. W. Mossberg, 1990, Phys. Rev. Lett. **64**, 2499.
Zimmermann, R., 1988, *Many Particle Theory of Highly Excited Semiconductors* (Teubner Texte zur Physik, Leipzig).
Zimmermann, R., 1990, Phys. Status Solidi B **159**, 317.
Zimmermann, R., 1992, J. Lumin. **53**, 187.
Zimmermann, R., K. Kilimann, W. D. Kraeft, D. Kremp, and G. Röpke, 1978, Phys. Status Solidi B **90**, 175.